Universidad de Huelva

Departamento de Química “Profesor José Carlos Vílchez Martín”

Synthesis, reactivity and catalytic applications of iridium and copper complexes bearing bulky phosphines in conventional and exotic electronic configurations

Memoria para optar al grado de doctora presentada por:

Alejandra Pita Milleiro

Fecha de lectura: 4 de abril de 2025

Bajo la dirección de los doctores:

Pedro José Pérez Romero

Jesús Campos Manzano

Huelva, 2025

UNIVERSIDAD DE HUELVA

Departamento de Química "Profesor José Carlos Vílchez Martín"

CONSEJO SUPERIOR DE INVESTIGACIONES CIENTÍFICAS

Instituto de Investigaciones Químicas

Synthesis, Reactivity And Catalytic Applications Of Iridium And Copper Complexes Bearing Bulky Phosphines In Conventional And Exotic Electronic Configurations

Programa de Doctorado: Ciencia y Tecnología Industrial y Ambiental

Alejandra Pita Milleiro

Huelva, 2025

Synthesis, Reactivity And Catalytic Applications Of Iridium And Copper Complexes Bearing Bulky Phosphines In Conventional And Exotic Electronic Configurations

por

Alejandra Pita Milleiro

Trabajo presentado para aspirar
al Título de Doctora en Química
Huelva, 2025

Alejandra Pita Milleiro

Directores de Tesis

Pedro José Pérez Romero
Catedrático de
Química Inorgánica
(Universidad de Huelva)

Jesús Campos Manzano
Investigador
Científico
(CSIC)

A mi abuelo Jose

AGRADECIMIENTOS

La mayor alegría de esta tesis ha sido, sin ninguna duda, las personas que he podido conocer dentro y fuera del laboratorio a lo largo de estos años. En las siguientes líneas intentaré transmitir mi agradecimiento a todas vosotras.

Marta y Kike, nos hemos dicho muchas cosas bonitas, dentro y fuera de la Alameda, pero aquí van más: os doy las gracias por todo el apoyo que he sentido gracias a vosotros, escribir la tesis en paralelo ha hecho de una experiencia tan individual algo mucho más agradable. Gracias Marta, además de ser una tía chulísima, siempre has tenido una mano que prestar, incluso aunque fuera solo martes y ya hubiera ganas de ir al laboratorio con americana. Kike, gracias por todo tu cariño y todos los abrazos, que a veces son tan necesarios en el laboratorio.

Helena y Martina, como os he dicho muchas veces, me alegro mucho de que seamos amigas porque si no lo fuéramos me daríais pánico. Helena, gracias por estar ahí siempre que te he necesitado, estos últimos meses han sido muy estresantes por muchos motivos, pero gracias a ti ha sido más fácil, lo aprecio mucho. Martina, gracias por toda tu ayuda cerrando cosas de la tesis, por los ochocientos archivos de DRX que te he pedido, pero, especialmente, gracias por la carbonara y los Aperol, ya que yo no pude ir a tu defensa (a pesar de cierta promesa en vídeo) vamos a tener que celebrar el doble esta.

Nadir, tu amistad ha sido de lo más inesperado, pero que bueno que las sorpresas sean a veces positivas. Gracias por todos los cafés con alfajores, por mantenerme informada de todo (quizá demasiado) los tres meses que estuve en Oslo y por ofrecerme tu sofá de Erlangen. Has sido un apoyo extraordinario en esta última etapa y lo agradeceré siempre.

Agradecimientos

Gracias a todas las personas con las que he podido trabajar: a Emmanuel, por su tranquilidad y buen-rollismo; a Alba, por estar siempre dispuesta a una cervecita y compartir dramas; a Pilar, que no me mató cuando le tiré 200 mg de platino; a Jeff, que para bien o para mal se dio cuenta de que la combinación Martina + yo + comida de grupo le iba a sentar fatal siempre, pero ahí sigue; a Antonio, por sus marchas de Semana Santa, su playlist compartida de Spotify y sus chistes malos. Gracias, Miquel, por todos tus consejos no solo de química, sino también sobre *el juego de la academia* o sobre dónde encontrar el mejor rabo de toro de Sevilla. Félix, gracias por el descubrimiento de América, fecha señalada con la que espero contar en la celebración post-defensa. Juanjo, si no hubiera empezado a aprender contigo computacional esta tesis y mi trayectoria hubieran sido muy distintas, gracias por todo lo que me enseñaste y por tu apoyo durante estos años.

Javi, mis agradecimientos a ti ya sabes que se extienden mucho más allá de los años de tesis. Menos mal que te hicieron gracia los gritos que, cuenta la leyenda, dedique yo a una señora-bien-señora-fetén allá por 2016. Gracias por todas las horas compartidas y por estar siempre a favor de una buena anécdota. No sabes lo que me alegro de tener como amigo a, como diría Toñi Moreno, una *persona* tan *maravillosa*.

Gracias, Dani y a Susana, de la Complu, por recibirme con tanta amabilidad esas semanas en Madrid. Isra, gracias por la acogida y compartir tus trucos para hacer unas figuras tan chulas.

De mi etapa en Oslo, gracias, Lucía, no solo por ser una gran postdoc, dispuesta a resolver cualquier duda, sino también por todos los días de escalada y todos los *coffee breaks*. To Hannan and Manuela, for all your kindness, all the gossip and all the hiking. David, muchas gracias por tu entusiasmo y tu confianza desde el primer día.

Agradecimientos

Por supuesto, sin directores no hay tesis. Gracias, Jesús y Pedro, por todo lo que he aprendido con vosotros, por la ayuda, el entusiasmo y, especialmente, por la generosidad con vuestro tiempo, incluso con Navidades de por medio, para hacer correcciones a esta *high-speed thesis*.

Gracias a toda mi familia por darme un lugar al que sé que siempre puedo volver. Papá, gracias tu confianza, por tu apoyo y por todo lo que me has enseñado, no sería la persona que soy sin ti.

Un abrazo,

Ale

TABLE OF CONTENTS

ABBREVIATIONS

Me	methyl, -CH_3
Et	ethyl, -CH_2CH_3
^{i}Pr	*iso*-propyl, -$CH(CH_3)_2$
^{t}Bu	*tert*-butyl, -CMe_3
Ph	phenyl, -C_6H_5
Ar	aryl
Ar’	terphenyl
Xyl	xylyl, 2,6-$Me_2C_6H_3$
Dipp	diisopropylphenyl, 2,6-$^{i}Pr_2C_6H_3$
BAr^F	$[\{3,5\text{-}(CF_3)_2\text{-}C_6H_3)_4\}B]^-$
THF	tetrahydrofuran, C_4H_8O
Tol	toluene, C_7H_8
acac	acetylacetonate
L	2-electron donor ligand
X	1-electron donor ligand
C_5Me_5	pentamethylcyclopentadienyl
NHC	N-Heterocyclic Carbene
η	ligand hapticity
ν	infrared vibrational wavenumber (cm^{-1})
min	minutes
h	hours
equiv.	equivalents
Anal. Calc.	analysis calculated

Abbreviations

Exp.	experimental
kcal	kilocalorie
g	grams
mmol	millimol
mL	milliliter
Å	angstrom
º	degree
C	Celsius
K	Kelvin
ref.	reference
ORTEP	crystallographic representation (Oak Ridge Thermal Ellipsoid Program)
IR	infrared
k	rate constant
OA	Oxidative Addition
RE	Reductive Elimination
σ-BM	σ-Bond Metathesis
MAσBM	Metal Assisted σ-Bond Metathesis
σ-CAM	σ-Complex Assisted Metathesis
OATS	Oxidatively Added Transition State
AMLA	Ambiphilic Metal Ligand Assistance
CMD	Concerted Metalation Deprotonation
NAD	Nicotinamide Adenine Dinucleotide
DFT	Density Functional Theory
TS	Transition State

Abbreviations

QTAIM	Quantum Theory of Atoms in Molecules
IRC	Intrinsic Reaction Coordinate
SMD	Solvation Model based on Density
SCF	Self-Consistent Field
bcp	bond critical point
MECP	Minimum Energy Crossing Point
ASM	Activation Strain Model
EDA	Energy Decomposition Analysis
NOCV	Natural Orbitals for Chemical Valence

Abbreviations

NMR Abbreviations

NMR	Nuclear Magnetic Resonance
δ	chemical shift in ppm
ppm	parts per million
NOESY	Nuclear Overhauser Enhancement SpectroscopY
EXSY	EXchange SpectroscopY
COSY	^{1}H-^{1}H correlation spectroscopy
HSQC	^{1}H-^{13}C correlation spectroscopy (Heteronuclear Single Quantum Coherence)
HMBC	^{1}H-^{13}C correlation spectroscopy (Heteronuclear Multiple Bond Correlation)
s	singlet
d	doublet
t	triplet
sept	septet
m	multiplet
br.	broad
$^{n}J_{AB}$	coupling constant (Hz) between A and B nuclei separated by n bonds
Hz	hertz

CONSIDERACIONES GENERALES

Esta Tesis Doctoral se ha desarrollado en el marco de una colaboración entre el Laboratorio de Catálisis Homogénea (Universidad de Huelva-CIQSO) y el grupo de Química Organometálica: Estructura, Reactividad y Aplicaciones (CSIC-Universidad de Sevilla). Esta Tesis Doctoral ha sido financiada por una ayuda *"La Caixa" Doctoral INPhINIT fellowship*. El objetivo central de la tesis consiste en el estudio de conceptos de interés en el campo de la catálisis homogénea.

La Memoria tiene una estructura clásica basada en: **Introducción**, **Resultados y Discusión**, y **Parte Experimental**, para cada uno de los tres capítulos independientes que la componen. Para facilitar su lectura, la bibliografía aparece tanto a pie de página como al final de cada capítulo y de forma independiente en cada uno de ellos. Esta distribución hace que algunas referencias puedan aparecer en distintos capítulos. La numeración de los esquemas, figuras y compuestos es independiente en cada uno de ellos.

El primero de los capítulos incluye la síntesis de compuestos organometálicos de Ir estabilizados por ligandos fosfina voluminosos de composición PMe_2Ar', donde Ar' es un sustituyente de tipo terfenilo, y el estudio de su reactividad. El segundo capítulo consiste en la síntesis de complejos monoméricos de Ir(II) y su uso como catalizadores para la isomerización de olefinas. El último capítulo incluye la síntesis de diversos complejos de cobre con una fosfina voluminosa y su uso como catalizadores en reacciones de aziridinación. Todos los resultados experimentales se complementan con estudios computacionales. Todos los estudios computacionales son obra de la autora de este trabajo.

Consideraciones Generales

Los nuevos compuestos sintetizados se han caracterizado fundamentalmente mediante espectroscopía de Resonancia Magnética Nuclear y estudios de difracción de rayos X de monocristal. Estas determinaciones cristalográficas se llevaron a cabo de manera independiente por distintos miembros del grupo dirigido por el Dr. Jesús Campos. Tanto las medidas de Resonancia Paramagnética Electrónica como las simulaciones de los espectros fueron realizadas de manera independiente por la Dra. Nereida Hidalgo. Los resultados catalíticos del capítulo III son obra de Jorge Pérez Ruíz (Universidad de Huelva-CIQSO) y se exponen como contexto para los estudios computacionales.

Durante el desarrollo de la tesis doctoral se ha realizado una estancia breve de tres meses en la *Universitetet i Oslo*, en Oslo (Noruega), bajo la supervisión del Dr. David Balcells. Por motivos de espacio, los resultados experimentales obtenidos durante dicha estancia no se han incluido en el manuscrito. Estos resultados incluyen la aplicación de técnicas de *machine learning* a complejos bimetálicos con fines catalíticos. Con el objeto de obtener la mención de "Doctorado Internacional" (RD 99/2011; BOE 10-02-2011, Art. 15), la mayor parte de la Tesis se ha redactado en inglés, exceptuando las Consideraciones Generales, el Resumen y las Conclusiones finales, secciones escritas tanto en inglés como en español.

RESUMEN

CAPÍTULO I

El objetivo fundamental del **primer capítulo** de esta Tesis Doctoral es el estudio de la reactividad de complejos catiónicos y coordinativamente insaturados de Ir(III) estabilizados por ligandos pentametilciclopentadienilo (C_5Me_5) y fosfinas voluminosas de terfenilo (PMe_2Ar', Ar' = 2,6-diarilfenil). El ligando C_5Me_5 se comporta de manera general como un espectador robusto. Sin embargo, en nuestros estudios se demuestra una notable electrofilia en la reacción de estos complejos insaturados con reactivos alquil-litiados, evidenciando el carácter no inocente del ligando C_5Me_5. Frente a otro tipo de nucleófilos, como son los reactivos de Grignard, la reactivad es marcadamente distinta consiguiéndose en este caso alquilar el centro metálico.

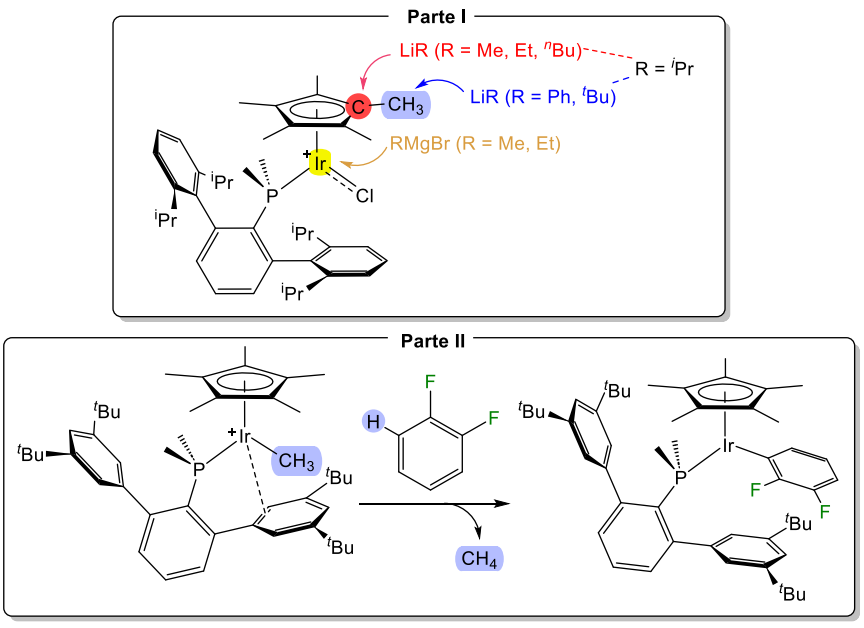

Resumen esquemático del primer capítulo: reactividad frente a diferentes agentes nucleófilos (arriba) y activación de enlace C–H (abajo).

En la segunda parte de los resultados del **primer capítulo**, se expone la obtención de complejos neutros de Ir(I) altamente insaturados y basados en el mismo tipo de ligandos. En el caso de un menor impedimento estérico de la fosfina de terfenilo, es posible metilar el iridio, obteniendo un complejo de Ir(III) capaz de llevar a cabo reacciones de activación C–H inter- e intramolecularmente. Una parte de los resultados obtenidos en este capítulo se ha publicado, mientras que otras secciones son todavía inéditas.

CAPÍTULO II

En el **segundo capítulo** de esta Tesis Doctoral se explora la posibilidad de acceder a estados de oxidación poco usuales en complejos de iridio. En concreto, se describen la síntesis de complejos mononucleares de Ir(II). Se expone el estudio de la relación entre estructura y propiedades, como las distancias en sus estructuras cristalinas o la localización de su densidad de espín. Estos compuestos exóticos son catalíticamente activos para la isomerización de olefinas y, además, son más activos que su análogo común de Ir(I). El mecanismo catalítico ha sido estudiado computacionalmente. Adicionalmente, la diferencia en reactividad ha sido racionalizada por medio de *Activation Strain Analysis*. Los resultados obtenidos en este capítulo han sido publicados.

Resumen

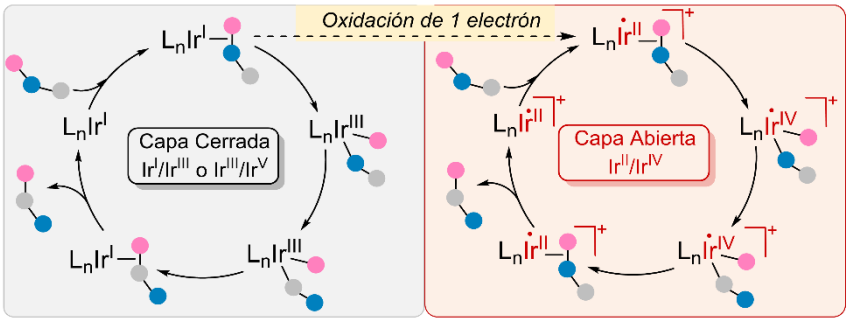

Resumen esquemático del segundo capítulo: comparación de mecanismo de capa cerrada (izquierda) y capa abierta (derecha) para la isomerización de olefinas con un catalizador basado en iridio.

CAPÍTULO III

El **tercer capítulo** de esta tesis se divide en dos secciones principales. En la primera, se presenta la síntesis de complejos de cobre utilizando una fosfina de muy alto volumen estérico. En este apartado, se describen los aductos obtenidos con pequeñas moléculas, como etileno, acetileno y monóxido de carbono, cuyas propiedades de enlace han sido estudiadas en profundidad mediante cálculos computacionales. En la segunda sección, se explora el potencial de uno de estos complejos de cobre como precatalizador en la aziridinación de olefinas. A través de técnicas computacionales, se analiza el mecanismo catalítico asociado, permitiendo racionalizar los resultados experimentales y aportar una comprensión detallada del sistema. Los resultados de este capítulo son todavía inéditos y los manuscritos correspondientes se encuentran en preparación.

Resumen

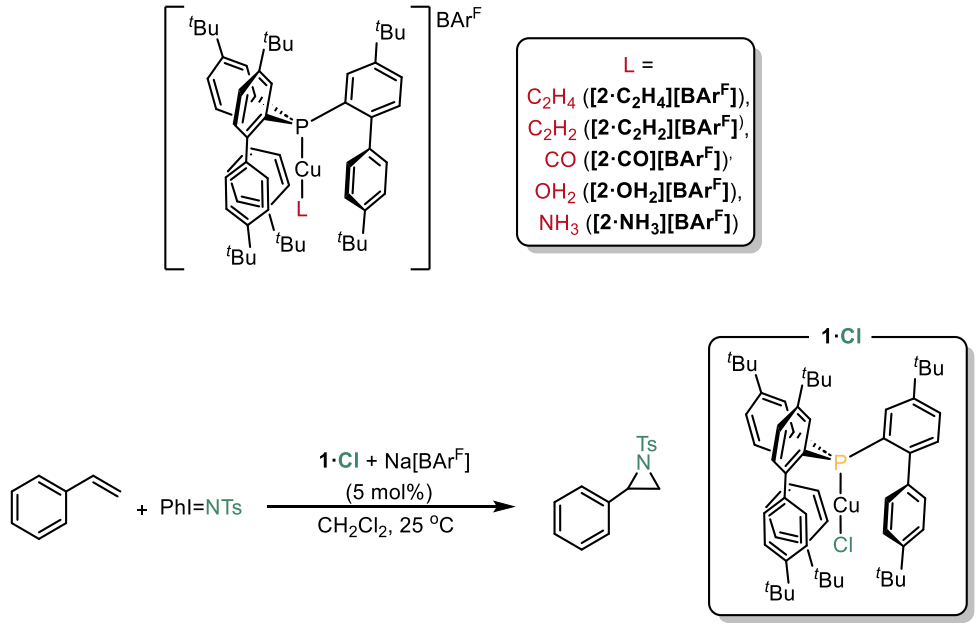

Resumen esquemático del tercer capítulo: aductos de fosfina-cobre y pequeñas moléculas (arriba) y reacción de aziridinación catalizada por el complejo ***1·Cl*** *(abajo).*

GENERAL CONSIDERATIONS

This Ph.D. Thesis was developed as part of a collaboration between the Homogeneous Catalysis Laboratory (University of Huelva-CIQSO) and the Organometallic Chemistry: Structure, Reactivity, and Applications group (CSIC-University of Seville). This Ph.D. Thesis was funded by a *"La Caixa" Doctoral INPhINIT* fellowship. The central objective of the thesis is the study of concepts of interest in the field of homogeneous catalysis.

The Thesis is structured in a classical format comprising **Introduction, Results and Discussion,** and **Experimental Section** for each of the three independent chapters. To facilitate reading, references are included as footnotes and at the end of each chapter, presented independently in each case. This organization may result in some references appearing in multiple chapters. The numbering of schemes, figures, and compounds is also independent for each chapter.

The first chapter involves the synthesis of organometallic Ir compounds stabilized by bulky phosphine ligands with the composition PMe_2Ar', where Ar' is a terphenyl-type substituent, and the study of their reactivity. The second chapter focuses on the synthesis of monomeric Ir(II) complexes and their use as catalysts for olefin isomerization. The final chapter addresses the synthesis of various copper complexes with a bulky phosphine and their application as catalysts in aziridination reactions. All experimental results are complemented by computational studies, which were performed entirely by the author of this work.

The newly synthesized compounds were primarily characterized using Nuclear Magnetic Resonance spectroscopy and single-crystal X-ray diffraction studies. These crystallographic determinations were

independently conducted by various members of the group led by Dr. Jesús Campos. Electron Paramagnetic Resonance measurements and spectral simulations were independently carried out by Dr. Nereida Hidalgo. The catalytic results in Chapter III were provided by Jorge Pérez Ruíz (University of Huelva-CIQSO) and are presented as context for the computational studies.

During the development of this Ph.D. thesis, a three-month research stay was conducted at the *Universitetet i Oslo*, in Oslo (Norway), under the supervision of Dr. David Balcells. Due to space constraints, the experimental results obtained during this stay have not been included in the manuscript. These results involve the application of machine learning techniques to bimetallic complexes for catalytic purposes. To obtain the "International Ph.D." distinction (RD 99/2011; BOE 10-02-2011, Art. 15), most of the thesis has been written in English, except for the General Considerations, Summary, and final Conclusions, which are presented in both English and Spanish.

SUMMARY

CHAPTER I

The fundamental objective of the **first chapter** of this Ph.D. Thesis is to study the reactivity of cationic and coordinatively unsaturated Ir(III) complexes stabilized by pentamethylcyclopentadienyl (C_5Me_5) ligands and bulky terphenyl phosphines (PMe_2Ar', Ar' = 2,6-diarylphenyl). The C_5Me_5 ligand generally acts as a robust spectator. However, our studies reveal significant electrophilicity in the reaction of these unsaturated complexes with alkyl-lithium reagents, highlighting the non-innocent nature of the C_5Me_5 ligand. In contrast, when using other nucleophiles such as Grignard reagents, markedly different reactivity is observed, enabling metal-centered alkylation.

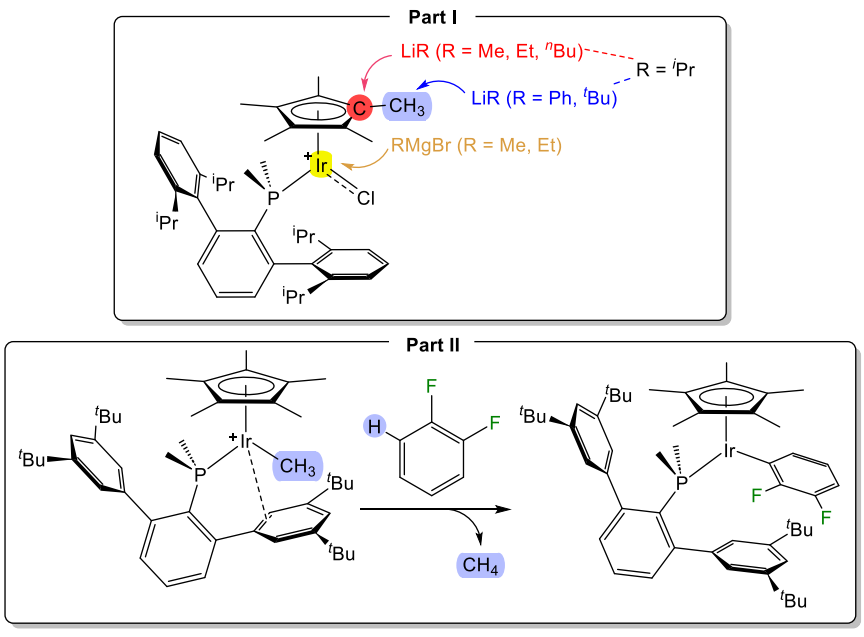

Schematic summary of the first chapter: divergent reactivity toward nucleophilic agents (top) and C–H bond activation (bottom).

Summary

In the second part of the **first chapter**, neutral, highly unsaturated Ir(I) complexes based on similar ligands are synthesized. With reduced steric hindrance of the terphenyl phosphine, methylation of iridium is possible, resulting in an Ir(III) complex capable of inter- and intramolecular C–H activation. Some of the results from this chapter have been published, while others remain unpublished.

CHAPTER II

The **second chapter** explores the accessibility of uncommon oxidation states in iridium complexes. Specifically, it describes the synthesis of mononuclear Ir(II) complexes and the study of their structure-property relationships, such as distances in crystal structures and spin density localization. These exotic compounds are catalytically active for olefin isomerization and are more active than their common Ir(I) analog. The catalytic mechanism was investigated computationally. Additionally, the difference in reactivity has been rationalized using Activation Strain Analysis. The results from this chapter have been published.

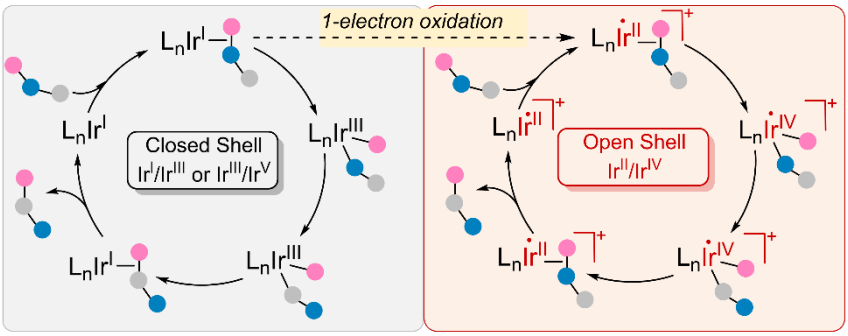

Schematic summary of the second chapter: comparison of closed-shell (left) and open-shell (right) mechanisms for olefin isomerization with an iridium-based catalyst.

Summary

CHAPTER III

The **third chapter** is divided into two main sections. The first presents the synthesis of copper complexes using a phosphine with very high steric bulk. This section describes the adducts obtained with small molecules such as ethylene, acetylene, and carbon monoxide, whose bonding properties have been thoroughly studied via computational calculations. In the second section, the potential of one of these copper complexes as a precatalyst in olefin aziridination is explored. Computational techniques were used to analyze the associated catalytic mechanism, allowing for rationalization of the experimental results and providing a detailed understanding of the system. The results from this chapter are currently unpublished as the corresponding manuscripts are in preparation.

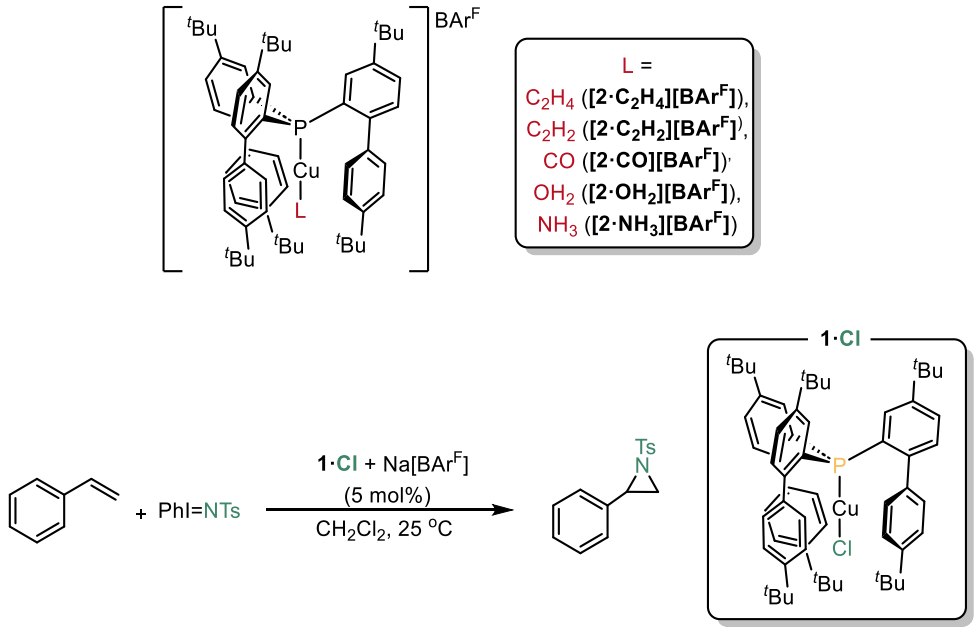

*Schematic summary of the third chapter: phosphine-copper and small molecules adducts (above) and aziridination reaction catalyzed by **1·Cl** (bottom).*

PUBLICATIONS

Research articles directly related to this thesis

Chapter I

Part 1. Pita-Milleiro, A.; Alférez, M. G.; Moreno, J. J.; Espada, M. F.; Maya, C.; Campos, J. Unveiling the Latent Reactivity of Cp* Ligands ($C_5Me_5^-$) toward Carbon Nucleophiles on an Iridium Complex. *Inorg. Chem.* **2023**, *62*, 5961–5971.

Part 2. Manuscript in preparation.

Chapter II

Pita-Milleiro, A.; Hidalgo, N.; Moreno, J. J.; Fernández, I.; Campos, J. An Open-Shell Ir(II)/Ir(IV) Redox Couple Outperforms an Ir(I)/Ir(III) Pair in Olefin Isomerization. *Nat. Chem.* **2025**.

Chapter III

Part 1. Manuscript in preparation.

Part 2. Manuscript in preparation.

Publicaciones

Debido a restricciones relativas a derechos de autor, los capítulos 2 y 3 (en proceso de publicación), han sido retirado de la tesis. En sustitución del artículo publicado ofrecemos la siguiente información: referencia bibliográfica, resumen y palabras claves.

- Pita-Milleiro, A., Hidalgo, N., Moreno, J.J. et al. An open-shell Ir(II)/Ir(IV) redox couple outperforms an Ir(I)/Ir(III) pair in olefin isomerization. Nat. Chem. 17, 606–613 (2025). https://doi.org/10.1038/s41557-024-01722-7

Enlace al texto completo: https://doi.org/10.1038/s41557-024-01722-7

RESUMEN:

Open-shell systems based on first-row transition metals and their involvement in various catalytic processes are well explored. By comparison, mononuclear open-shell complexes of precious transition metals remain underdeveloped. This is particularly true for IrII complexes, as there is very limited information available regarding their application in catalysis. Here we show that a family of IrII metalloradicals, featuring a C6H3-2,6-(OP(tBu)2)2 (POCOP) pincer ligand, effectively catalyses olefin isomerization—a key step in alkane metathesis—exhibiting up to 20 times higher activity than their IrI counterparts. Computational studies reveal that the IrII/IrIV redox cycling enables faster kinetics than the traditional IrI/IrIII pathway owing to reduced barriers for the oxidative addition and reductive elimination steps. Thus, this study presents a redox catalyst involving an IrII/IrIV pair, highlighting the capabilites of precious-metal systems that extend beyond traditional redox cycles. These findings emphasize the need for expanding catalytic design principles, especially for platinum-group metals.

- Copper(I)-Phosphine Complexes: Bonding and Catalytic Properties. (En proceso de publicación)

Publications

Other research articles

Serrano-Díez, E.; Pita-Milleiro, A.; Rangel-García, J.; Moreno, J. J.; Roselló-Merino, M.; Campos, J. Reversible Bimetallic Inhibition to Modulate Selectivity During Catalysis. *J. Am. Chem. Soc.* **2025**, *147*, 1271–1281.

Moreno, J. J.; Pita-Milleiro, A.; Luque-Gómez, A.; Espada, M. F.; López-Serrano, J.; Campos, J. Mechanism of Dihydrogen Splitting by an Apparent Bimetallic Frustrated Lewis Pair Based on Ir(III)/Pt(0). *Z. Anorg. Allg. Chem.* **2023**, *649*, e202300003.

CHAPTER I

Chapter I. Pentamethylcyclopentadienyl Iridium Complexes Bearing Bulky Phosphine Ligands as Platforms to Investigate Ligand Non-Innocence and C–H Activation Processes

I.1 INTRODUCTION

I.1.1 Transition metal mediated C−H activation

Carbon−hydrogen bonds are almost ubiquitous in organic molecules; however, they do not usually partake in productive reactions. The inherent inertness of these typically non-polar bonds, along with the difficulty in selectively transforming the numerous chemically similar C−H bonds present in organic compounds, present significant challenges to their functionalization.[1] Despite these challenges, the significance of C−H bond activation is undeniable.

After decades of seminal advances, C−H bond activation now serves as a critical tool for the chemical industry.[1] However, hydrocarbons are still primarily utilized as fuels to harness the energy stored in their chemical bonds, and their potential as cost-effective feedstocks remain underutilized due to the lack of efficient methods for converting them into synthetically valuable compounds.[2] For example, the activation of methane, the simplest hydrocarbon, has been a focal point of chemical research since the early 1950s. As the primary component of natural and shale gas, methane represents an abundant, low-cost feedstock, particularly for the chemical industry (Figure 1).[3] The activation of methane's strong C−H bonds is a complex process, typically requiring high temperatures. Despite these challenges, significant progress has been made in developing methods to

[1] a) Goldberg, K. I.; Goldman, A. S. *Activation and Functionalization of C−H bonds*. ACS Symposium Series 885, American Chemical Society, Washington DC, 2004; b) Bergman, R. G. *Nature* **2007**, *446*, 391–393.
[2] a) Hill, C. L. *Activation and functionalization of alkanes*. John Wiley & Sons, New York, 1989. b) Pérez, P. J. *Alkane C−H Activation by Single-Site Metal Catalysis*. Springer, Dordrecht, 2012. c) Labinger, J. A.; Bercaw, J. E. *Nature* **2002**, *417*, 507–514.
[3] Caballero, A.; Pérez, P. J. *Chem. Soc. Rev.* **2013**, *42*, 8809–8820.

convert methane directly into added-valued chemicals[4] such as higher hydrocarbons,[5] and oxidated derivatives, including carboxylic acids,[6] esters[7] and methanol.[8] Such a conversion would not only address logistical challenges associated with the transportation of methane, often located in remote areas,[4] but also create a versatile feedstock that could be used in the production of a wide range of chemicals.

[4] Gunsalus, N. J.; Koppaka, A.; Park, S. H.; Bischof, S. M.; Hashiguchi, B. G.; Periana, R. A. *Chem. Rev.* **2017**, *117*, 8521–8573.

[5] a) Belgued, M., Pareja, P., Amariglio, A., Amariglio, H. *Nature* **1991**, *352*, 789–790. b) Guo, X.; Fang, G.; Li, G.; Ma, H.; Fan, H.; Yu, L.; Ma, C.; Wu, X.; Deng, D.; Wei, M.; Tan, D.; Si, R.; Zhang, S.; Li, J.; Sun, L.; Tang, Z.; Pan, X.; Bao, X. *Science* **2014**, *344*, 616–619. c) Morejudo, S. H.; Zanon, R.; Escolastico, S.; Yuste-Tirados, I.; Malerod-Fjeld, H.; Vestre, P. K.; Coors, W. G.; Martinez, A.; Norby, T.; Serra, J. M.; Kjølseth, C. *Science* **2016**, *353*, 563–566.

[6] a) Lin, M.; Sen, A. *Nature* **1994**, *368*, 613–615. b) Periana, R. A., Mironov, O., Taube, D., Bhalla, G., Jones, C. J. *Science* **2003**, *301*, 814–818. c) Cui, X.; Li, H.; Wang, Y.; Hu, Y.; Hua, L.; Li, H.; Han, X.; Liu, Q.; Yanf, F.; He, L.; Chen, X.; Li, Q.; Xiao, J.; Deng, D.; Bao, X. *Chem* **2018**, *4*, 1902–1910.

[7] a) Periana, R. A.; Taube, D. J.; Gamble, S.; Taube, H.; Satoh, T.; Fujii, H. *Science* **1998**, *280*, 560–564. b) Caballero, A.; Despagnet-Ayoub, E.; Díaz-Requejo, M. M.; Díaz-Rodríguez, A.; González-Núñez, M. E.; Mello, R.; Muñoz, B. K.; Ojo, W.-S.; Asensio, G.; Etienne, M.; Pérez, P. J. *Science* **2011**, *332*, 835–838.

[8] a) Periana, R. A.; Taube, D. J.; Evitt, E. R.; Löffler, D. G.; Wentrcek, P. R.; Voss, G.; Masuda, T. *Science* **1993**, *259*, 340–343. b) Hammond, C.; Forde, M. M.; Rahim, M. H. A.; Thetford, A.; He, Q.; Jenkins, R. L.; Dimitratos, N.; Lopez-Sanchez, J. A.; Dummer, N. F.; Murphy, D. M.; Carley, A. F.; Taylor, S. H.; Willock, D. J.; Stangland, E. E.; Kang, J.; Hagen, H.; Kiely, C. J.; Hutchings, G. J. *Angew. Chem., Int. Ed.* **2012**, *51*, 5129–5133. c) Sushkevich, V.L., Palagin, D., Ranocchiari, M., van Bokhoven, J.A. *Science* **2017**, *356*, 523–527. d) Agarwal, N.; Freakley, S. J.; McVicker, R. U.; Althahban, S. M.; Dimitratos, N.; He, Q.; Morgan, D. J.; Jenkins, R. L.; Willock, D. J.; Taylor, S. H.; Kiely, C. J.; Hutchings, G. J. *Science* **2017**, *358*, 223–227. e) Baek, J.; Rungtaweevoranit, B.; Pei, X.; Park, M.; Fakra, S. C.; Liu, Y.-S.; Matheu, R.; Alshmimri, S. A.; Alshehri, S.; Trickett, C. A.; Somorjai, G. A.; Yaghi, O. M. *J. Am. Chem. Soc.* **2018**, *140*, 18208–18216.

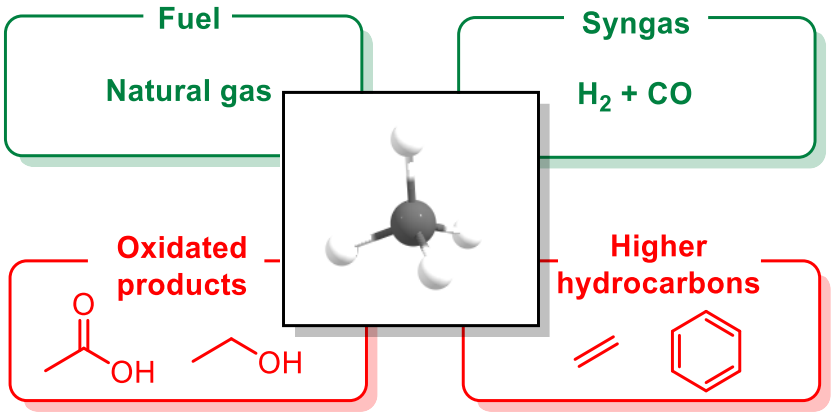

Figure 1. In green, current uses of methane, in red, some examples of desired products into which directly convert methane.

The preeminence of transition metals in the field of catalytic C−H bond functionalization is well known. Transition metal compounds capable of promoting C–H bond activation followed by C–C (or C–X, where X = O, N, S) bond formation offer significant potential for converting simple, readily available raw materials into value-added molecules, such as pharmaceuticals and natural products. The functionalization of alkanes through the formation of new C–X bonds opens numerous opportunities for more efficient utilization of natural hydrocarbon resources, as well as the synthesis of high-value organic compounds.[9]

[9] a) Godula, K.; Sames, D. *Science* **2006**, *312*, 67–72. b) Rech, J. C.; Yato, M.; Duckett, D.; Ember, B.; LoGrasso, P. V.; Bergman, R. G.; Ellman, J. A. *J. Am. Chem. Soc.* **2007**, *129*, 490–491. c) Davies, H. M. L.; Manning, J. R. *Nature* **2008**, *451*, 417–424. d) McMurray, L.; O'Hara, F.; Gaunt, M. J. *Chem. Soc. Rev.* **2011**, *40*, 1885–1898. e) Yamaguchi, J.; Yamaguchi, A. D.; Itami, K. *Angew. Chem. Int. Ed.* **2012**, *51*, 8960–9009. f) Wencel-Delord, J.; Glorius, F. *Nat. Chem.* **2013**, *5*, 369–375. g) He, J.; Hamann, L. G. H.; Davies, H. M. L.; Beckwith, R. E. J. *Nat. Commun.* **2015**, *6*, 5943.

From a historical perspective, the first activation of a C−H bond is sometimes attributed to Dimroth's report[10] of 1898 (Scheme 1), yet, since the term "C−H bond activation" has acquired mechanistic connotations, it is argued that, as the aforementioned reaction involves an electrophilic attack on an arene π-system followed by deprotonation of the resulting cation, this does not qualify as such.[1]

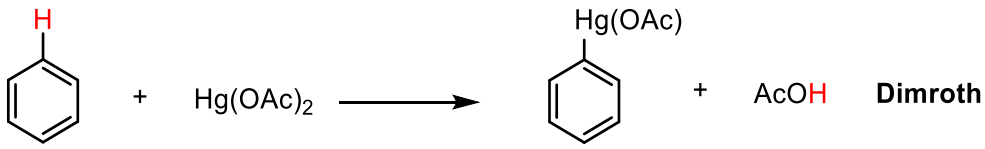

Scheme 1. Dimroth's reaction, considered by some the first C−H bond activation example.

In agreement with the current mechanistic connotations, the first example of a truly C−H bond activation is attributed to Chatt,[11] who disclosed the oxidative addition of naphthalene to a Ru(0) complex (Scheme 2), whereas Shilov[12] made pioneer advances in the catalytic oxidation of alkanes to alcohols and alkyl halides, including the challenging transformation of methane (Scheme 2).

[10] a) Dimroth, O. *Ber. Dtsch. Chem. Ges.* **1898**, *31*, 2154–2156. b) Dimroth, O. *Ber. Dtsch. Chem. Ges.* **1902**, *35*, 2032–2045.
[11] Chatt, J.; Watson, H. R. *J. Chem. Soc.* **1962**, 2545–2549.
[12] a) Gol'dshleger, N.F.; Tyabin, M.B.; Shilov, A.E.; Shteinman, A. A. *Zh. Fiz. Khim.* **1969**, *43*, 2174–2175. b) Gol'dshleger, N. F.; Shteinman, A. A.; Shilov, A. E.; Eskova, V. V. *Zh. Fiz. Khim.* **1972**, *46*, 1353–1354.

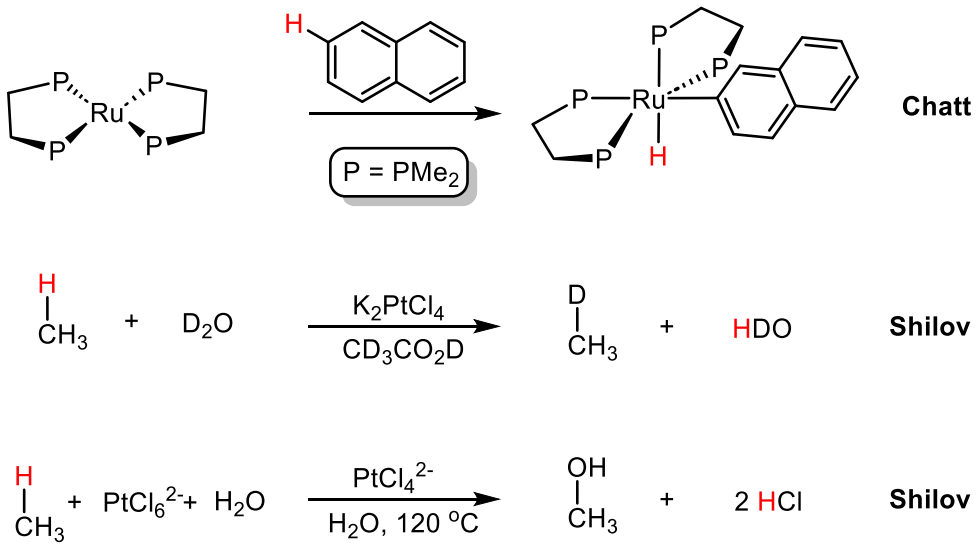

Scheme 2. First examples of C−H bond activation (Chatt) and functionalization (Shilov).

I.1.2 Mechanisms of C−H bond activation

In the past years, much knowledge has been acquired regarding the mechanisms of C−H bond activation reactions.[13] In the following, we will focus on oxidative addition, σ-bond metathesis, electrophilic substitution, and 1-2 addition mechanisms (Figure 2).

Oxidative addition is the most prevalent mechanism for C–H bond activation. It can be initiated by the coordination of the C–H bond to a vacant metal site, leading to the formation of a σ-complex. Electron-rich, low-valent complexes of late transition metals, with readily accessible higher oxidation states, commonly activate C–H bonds via this pathway.

The **σ-bond metathesis** mechanism involves an alkyl or hydride metal complex (M–R or M–H, respectively) and is the preferred pathway for C–H activation by early transition metals, lanthanides, and actinides with a d^0 electronic configuration. There are different intermediate scenarios[14] within σ-bond metathesis which include metal-assisted σ-bond metathesis (MAσBM), σ-complex assisted metathesis (σ-CAM, also known as oxidatively added transition state, OATS) and oxidative hydrogen migration (OHM), whose key transition states are represented in Figure 2b.

[13] a) Hartwig, J. F. *J. Am. Chem. Soc.* **2016**, *138*, 2–24. b) Altus, K.M.; Love, J.A.; *Commun. Chem*. **2021**, *4*, 173.
[14] a) Roudesly, F.; Oble, J.; Poli, G. *J. Mol. Catal. A: Chem* **2017**, *426*, 275–296. b)Vastine, B. A.; Hall, M. B. *J. Am. Chem. Soc.* **2007**, *129*, 12068–12069.

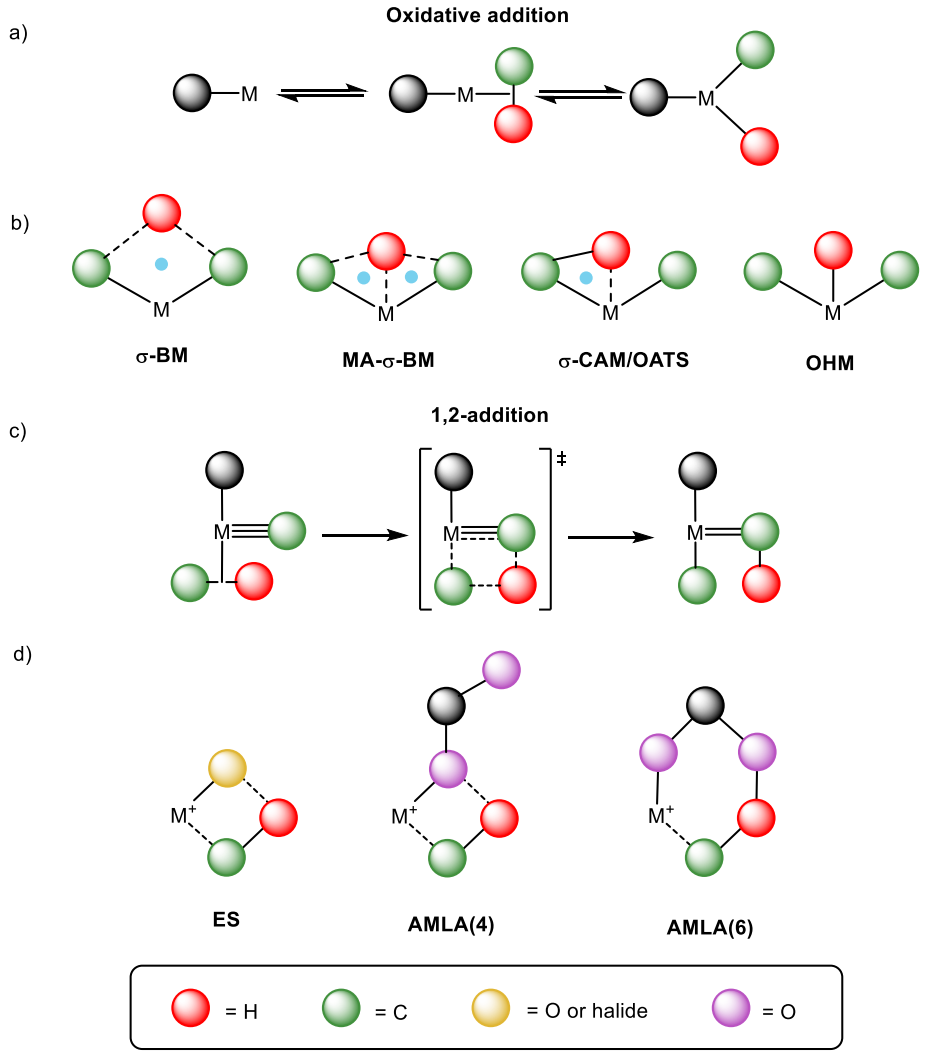

Figure 2. a) Simplified depiction of the oxidative addition mechanism; b) Transition states encountered during the different σ-bond metathesis mechanisms; blue dots represent the ring critical points of the interaction; c) Simplified depiction of the 1,2-addition mechanism; d) The three most common transition states found during electrophilic C−H activation. Figure adapted from ref. 13b.

For a C–H activation to be classified as an **electrophilic mechanism**, it must involve the abstraction of a proton by a lone pair on a neighboring

heteroatom during the transition state (Scheme 2c). This defining characteristic sets the electrophilic substitution (ES) mechanism apart from σ-bond metathesis, which also involves a four-centered transition state but lacks lone pair involvement. In electrophilic mechanisms, the metal's oxidation state typically remains unchanged throughout the process. These reactions often feature the formation of a ring structure comprising the metal, the C–H fragment, and the heteroatom. Similar to the ES transition state is the amphiphilic metal-ligand activation transition state, an alternative also categorized as electrophilic mechanism. This consists of a four-membered, cyclic, chelate-assisted transition state (AMLA(4)), in which one of the acetate oxygen atoms engages in the C–H bond substitution event while simultaneously forming M–C and O–H bonds. Alternatively, a six-membered (AMLA(6)) transition state can occur, in which the hydrogen is transferred to the pendant acetate oxygen.[15]

Finally, **1,2-addition** is typically associated with early transition metals. In this mechanism, the C–H bond of an alkane adds across an M=X double bond (or an M≡X triple bond), resulting in the formation of M–C and X–H bonds, as illustrated in Figure 2c. Notably, the metal's oxidation state remains unchanged throughout the process.[16]

In general, homogeneous C−H functionalization has been dominated by complexes of late transition metals belonging to the second (Ru, Rh, Pd) and third (Ir, Pt) rows. In the context of this PhD thesis, it is relevant to

[15] Ess, D. H.; Bischof, S. M.; Oxgaard, J.; Periana, R. A.; Goddard, W. A. *Organometallics*, **2008**, *27*, 6440–6445.
[16] Cheng, Y.-H.; Ho, Y.-S.; Yang, C.-J.; Chen, C.-Y.; Hsieh, C.-T.; Cheng, M.-J. *J. Phys. Chem. A* **2024**, *128*, 4638–4650.

highlight that decisive mechanistic advances have been made with the investigation of C−H bond activation at electrophilic (η^5-C_5Me_5)Ir(III) centers,[17] which is the core fragment of this work. Nevertheless, before entering into discussing the specific chemistry of iridium in the following section, it is also important to acknowledge that relevant advances have been achieved more recently employing first row transition metal complexes, including Fe,[18] Co,[19] Ni[20] and Cu.[21]

[17] a) Klei, S. R.; Tilley, T. D.; Bergman, R. G. *J. Am. Chem. Soc.* **2000**, *122*, 1816–1817. b) Balcells, D.; Clot, E.; Eisenstein, O.; *Chem. Rev.* **2010**, *110*, 749–823. c) Carlsen, R.; Wohlgemuth, N.; Carlson, L.; Ess, D. H. *J. Am. Chem. Soc.* **2018**, *140*, 11039–11045. d) Taw, F.L.; Mellows, H.; White, P. S.; Hollander, F. J.; Bergman, R. G.;Brookhart, M.; Heinekey, D. M. *J. Am. Chem. Soc.* **2002**, *124*, 5100–5108.

[18] Shang, R.; Ilies, L.; Nakamura, E. *Chem. Rev.* **2017**, *117*, 9086–9139.

[19] a) Moselage, M.; Li, J.; Ackermann, L. *ACS Catal.* **2016**, *6*, 498–525. b) Yoshino, T.; Matsunaga, S. *Adv. Organomet. Chem.* **2017**, *68*, 197–247.

[20] a) Zhou, W.; Zheng, S.; Schultz, J. W.; Rath, N. P.; Mirica, L. M. *J. Am. Chem. Soc.* **2016**, *138,* 5777–5780. b) Chong, E.; Kampf, J. W.; Ariafard, A.; Canty, A. J.; Sanford, M. S. *J. Am. Chem. Soc.* **2017**, *139*, 6058–6061.

[21] a) Gava, R.; Olmos, A.; Noverges, B.; Varea, T.; Álvarez, E.; Belderrain, T. R.; Caballero, A.; Asensio, G.; Pérez, P. J. *ACS Catal.* **2015**, *5,* 3726–3730. b) Guo, X.-X.; Gu, D.-W.; Wu, Z.; Zhang, W. *Chem. Rev.* **2015**, *115*, 1622–1651.

I.1.3 Iridium complexes in C−H bond activation

Iridium complexes have provided relevant breakthroughs in the C−H activation field during the past 50 years. For example, Crabtree[22] and Felkin[23] described alkane dehydrogenation mediated by Ir complexes. Their groundbreaking work introduced an unsaturation susceptible of further functionalization into an otherwise inert alkane (Scheme 3). This field was further advanced by Jensen and Goldman through the use of pincer ligands,[24] and the subsequent seminal discovery of highly efficient alkane metathesis processes (Scheme 3),[25] which permitted the production of long chain alkanes of importance for diesel production from short alkanes. In fact, the same concept using pincer iridium catalysts was more recently applied for plastic depolymerization.[26]

[22] Crabtree, R. H., Mihelcic, J. M.; Quirk, J. M. *J. Am. Chem. Soc.* **1979**, *101*, 7738–7740.
[23] Felkin, H.; Fillebeen-Khan, T.; Gault, Y.; Holmes-Smith, R.; Zakrzewski, J. *Tetrahedron Lett.* **1984**, *25*, 1279–1282.
[24] Liu, F.; Pak, E. B.; Singh, B.; Jensen, C. M.; Goldman, A. S. *J. Am. Chem. Soc.* **1999**, *121*, 4086–4087.
[25] Goldman, A. S.; Roy, A. H.; Huang, Z.; Ahuja, R.; Schinski, W.; Brookhart, M. *Science* **2006**, *312*, 257–261.
[26] Conk, R. J.; Hanna, S.; Shi, J. X.; Yang, J.; Ciccia, N. R.; Qi, L.; Bloomer, B. J.; Heuvel, S.; Wills, T.; Su, J.; Bell, A. T.; Hartwig, J. F. *Science* **2022**, *377*, 1561–1566.

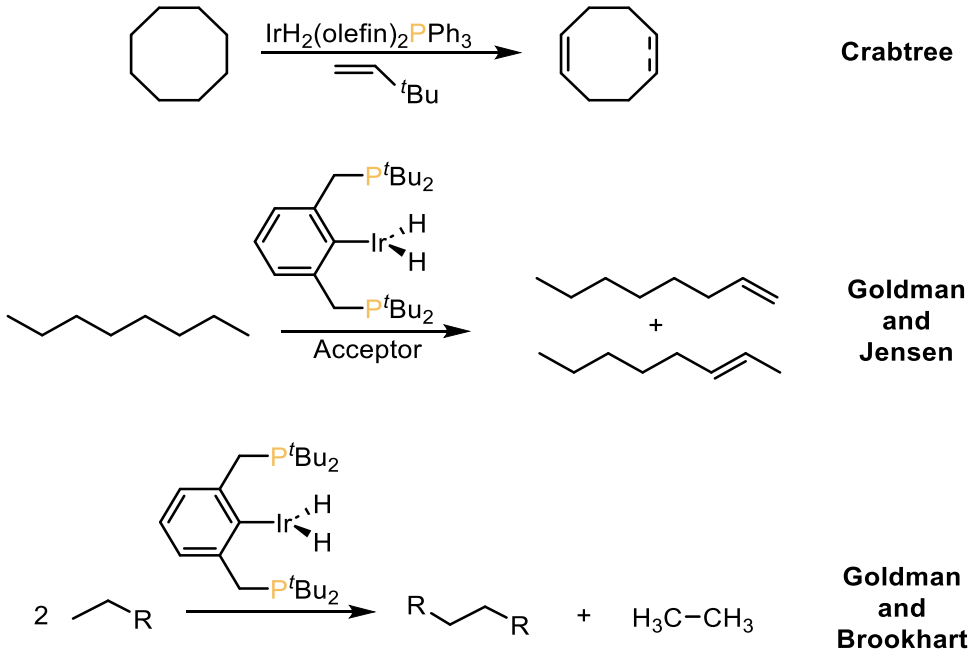

Scheme 3. Early reports on alkane dehydrogenation mediated by Ir complexes pioneered by Crabtree, Goldman, Jensen and Brookhart.

In an alternative approach, also based on iridium and inspired by Green's groundbreaking contributions,[27] Bergman[28] and Graham[29] independently reported in 1982 the first examples of oxidative addition reactions of saturated hydrocarbons, which were accomplished via photochemically generated iridium(I) cyclopentadienyl complexes (Scheme 4). In 1995, in another groundbreaking contribution, Bergman reported a cationic [(η^5-

[27] Green, M. L. H.; Knowles, P. J. *J. Chem. Soc. D* **1970**, 1677–1677.
[28] Janowicz, A.H.; Bergman, R. G. *J. Am. Chem. Soc.* **1982**, *104*, 352–354.
[29] Hoyano, J. K.; Graham, W.A.G. *J. Am. Chem. Soc.* **1982**, *104*, 3723–3725.

C_5Me_5)Ir(III)] complex that enabled the facile activation of hydrocarbons, including methane under mild conditions (–10 ºC)[30] (Scheme 4).

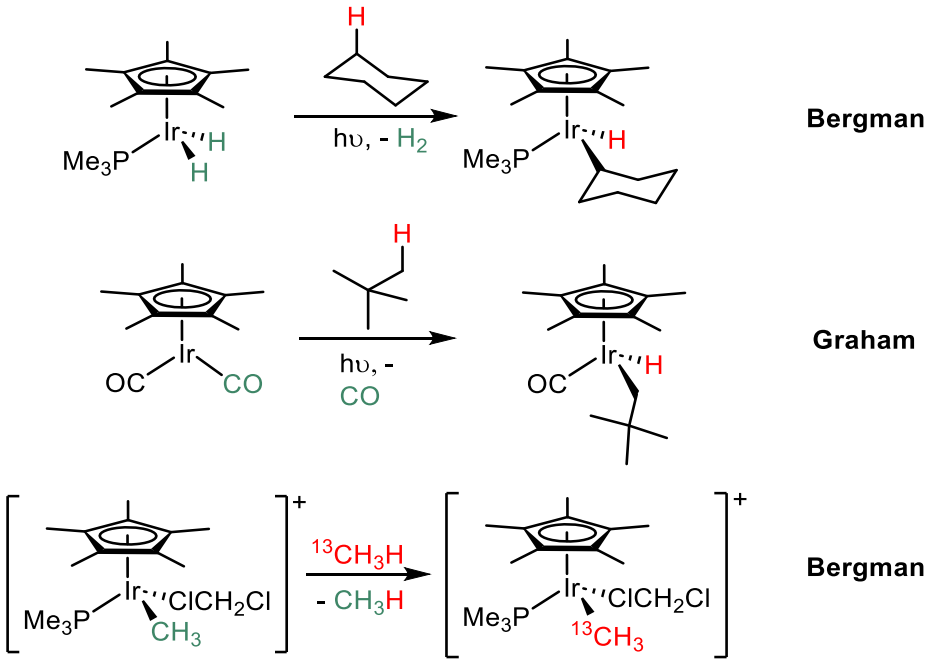

Scheme 4. Examples of C−H activation of hydrocarbons employing Ir(C_5Me_5) complexes.

This latter breakthrough paved the way for numerous subsequent examples of C–H bond activation and functionalization based on iridium,[31] including many systems that still capitalize on the (C_5Me_5)Ir fragment. In this regard, some recent examples of C−H functionalization include Miura's C−H arylation to afford fluorenes[32] (Scheme 5), Crabtree's C−H hydroxylation

[30] Arndtsen, B. A.; Bergman, R. G. *Science* **1995**, *270*, 1970–1973.
[31] For a review on this topic see: Shilov, A. E.; Shul'pin, G. B. *Activation and Catalytic Reactions of Saturated Hydrocarbons in the Presence of Metal Complexes*, 2000, Kluwer Academic, Dordrecht.
[32] Itoh, M.; Hirano, K.; Satoh, T.; Shibata, Y.; Tanaka, K.; Miura, M. *J. Org. Chem.* **2013,** *78,* 1365–1370.

of alkanes with water under oxidative conditions[33] (Scheme 5), or Martín-Matute's C−H amination[34] (Scheme 5).

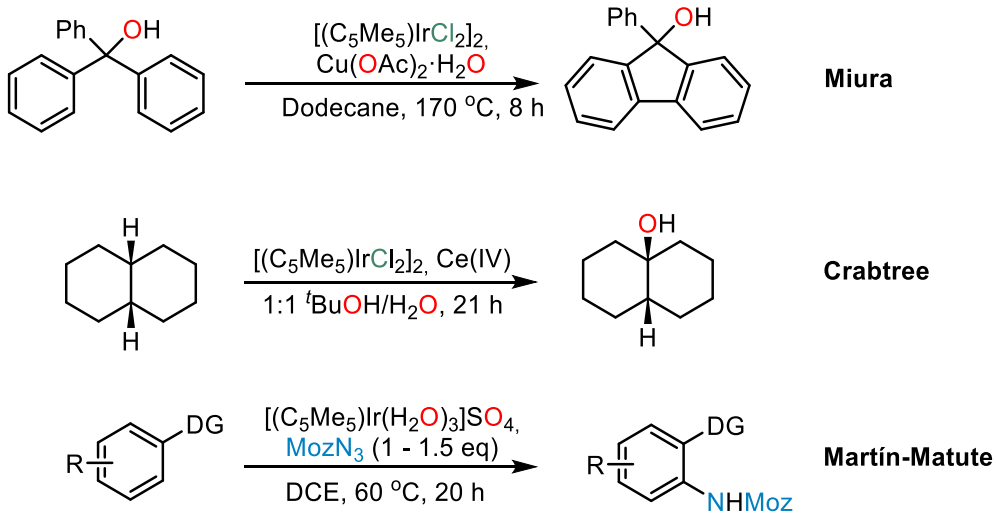

Scheme 5. Iridium(III)-catalyzed C−H arylation (top), alkane hydroxylation (middle) and selective amination (bottom). Moz = p-methoxybenzyloxycarbonyl. DG =Directing Group.

[33] a) Zhou, M.; Schley, N. D.; Crabtree, R. H. *J. Am. Chem. Soc.* **2010**, *132*, 12550–12551. b) Zhou, M.; Balcells, D.; Parent, A. R.; Crabtree, R. H.; Eisenstein, O. *ACS Catal.* **2012**, *2*, 208–218.

[34] Weis, E.; Johansson, M.; Korsgren, P.; Martín-Matute, B.; Johansson, M. J. *JACS Au* **2022,** *2*, 906–916.

I.1.4 Non-innocence of cyclopentadienyl ligands

As described in the previous section, the cyclopentadienyl ligand has played an important role in the development of iridium-based C–H bond activation processes, thereby a more detailed discussion about its nature and properties is due. Since the serendipitous discovery of ferrocene in 1951,[35] cyclopentadienyl ligands, $[C_5R_5]^-$, have become indisputably one of the most important ligands in organometallic chemistry and homogeneous catalysis.[36] In fact, their coordination complexes extend to virtually every metal in the periodic table.[37] Their versatility is evidenced, as well, by their variable hapticity (from η^1 to η^5)[38] and synthetic flexibility. Beyond the foremost and simplest $[C_5R_5]^-$ ligands, many versions have been developed, including mono and polyfunctionalized derivatives where R accounts for simple alkyl or aryl groups,[39] or even bulky substituent to access extremely congested cyclopentadienyl ligands,[40] heteroatom-containing fragments for cooperative reactivity with

[35] a) Kealy, T. J.; Pauson, P. L. *Nature* **1951**, *168*, 1039−1040. b) Miller, A.; Tebboth, J. A.; Tremaine, F. *J. Chem. Soc.* **1952**, 632−635.
[36] Crabtree, R. H. *J. Organomet. Chem.* **2005**, *690*, 5451−5457.
[37] a) Poli, R. *Chem. Rev*. **1991**, *91*, 509−551. b) Budzelaar, P. H. M.; Engelberts, J. J.; van Lenthe, J. H. *Organometallics* **2003**, *22*, 1562−1576. c) Evans, W. J. *Organometallics* **2016**, *35*, 3088−3100.
[38] a) O'Connor, J. M.; Casey, C. P. *Chem. Rev.* **1987**, *87*, 307−318. b) Veiros, L. F. *Organometallics* **2000**, *19*, 3127−3136.
[39] Deck, P. A. *Coord. Chem. Rev*. **2006**, *250*, 1032−1055.
[40] a) Ruspic, C.; Moss, J. R.; Schü rmann, M.; Harder, S. *Angew. Chem. Int. Ed*. **2008**, *47*, 2121−2126. b) Meyer, G. *Angew. Chem., Int. Ed.* **2008**, *47*, 4962−4964. c) Harder, S.; Naglav, D.; Schwerdtfeger, P.; Nowik, I.; Herber, R.H. *Inorg. Chem.* **2014**, *53*, 2188−2194. d) van Velzen, N. J. C.; Harder, S. *Organometallics* **2018**, *37*, 2263−2271. e) Giesbrecht, G. R.; Gordon, J. C.; Clark, D. L.; Scott, B. L. *Dalton Trans.* **2003**, *3*, 2658−2665. f) Orzechowski, L.; Piesik, D. F. J.; Ruspic, C.; Harder, S. *Dalton Trans.* **2008**, *35*, 4742−4746. g) Harder, S.; Ruspic, C. *J. Organomet. Chem.* **2009**, *694*, 1180−1184.

the metal,[41] bridging anchors to access ansa-metallocenes,[42] or chiral moieties to mediate asymmetric catalysis.[43] However, the permethylated $[C_5Me_5]^-$ ligand (Cp*), which was extensively used by Bergman in the area of C–H bond activation, as described in the previous section, is likely the one that has enjoyed the widest popularity.

A crucial driving force for the widespread use of cyclopentadienyl ligands is their robust spectator behavior, which is particularly strong in the case of Cp*. However, even for the later ligand, there are increasing examples of its non-innocent character (Figure 3), an aspect of utmost importance for the work described in this PhD Thesis. The methyl groups of Cp* can partake in several transformations, including, but not limited to, deprotonation by an external base or a bifunctional ligand,[44,45,46] hydride

---

[41] a) Blais, M. S.; Rausch, M. D. *J. Organomet. Chem.* **1995**, *502*, 1−8. b) Conway, B. G.; Rausch, M. D. *Organometallics* **1985**, *4*, 688−693.

[42] a) Chen, E. Y.-X.; Kruper, W. J.; Roof, G.; Wilson, D. R. *J. Am. Chem. Soc.* **2001**, *123*, 745−746. b) Mitchell, J. P.; Hajela, S.; Brookhart, S. K.; Hardcastle, K. I.; Henling, L. M.; Bercaw, J. E. *J. Am. Chem. Soc.* **1996**, *118*, 1045−1053. c) Busico, V.; Cipullo, R. *J. Am. Chem. Soc.* **1994**, *116*, 9329−9330. d) Wang, B. *Coord. Chem. Rev*. **2006**, *250*, 242−258.

[43] Mas-Roselló, J.; Herraiz, A. G.; Audic, B.; Laverny, A.; Cramer, N. *Angew. Chem., Int. Ed.* **2021**, *60*, 13198−13224.

[44] a) Bernechea, M.; Berenguer, J. R.; Lalinde, E.; Torroba, J. *Organometallics* **2009**, *28*, 312−320. b) Fan, L.; Wei, C.; Aigbirhio, F. I.; Turner, M. L.; Gusev, O. V.; Morozova, L. N.; Knowles, D. R. T.; Maitlis, P. M. *Organometallics* **1996**, *15*, 98−104. c) Glueck, D. S.; Bergman, R. G. *Organometallics* **1990**, *9*, 2862−2863. d) Caldwell, H.; Pregosin, P. S. *Organometallics* **2008**, *27*, 1591−1595.

[45] Moreno, J. J.; Espada, M. F.; Campos, J.; López-Serrano, J.; MacGregor, S. A.; Carmona, E. *J. Am. Chem. Soc.* **2019**, *141*, 2205−2210.

[46] a) Takemoto, S.; Morita, H.; Karitani, K.; Fujiwara, H.;Matsuzaka, H. *J. Am. Chem. Soc.* **2009**, *131*, 18026−18027. b) Cloke, F. G. N.; Green, J. C.; Green, M. L. H.; Morley, C. P. *Chem. Commun*. **1985**, *14*, 945−946. c) Kupfer, V.; Thewalt, U.; Tišlerová, I.; Ště pnička, P.; Gyepes, R.; Kubiš ta, J.; Horáček, M.; Mach, K. *J. Organomet. Chem.* **2001**, *620*, 39−50. d) Sun, Y.; Spence, R. E. V. H.; Piers, W. E.; Parvez, M.; Yap, G. P.A. *J. Am. Chem. Soc.* **1997**, *119*, 5132−5143. e)

abstraction which tends to proceed through single-electron processes,[47] C−H oxidative addition to an adjacent transition metal in bimetallic structures,[48] or direct and reversible methyl-to-metal hydride migration, which was soon identified in early transition metals[49] and recently unlocked by our group as a viable process for late transition metals.[50] In addition, the protonation of the internal ring has been exploited in proton-couple-electron-transfer (PCET) catalysis capitalizing on the reversible

---

Mori, Y.; Ando, T.; Matsumoto, T.; Yatabe, T.; Kikkawa, M.; Yoon, K.-S.; Ogo, S. *Angew. Chem., Int. Ed.* **2018**, *57*, 15792−15796. f) Rodríguez-Bárzano, A.; Blacker, A. J.; McGowan, P. C. *Dalton Trans*. **2013**, *42*, 16669−16671. g) Holland, P. L.; Andersen, R. A.; Bergman, R. G.; Huang, J.; Nolan, S. P. *J. Am. Chem. Soc.* **1997**, *119*, 12800−12814. i) Rüba, E.; Mereiter, K.; Schmid, R.; Kirchner, K.; Bustelo, E.; Puerta, M. C.; Valerga, P. *Organometallics* **2002**, *21*, 2912−2920.

[47] a) Klet, R. C.; Kaphan, D. M.; Liu, C.; Yang, C.; Kropf, A. J.; Perras, F. A.; Pruski, M.; Hock, A. S.; Delferro, M. *J. Am. Chem. Soc*. **2018**, *140*, 6308−6316. b) Li, S.; Wang, X.; Zhang, Z.; Zhao, Y.; Wang, X. *Dalton Trans*. **2015**, *44*, 19754−19757. c) Meredith, J. M.; Goldberg, K. I.; Kaminsky, W.; Heinekey, D.M. *Organometallics* **2012**, *31*, 8459−8462.

[48] a) Einstein, F. W. B.; Jones, R. H.; Zhang, X.; Yan, X.; Nagelkerke, R.; Sutton, D. *Chem. Commun.* **1989**, *19*, 1424−1426. b) Wang, W.; Davis, H. B.; Einstein, F. W. B.; Pomeroy, R. K. *Organometallics* **1994**, *13*, 5113−5121. c) Evans, W. J.; Perotti, J. M.; Ziller, J. W. *Inorg. Chem.* **2005**, *44*, 5820−5825. d) Takahashi, Y.; Fujita, K.; Yamaguchi, R. *Eur. J. Inorg. Chem.* **2008**, *28*, 4360−4368. e) Carbó, J. J.; García-López, D.; Gómez-Pantoja, M.; González-Pérez, J. I.; Martín, A.; Mena, M.; Santamaría, C. *Organometallics* **2017**, *36*, 3076−3083. f) Dyllick-Brenzinger, R.; Olsen, H. *J. Am. Chem. Soc.* **1981**, *103*, 704−706. g) Chung, C.; Tseng, W.-C.; Chi, Y.; Peng, S.-M.; Lee, G.-H. *Organometallics* **1998**, *17*, 2207−2214. h) Shima, T.; Hou, Z. *Organometallics* **2009**, *28*, 2244−2252.

[49] a) McDade, C.; Green, J. C.; Bercaw, J. E. A. *Organometallics* **1982**, *1*, 1629−1634. b) Bulls, A. R.; Schaefer, W. P.; Serfas, M.; Bercaw, J. E. *Organometallics* **1987**, *6*, 1219−1226. c) Bercaw, J. E. *J. Am. Chem. Soc.* **1974**, *96*, 5087−5095. d) Cloke, F. G. N.; Day, J. P.; Green, J. C.; Morley, C. P.; Swain, A. C. *Dalton Trans*. **1991**, 789−796.

[50] Alférez, M. G.; Moreno, J. J.; Hidalgo, N.; Campos, J. *Angew. Chem., Int. Ed.* **2020**, *59*, 20863−20867.

migration of the proton between the ring and the metal.[51] Moreover, several radical routes have been identified for Cp*-containing species resulting in ligand functionalization.[52]

[51] a) Chalkley, M. J.; del Castillo, T. J.; Matson, B. D.; Roddy, J. P.; Peters, J. C. *ACS Cent. Sci.* **2017**, *3*, 217−223. b) Chalkley, M. J.; del Castillo, T. J.; Matson, B. D.; Peters, J. C. *J. Am. Chem. Soc*. **2018**, *140*, 6122−6129. c) Chalkley, M. J.; Oyala, P. H.; Peters, J. C. *J. Am. Chem. Soc*. **2019**, *141*, 4721−4729. d) Quintana, L. M. A.; Johnson, S. I.; Corona, S. L.; Villatoro, W.; Goddard, W. A.; Takase, M. K.; VanderVelde, D. G.; Winkler, J. R; Gray, H. B.; Blakemore, J. D. *Proc. Natl. Acad. Sci. U. S. A*. **2016**, *113*, 6409−6414. e) Pitman, C. L.; Finster, O. N. L.; Miller, A. J. M. *Chem. Commun.* **2016**, *52*, 9105−9108. f) Pal, S.; Kusumoto, S.; Nozaki, K. *Organometallics* **2018**, *37*, 906−914. g) Kefalidis, C. E.; Perrin, L.; Burns, C. J.; Berg, D. J.; Maron, L.; Andersen, R. A. *Dalton Trans.* **2015**, *44*, 2575−2587.

[52] a) Gusev, O.; Denisovich, L. I.; Peterleitner, M. G.; Rubezhov, A. Z.; Ustynyuk, N. A.; Maitlis, P. M. *J. Organomet. Chem.* **1993**, *452*, 219−222. b) Gusev, O. V.; Peterleitner, M. G.; Ievlev, M. A.; Kal'sin, A. M.; Petrovskii, P. V.; Denisovich, L. I.; Ustynyuk, N. A. *J. Organomet. Chem.* **1997**, *531*, 95−100. c) Blaha, J. P.; Wrighton, M. S. *J. Am. Chem. Soc.* **1985**, *107*, 2694−2702.

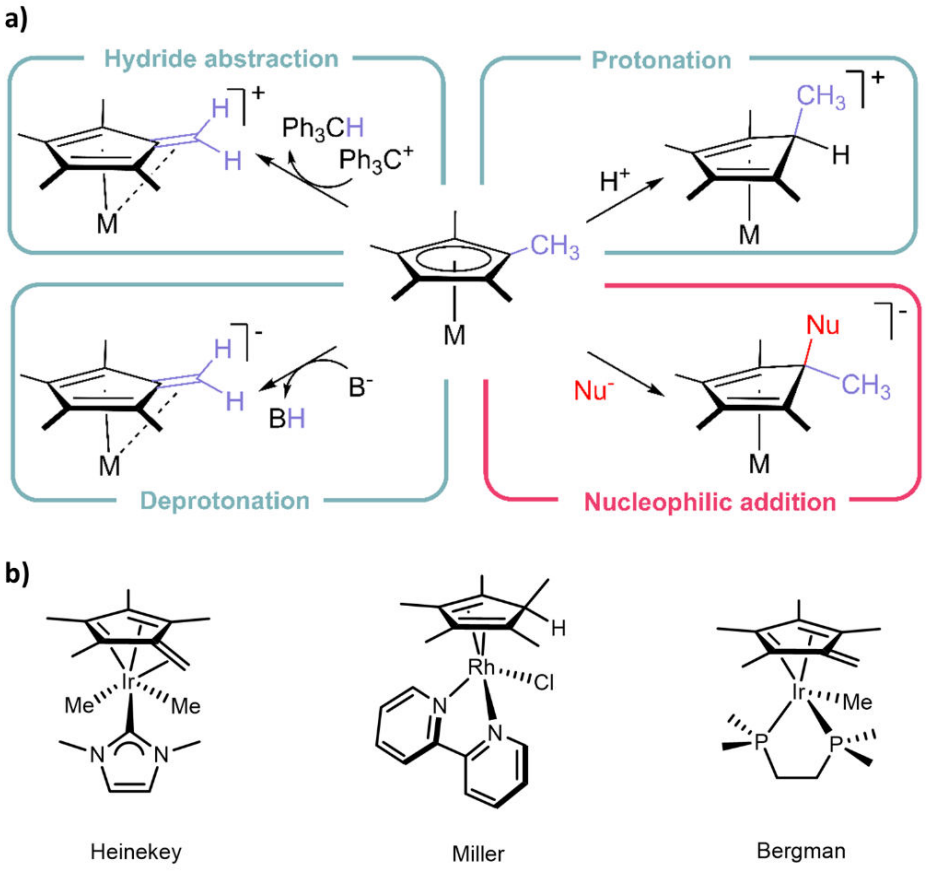

Figure 3. a) Most common intermolecular pathways for the activation of the Cp ligand in transition metal complexes; b) Some examples of C_5Me_5 participation in the reactivity of iridium and rhodium complexes.*

I.1.5 (η^5-C_5Me_5)Ir complexes with bulky terphenyl phosphine ligands

As stated previously, one of the most promising strategies for C−H bond activation involves the use of transition metal complexes.[13] Since the pioneering work by Bergman and his collaborators on Ir(III) complexes such as $[(\eta^5\text{-}C_5Me_5)Ir(Me)(PMe_3)(ClCH_2Cl)]^+$ and other similar species,[30] significant advances have been made in understanding how transition metal complexes can promote C−H activation. But those original designs have garnered continuous attention along the years, focusing primarily on neutral or cationic Rh and Ir complexes that incorporate Cp*M (M = Rh, Ir) fragments.[17] One interesting observation from these studies is that the reactivity of related complexes can vary significantly depending on the co-ligands surrounding the metal center. For example, the iridium complex $[(\eta^5\text{-}C_5Me_5)Ir(Me)(P(OMe)_3)(ClCH_2Cl)]^+$, where PMe_3 is replaced by $P(OMe)_3$, shows reduced reactivity toward C−H bond activation, likely due to the lower electron density at the metal center.[53] This clearly manifest the relevant role that the phosphine ligand plays tuning the properties of such organometallic complexes.

Similarly, our group has recently investigated cationic iridium(III) complexes of the general formula $[(\eta^5\text{-}C_5Me_5)IrCl(PMe_2Ar')]^+$, where PMe_2Ar' represents bulky terphenyl phosphine ligands (Scheme 6).[45,54] This previous research has focused on two key systems, PMe_2Ar^{Xyl2} and PMe_2Ar^{Dipp2} (Ar^{Dipp2} = C_6H_3-2,6-(C_6H_3−2,6-$^i Pr_2$)$_2$, Ar^{Xyl2} = C_6H_3-2,6-(C_6H_3−2,6-Me_2)$_2$), which exhibit distinct steric hindrance close to the

[53] Tellers, D. M.; Yung, C. M.; Arndtsen, B.; Adamson, D. R.; Bergman, R. G. *J. Am. Chem. Soc.* **2002**, *124*, 1400–1410.
[54] Moreno, J. J.; Espada, M. F.; Maya, C.; Campos, J.; López-Serrano, J.; MacGregor, S. A.; Carmona, E. *Polyhedron* **2021**, *207*, 115363.

metal center due to the different bulkiness of *iso*-propyl and methyl groups, respectively. These complexes were able to promote an intriguing remote electrophilic C–H bond activation, mediated by the iridium center and facilitated by the steric bulk of the terphenyl ligands. Notably, this transformation, which is represented in Scheme 6, involves an unprecedented and reversible C–C bond formation that results in an unexpected coupling of the phosphine and the Cp* ligand. The intermediate features a unique 10-membered phospha-iridacycle structure, resulting from C_5Me_5 deprotonation and subsequent nucleophilic attack on a dearomatized phosphine ring (Scheme 6).[45,54]

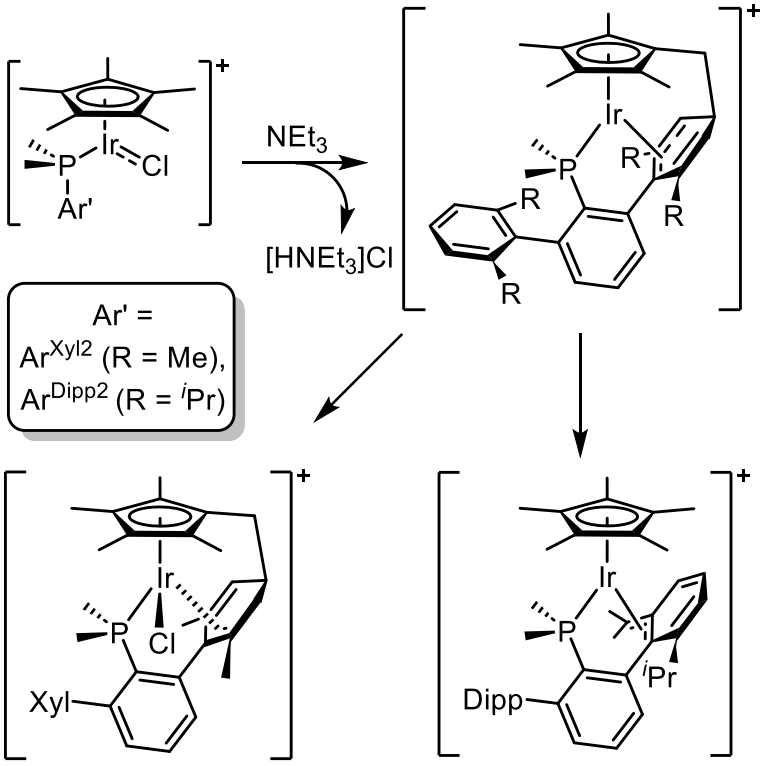

Scheme 6. Formation of a 10-membered phospha-iradacycle intermediate from the reaction of a cationic (η^5-C_5Me_5)Ir(III)-phosphine complex and NEt_3, and subsequent reactivity: for the xylyl system, the formal addition of HCl leads to a cationic chloride species; for the di-iso-propyl system a pseudoallylic species is formed. (Ar^{Dipp2} = C_6H_3-2,6-(C_6H_3-2,6-$^iPr_2$)$_2$, Ar^{Xyl2} = C_6H_3-2,6-(C_6H_3-2,6-Me_2)$_2$).

In the case of the Dipp system, the reaction proceeds to give a pseudoallylic complex, while only traces of the analogous species was found for the xylyl system.[54] Computational investigations revealed that a higher energy barrier for the C–H deprotonation step for the xylyl system seem to be responsible for the dissimilar reactivity exhibited by the two apparently similar phosphines. Thus, the alternative pathway consisting of the formal addition of HCl to the intermediate competes and leads to a

different reaction outcome, precluding the formation of the pseudoallylic structure in the presence of NEt_3.[54]

These early results from our group open up two clear avenues for further investigation, which constitute the grounds over which the present Chapter is built upon. The first involves the exploration of the non-innocent nature of the Cp* ligand in even greater depth, for instance by incorporating alternative nucleophiles into the system to probe the full scope of its reactivity. The second objective focuses on avoiding the intramolecular activation of the phosphine ligand, as this hampers potential routes toward effective intermolecular C–H bond activation. In fact, earlier studies in our group based on phosphine $PMeXyl_2$,[55] further confirmed the propensity of these electrophilic Ir(III) systems to intramolecularly activate C–H bonds when available, illustrating the challenges of achieving the desired intermolecular reactivity. To address this, we propose modifying the ligand environment of the terphenyl phosphine, particularly by replacing the *iso*-propyl groups in 2- and 6- positions of the lateral aryl rings of the terphenyl phosphine, by bulkier ^{t}Bu substituents located at 3- and 5-positions. These groups lack benzylic C–H groups that are more susceptible to activation while their further positioning may facilitate the approach of the iridium center to the lateral ring, potentially enhancing the stability. Moreover, as pinpointed by Scheme 6, subtle changes in the ligand environment for this type of complexes can impart a strong effect on reactivity.

[55] a) Campos, J.; López-Serrano, J.; Álvarez, E.; Carmona, E. *J. Am. Chem. Soc.* **2012**, *134*, 7165–7175. b) Campos, J.; Esqueda, A. C.; Carmona, E. *Chem. Eur. J.* **2010**, *16*, 419–422.

Chapter I. Pentamethylcyclopentadienyl Iridium Complexes Bearing Bulky Phosphine Ligands as Platforms to Investigate Ligand Non-Innocence and C–H Activation Processes

The upcoming **Results and Discussion** *section of this chapter is organized into two subsections. The first subsection,* **I.2.1 Divergent reactivity of a cationic pentamethylcyclopentadienyl iridium complex toward carbon nucleophiles**, *focuses on the reactivity of a cationic (η^5-C_5Me_5)Ir(III) complex with carbon nucleophiles. Depending on the nature of the carbon nucleophile, distinctive reactivity patterns arise, some involving the non-innocent behavior of the η^5-C_5Me_5 ligand. The second subsection,* **I.2.2 C−H activation by an unsaturated Ir(III)-Me complex**, *details our investigation into the potential of a different cationic (η^5-C_5Me_5)Ir(III) complex for C–H bond activation.*

I.2 RESULTS AND DISCUSSION

I.2.1 Divergent reactivity of a cationic pentamethylcyclopentadienyl iridium complex toward carbon nucleophiles

I.2.1.1 Introductory remarks

Cyclopentadienyl ligands, in particular Cp*, continue to be extensively employed in fundamental organometallic chemistry and homogeneous catalysis. Yet, as stated in the introduction, the methyl groups of the Cp* ligand can partake in a variety of transformations. In contrast, the reactivity of the internal carbon centers of the Cp* ligand toward nucleophiles has only been observed in a limited number of cases,[56] being more frequent on the less electron-rich and sterically hindered $[C_5H_5]^-$ upon addition of common highly polar reagents, typically organolithium and organomagnesium compounds.[57] These transformations are of high

[56] a) Yao, Z.-J.; Lin, Y.-J.; Xu, B.; Jin, G.-X. *Dalton Trans*. **2014**, *43*, 4938−4940. b) Moseley, K.; Kang, J. W.; Maitlis, P.M. *J. Chem. Soc. A: Inorg. Phys. Theor.* **1970**, 2875−2883. c) Razuvaev, G. A.; Maryin, V. P.; Vyshinskaya, L. I.; Ya, G.; Mal'kova, Y.; Andrianov, A.; Druzhkov, O.N. *Dokl. Akad. Nauk SSSR* **1987**, *294*, 614−617. d) Kochi, T.; Nomura, Y.; Tang, Z.; Ishii, Y.; Mizobe, Y.; Hidai, M. *Dalton Trans.* **1999**, *15*, 2575−2582.

[57] a) de Azevedo, C. G.; Calhorda, M. J.; de Carrondo, M. A. A. F.; Dias, A. R.; Duarte, M. T.; Galvão, A. M.; Gamelas, C. A.; Gonçalves, I. S.; da Piedade, F. M.; Romão, C. C. *J. Organomet. Chem.* **1997**, *544*, 257−276. b) Comte, V.; Blacque, O.; Kubicki, M. M.; Moïse, C. *Organometallics* **1997**, *16*, 5763−5769. c) Hughes, R. P.; Maddock, S. M.; Guzei, I. A.; Liable-Sands, L.M.; Rheingold, A. L. *J. Am. Chem. Soc.* **2001**, *123*, 3279−3288. d) Hughes, R. P.; Maddock, S. M.; Rheingold, A. L.; Liable-Sands, L. M. *J. Am. Chem. Soc.* **1997**, *119*, 5988−5989. e) Liu, R.; Zhou, X. *Chem. Commun*. **2013**, *49*, 3171−3187. f) Comte, V.; Blacque, O.; Kubicki, M. M.; Moïse, C. *Organometallics* **2001**, *20*, 5432−5439. g) Forschner, T. C.; Cooper, N. J. *J. Am. Chem. Soc*. **1989**, *111*, 7420−7424. h) Basato, M.; Biffis, A.; Buscemi, G.; Callegaro, E.; Polo, M.; Tubaro, C.; Venzo, A.; Vianini, C.; Graiff, C.; Tiripicchio, A.; Benetollo, F. *Organometallics* **2007**, *26*, 4265−4270. i) Basato, M.; Biffis, A.; Tubaro, C.; Graiff, C.; Tiripicchio. *Dalton Trans.* **2004**, *24*, 4092−4093. j) Fischer, E. O.;

relevance for a variety of catalytic processes involving cyclopentadienyl-bearing catalysts.[58] For instance, cyclopentadienyl iron and nickel complexes are very active Kumada cross-coupling catalysis, which involves organomagnesium reagents.[59] Additionally, cyclopentadienyl nickel complexes are active catalysts for polymerization reaction in the presence of Grignard reagents.[60] Organolithium and organomagnesium species are also used as initiators for olefin polymerization or diene isomerization with related catalysts.[61] Besides, the use of organolithium and organomagnesium reagents in the presence of Cp*M complexes of both early[62] and late-transition metals[63] have been reported in many

---

Herberich, G. E. *Chem. Ber*. **1961**, *94*, 1517−1523. k) Fischer, E. O.; Angelici, R. J. *J. Am. Chem. Soc.* **1963**, *85*, 3733−3735.

[58] a) Millward, D. B.; Waymouth, R. M. *Organometallics* **1997**, *16*, 1153−1158. b) Suzuki, N.; Kondakov, D. Y.; Takahashi, T. *J. Am. Chem. Soc.* **1993**, *115*, 8485−8486. c) Dzhemilev, U. M.; D'yakonov, V. A.; Khafizova, L. O.; Ibragimov, A. G. *Tetrahedron* **2004**, *60*, 1287−1291. c) Morken, J. P.; Didiuk, M. T.; Hoveyda, A. H. *J. Am. Chem. Soc.* **1993**, *115*, 6997−6998. d) Negishi, E.-I.; Takahashi, T. *Acc. Chem. Res.* **1994**, *27*, 124−130. e) Takahashi, T.; Seki, T.; Nitto, Y.; Saburi, M.; Rousset, C. J.; Negishi, E. *J. Am. Chem. Soc.* **1991**, *113*, 6266−6268. f) Farády, L.; Bencze, L.; Markó, L. *J. Organomet. Chem.* **1967**, *10*, 505−510. g) Farády, L.; Markó, L. *J. Organomet. Chem.* **1971**, *28*, 159−165. h) Negishi, E.; Rousset, C. J.; Choueiry, D.; Maye, J. P.; Suzuki, N.; Takahashi, T. *Inorg. Chim. Acta* **1998**, *280*, 8−20.

[59] a) Uemura, M.; Yorimitsu, H.; Oshima, K. *Chem. Commun*. **2006**, *45*, 4726−4728. b) Fürstner, A.; Martin, R.; Krause, H.; Seidel, G.; Goddard, R.; Lehmann, C. W. *J. Am. Chem. Soc.* **2008**, *130*, 8773−8787. c) Monnereau, L.; Sémeril, D.; Matt, D.; Toupet, L.; Mota, A. J. *Adv. Synth. Catal.* **2009**, *351*, 1383−1389. d) Goetz, A. E.; Garg, N. K. *Nat. Chem.* **2013**, *5*, 54−60. e) Macklin, T. K.; Snieckus, V. *Org. Lett*. **2005**, *7*, 2519−2522. f) Teo, W. J.; Wang, Z.; Xue, F.; Andy Hor, T. S.; Zhao, J. *Dalton Trans.* **2016**, *45*, 7312−7319.

[60] Tamba, S.; Fuji, K.; Meguro, H.; Okamoto, S.; Tendo, T.; Komobuchi, R.; Sugie, A.; Nishino, T.; Mori, A. *Chem. Lett.* **2013**, *42*, 281−283.

[61] a) Yanlong, Q.; Lu; Jiaqui; Weihua, X. *J. Mol. Catal.* **1986**, *34*, 31−38. b) Tao, X.; Qian, F.; Yong, L.; Qian, Y. *J. Mol. Catal. A: Chem*. **2000**, *156*, 121−126.

[62] a) Dysard, J. M.; Tilley, T. D. *J. Am. Chem. Soc.* **2000**, *122*, 3097−3105. b) Mohapatra, S. K.; Büschel, S.; Daniliuc, C.; Jones, P. G.; Tamm, M. *J. Am. Chem. Soc*. **2009**, *131*, 17014−17023. c) Chiu, M.; Hoyt, H. M.; Michael, F. E.;

occasions, but the direct reactivity of the Cp* ligand has been overlooked in all cases. On these bases, understanding these unforeseen reactions is crucial to avoid catalyst deactivation[64] or undesired catalytic outcomes,[65] and to further extend the utility of this platform beyond current capabilities, while gaining insight into the formation of active species from Cp*-bearing precatalysts in the presence of bases.

On these grounds, we selected the terphenyl phosphine iridium compound **1** [(η^5-C_5Me_5)Ir(Cl)-(PMe_2Ar^{Dipp2})][BAr^F] (Ar^{Dipp2} = C_6H_3-2,6-(C_6H_3-2,6-$^iPr_2$)$_2$, [BAr^F] = B(3,5-$C_6H_3(CF_3)_2$)$_4$)[45], recently reported by our group and discussed in detail in section I.1.4, to carry out a systematic study of its

---

Bergman, R. G.; vanHalbeek, H. *Angew. Chem., Int. Ed.* **2008**, *47*, 6073−6076. d) Martín, A.; Mena, M.; Morales-Varela, M. D. C.; Santamaría, C. *Eur. J. Inorg. Chem.* **2004**, *9*, 1914−1921. e) Hernán-Gómez, A.; Martín, A.; Mena, M.; Santamaría, C. *Dalton Trans.* **2013**, *42*, 5076−5084. f) Visser, C.; Meetsma, A.; Hessen, B. *Organometallics* **2002**, *21*, 1912−1918. g) Kirchbauer, F. G.; Pellny, P.-M.; Sun, H.; Burlakov, V. V.; Arndt, P.; Baumann, W.; Spannenberg, A.; Rosenthal, U. *Organometallics* **2001**, *20*, 5289−5296. h) García-Castro, M.; Martín, A.; Mena, M.; Yélamos, C. *Organometallics* **2004**, *23*, 1496−1500. i) Schock, L. E.; Marks, T. J. *J. Am. Chem. Soc.* **1988**, *110*, 7701−7715.

[63] a) Golden, J. T.; Peterson, T. H.; Holland, P. L.; Bergman, R. G.; Andersen, R. A. *J. Am. Chem. Soc.* **1998**, *120*, 223−224. b) Bretschneider-Hurley, A.; Winter, C. H. *J. Am. Chem. Soc*. **1994**, *116*, 6468−6469. c) Ohashi, M.; Matsubara, K.; Iizuka, T.; Suzuki, H. *Angew. Chem., Int. Ed.* **2003**, *42*, 937−940. d) Seneviratne, K. N.; Bretschneider-Hurley, A.; Winter, C. H. *J. Am. Chem. Soc.* **1996**, *118*, 5506−5507. e) Chao, S.; Robbins, J. L.; Wrighton, M. S. *J. Am. Chem. Soc.* **1983**, *105*, 181−188. f) Sun, X.; Singh, A. K.; Yadav, R.; Jin, D.; Haimerl, M.; Scheer, M.; Roesky, P. W. *Chem. Commun.* **2022**, *58*, 673−676. g) Weng, W.; Bartik, T.; Brady, M.; Bartik, B.; Ramsden, J. A.; Arif, A. M.; Gladysz, J. A. *J. Am. Chem. Soc*. **1995**, *117*, 11922−11931. h) Herring, F. G.; Legzdins, P.; Richter-Addo, G. B. *Organometallics* **1989**, *8*, 1485−1493. i) Glassman, T. E.; Liu, A. H.; Schrock, R. R. *Inorg. Chem.* **1991**, *30*, 4723−4732.

[64] Crabtree, R. H. *Chem. Rev.* **2015**, *115*, 127−150.

[65] a) Maimone, T. J.; Milner, P. J.; Kinzel, T.; Zhang, Y.; Takase, M.K.; Buchwald, S. L. *J. Am. Chem. Soc.* **2011**, *133*, 18106−18109. b) Milner, P. J.; Maimone, T. J.; Su, M.; Chen, J.; Müller, P.; Buchwald, S. L. *J. Am. Chem. Soc.* **2012**, *134*, 19922−19934. c) Sather, A. C.; Lee, H. G.; de La Rosa, V. Y.; Yang, Y.; Müller, P.; Buchwald, S. L. *J. Am. Chem. Soc.* **2015**, *137*, 13433−13438.

reactivity toward highly polarized organolithium and organomagnesium reagents. This platform is particularly attractive for these endeavors because (i) it presents a vacant coordination site at the electrophilic Ir(III) center and a chloride ligand susceptible of participating in salt metathesis, yet both the ring and methyl groups of the Cp* can react preferentially toward nucleophiles and/or bases; (ii) the proven noninnocence of the Cp* ligand in this complex, encompassing deprotonation, reversible C−C bond formation and C−H bond breaking, as discussed in section **I.1.5**;[45] (iii) its great stability toward cyclometallation;[45] (iv) the possibility of accessing a bulkier analogue of the iconic Bergman's complex [(η^5-C_5Me_5)Ir(Me)(PMe_3)($ClCH_2Cl$)]$^+$ described in the introduction;[30] and (v) the prominent position of Cp*Ir complexes in the field of C−H bond activation and functionalization (see for instance Scheme 5)[2c, 17]

I.2.1.2 Synthesis and characterization of complexes 2·Me, 2·Et, and 2·^{n}Bu

To start this systematic study, we first examined the equimolar reaction of complex **1** with the common nucleophile LiMe. As stated above, and considering the reduced size of the methyl anion, we anticipated the methyl group to either fill the vacancy of this unsaturated Ir(III) complex or replace the chloride to access a Bergman-type complex [(η^5-C_5Me_5)Ir(Me)(PR_3)($ClCH_2Cl$)]$^+$.[30] To our surprise, the only discernible product, which we have fully characterized, is a cationic Ir(I) complex (**2·Me**) featuring a new methyl group bonded to one of the internal carbon atoms of the former Cp* ligand, as shown in Scheme 7. Analogous reactivity was found with lithium alkyls LiEt and Li^{n}Bu (Scheme 7), whose equimolar addition to the iridium precursor **1** led respectively to compounds **2·Et** and **2·^{n}Bu**, in which a new hydrocarbyl fragment is installed in the *exo*-face of the parent Cp* ligand.

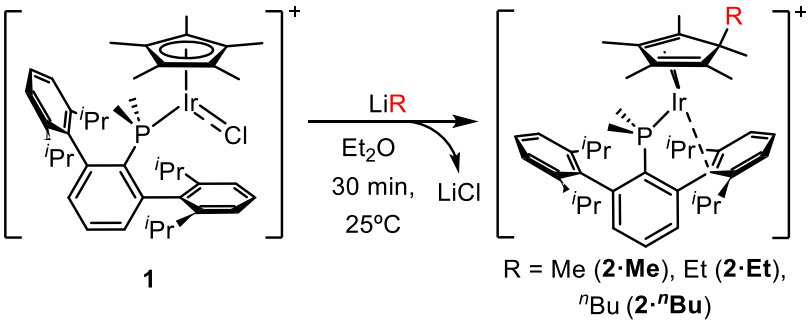

*Scheme 7. Syntheses of complexes **2·Me**, **2·Et**, and **2·^{n}Bu** from **1** and LiMe, LiEt, and Li^{n}Bu, respectively.*

The room temperature ^{1}H NMR spectrum of complex **2·Me** features broad resonances, suggestive of a dynamic solution process. This fluxional behavior arises from the rotation of the C_5Me_6 fragment, presumably through a tetrahedral coordination environment,[66] and not from the exchange of the flanking Dipp rings of the phosphine ligand, according to exchange spectroscopy (EXSY) experiments (Figure 4). In particular, cross-peaks of the same sign as the diagonal peaks at 1.86, 1.54, 0.73 and 0.32 ppm due to the methyl groups of the singly-methylated carbon atoms of the C_5Me_6 moiety account for this process. No exchange peaks were observed for the *m*-C_6H_3 protons of the central aryl ring.

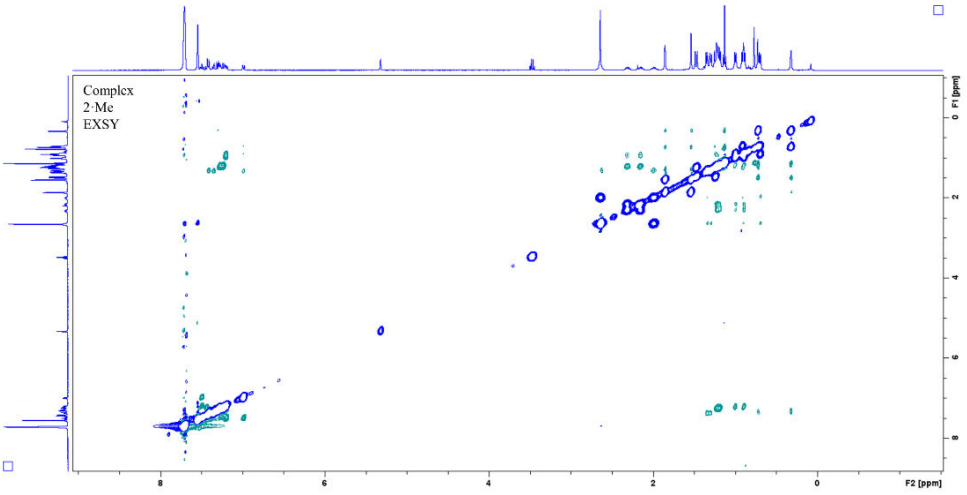

Figure 4. Exchange spectroscopy (EXSY) experiment of complex ***2·Me*** (25 ºC, mixing time = 0.80 s).

[66] a) Janowicz, A. H.; Bergman, R. G. *J. Am. Chem. Soc.* **1982**, *104*, 352−354. b) Marinelli, G.; Rachidi, I. E. I.; Streib, W. E.; Eisenstein, O.; Caulton, K. G. *J. Am. Chem. Soc*. **1989**, *111*, 2346−2347.

Nevertheless, at −20 °C, complex **2·Me** exhibits a rigid solution structure providing sharp, well-resolved resonances. The absence of symmetry elements in **2·Me** results in a complex ^{1}H NMR spectrum with six singlets, each with relative intensity corresponding to 3 H, recorded in the 1.84-0.32 ppm range for the Me groups of the newly formed C_5Me_6 diene ligand. Likewise, the four Dipp *iso*-propyl substituents are inequivalent and originate corresponding multiplets centered at 2.64, 2.32, 2.15 and 2.00 ppm for the methine C*H*Me$_2$ protons. To compensate unsaturation, complex **2·Me** features a secondary π-arene interaction with the metal center revealed by the low-frequency shift of one of the *ipso* carbon atoms of the flanking aryl rings (120.4 ppm, *cf.* the 135.7 ppm value for the corresponding carbon of the non-coordinated Dipp ring) and further supported by topological analysis (Figure 5 and Table 1).

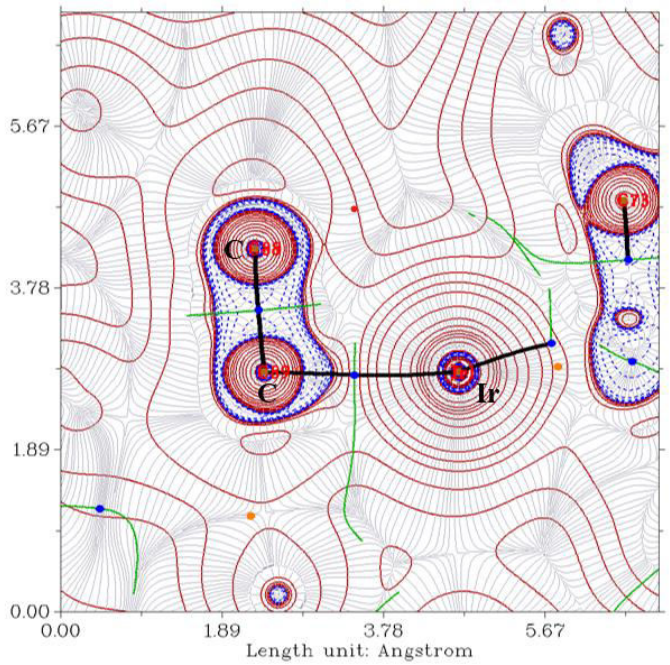

*Figure 5. Plot of the Laplacian of the electron density, $\nabla^2\rho$, of complex **2·Me** in the plane containing the Ir, C_{ipso}, and one of the C_{ortho} atoms. Both C atoms belong to the Dipp group which features an interaction with the metal center. The solid and dashed lines correspond to positive and negative values of $\nabla^2\rho$ respectively. Interatomic basins are represented in green. In plane bcps and bond paths of the electron density are superimposed.*

Table 1. Selected properties of the electron density at relevant bcps shown in the previous figure.

bond	ρ^b	$G_a{}^c$	$V_a{}^c$	$H_a{}^c$	$\lvert V_a \rvert / G_a$	$\nabla^2\rho^d$
Ir-C_{ipso}	0.0793	0.0575	− 0.0844	− 0.0269	1.471	0.1253

[a] average values, [b] e·bohr^{-3}, [c] Hartree, [d] e·bohr^{-5}, e = elementary charge.

One of the *ortho* carbon atoms of this ring seems to also participate in the bonding, resulting in η^2-coordination of the arene, as its chemical shift (132.5 ppm) is significantly shifted to lower frequencies compared to its counterparts (141.5 ppm for the other *ortho* carbon within the same ring, and 146.5 and 146.9 ppm for the ones belonging to the non-bound Dipp). This is also confirmed by EDA-NOCV[67] analysis of the bonding between the $[Ir\text{-}C_5Me_6]^+$ and phosphine fragments (Figure 6), which show that the orbital term is dominated by two different orbital interactions: i) the σ-donation from the HOMO of the phosphine moiety to the transition metal fragment (denoted as $\Delta E(\rho_1)$), and ii) donation from *ipso*- and *ortho*-carbons of the interacting Dipp unit to the $[Ir\text{-}C_5Me_6]^+$ fragment and backdonation of the latter (denoted as $\Delta E(\rho_2)$).

[67] te Velde, G.; Bickelhaupt, F. M.; Baerends, E. J.; Fonseca Guerra, C.; van Gisbergen, S. J. A.; Snijders, J. G.; Ziegler, T. *J. Comput. Chem*. **2001**, *22*, 931−967.

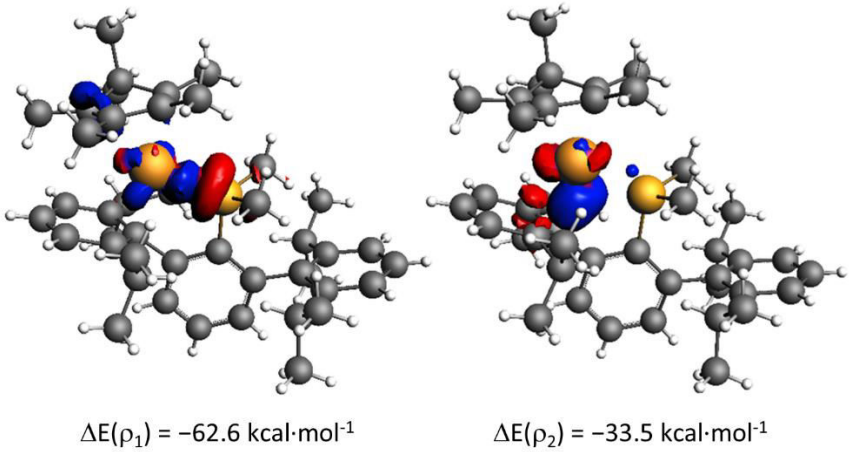

Figure 6. Contour plots of NOCV deformation densities Δρ and associated energies ΔE(ρ) (computed at the ZORA-BP86-D3/TZ2P/PBE0-D3/SDD(Ir)/6-31(d,p)(all other atoms) level) in ***2·Me****. The fragments are defined as the phosphine moiety and the rest of the complex. Electron-density charge flows in the direction red→blue.*

Interestingly, the $^{13}C\{^{1}H\}$ NMR spectrum of complex **2·Me** also exhibits a clear difference in the chemical shift of the two pairs of carbons involved in the two formal double bonds of the C_5Me_6 unit (122.5 and 114.6 *vs* 78.3 and 61.9 ppm). This experimental evidence together with the longer C−C distance for the formal double bond *trans* to the phosphine (C34−C33: 1.431(6) *vs* C35−C36: 1.338(6) Å) and corresponding closer distance to the metal center (C34−Ir1: 2.118(5) and C33−Ir1: 2.163(4) vs C35−Ir1: 2.265(5) and C36−Ir1: 2.437(4) Å) support our hypothesis that the formal coordinated diene is closer in nature to a double bond and a metalacyclopropane. This can be explained by the stronger trans influence

of the phosphine, also observed in a closely related system.[68] EDA-NOCV studies further sustain this idea. As shown in Figure 7, the carbon atoms with the longer C−C bond distance participate to a greater extent in the principal orbital interactions between the C_5Me_6 and [Ir-phosphine]$^+$ fragments. These spectroscopic features are similar to those found for compounds **2·Et** and **2·^{n}Bu**.

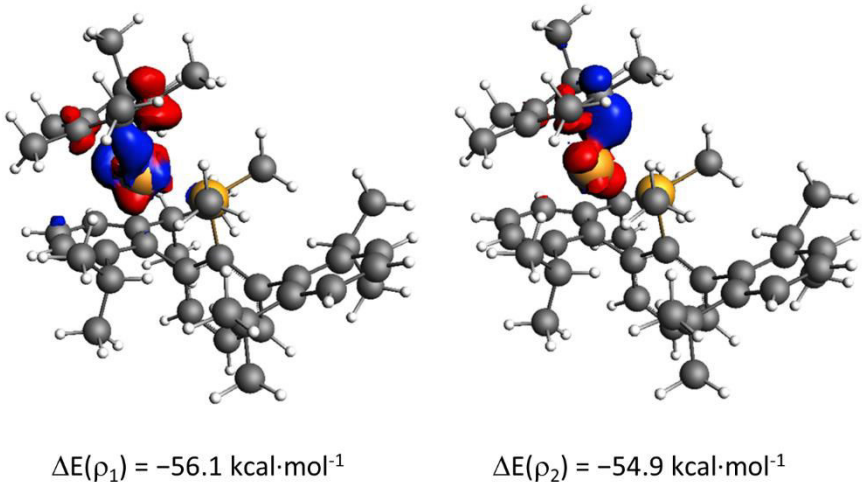

*Figure 7. Contour plots of NOCV deformation densities Δρ and associated energies ΔE(ρ) (computed at the ZORA-BP86-D3/TZ2P/*PBE0-*D3/*SDD(Ir)/6-31(d,p)(all other atoms) *level) in* **2·Me**. *The fragments are defined as the C_5Me_6 moiety and the rest of the complex. Electron-density charge flows in the direction re*d→*blue.*

The molecular formulation of the new compounds was corroborated by X-ray diffraction studies, confirming the *exo* attack on the Cp* and revealing a preferred η^1-arene coordination in the solid state, rather than η^2-binding as inferred from spectroscopic analysis. Thus, in complex **2·Me** the

[68] Moreno, J. J.; Espada, M. F.; Krüger, E.; López-Serrano, J.; Campos, J.; Carmona, E. *Eur. J. Inorg. Chem.* **2018**, 2309−2321.

Ir−C_{arene} bonding is characterized by an Ir−C_{ipso} bond distance of 2.249(4) Å, and by significantly longer, and therefore weaker, Ir−C_{ortho} interactions of length 2.544(5) and 2.686(4) Å (Figure 8). Similar geometric parameters are found in compounds **2·Et** and **2·^{n}Bu**, with notably shorter Ir−C_{ipso} (2.231(5), **2·Et**; 2.253(5) Å, **2·^{n}Bu**) distances compared to Ir−C_{ortho} (2.549(5), **2·Et**; 2.593(6) Å, **2·^{n}Bu**) interactions.

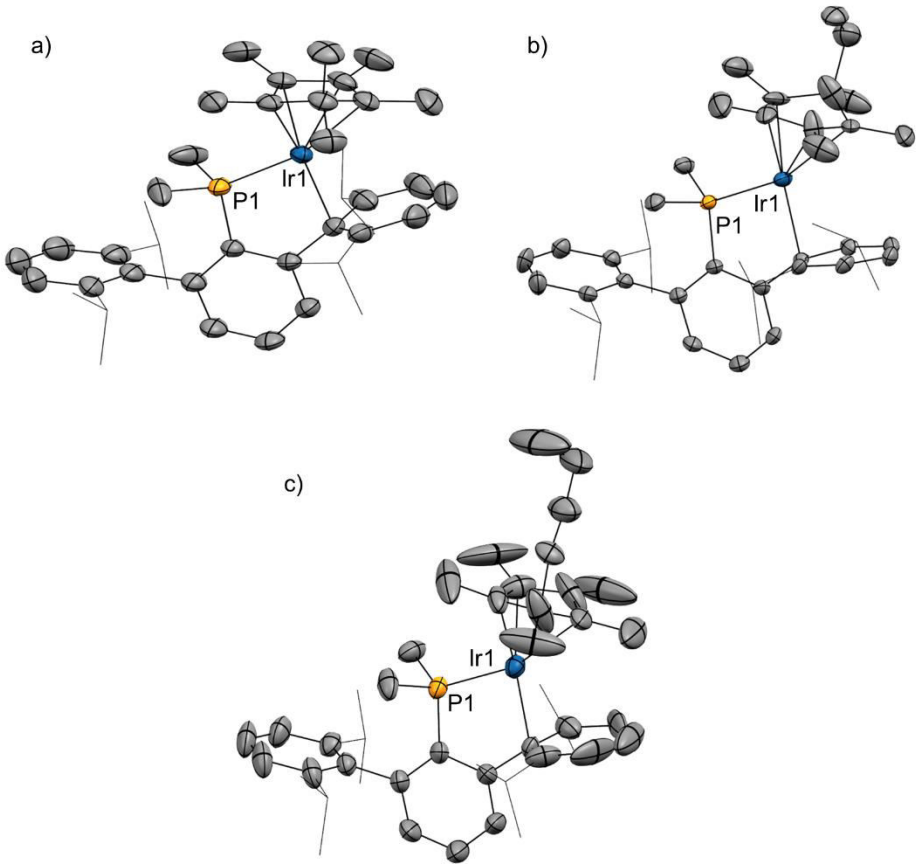

*Figure 8. ORTEP diagrams of the cation of complexes a) **2·Me**, b) **2·Et**, and c) **2·^{n}Bu**. Hydrogen atoms are excluded for clarity and thermal ellipsoids are set at 50% probability. Wireframe is used to represent the iso-propyl groups.*

We carried out Density Functional Theory studies to gain insight into the mechanism of the reactions depicted in Scheme 7. For convenience, we focused on the relatively simpler LiMe. It is possible to envision three different reaction pathways for the reaction between complex **1** and LiMe: i) an attack on the metal center, leading to a neutral Ir(I) species; ii) proton abstraction, producing a neutral fulvene species, or iii) a direct attack on one of the internal carbon atoms of the Cp* moiety. Our calculations indicate that all three routes have accessible barriers at room temperature (Figure 9).

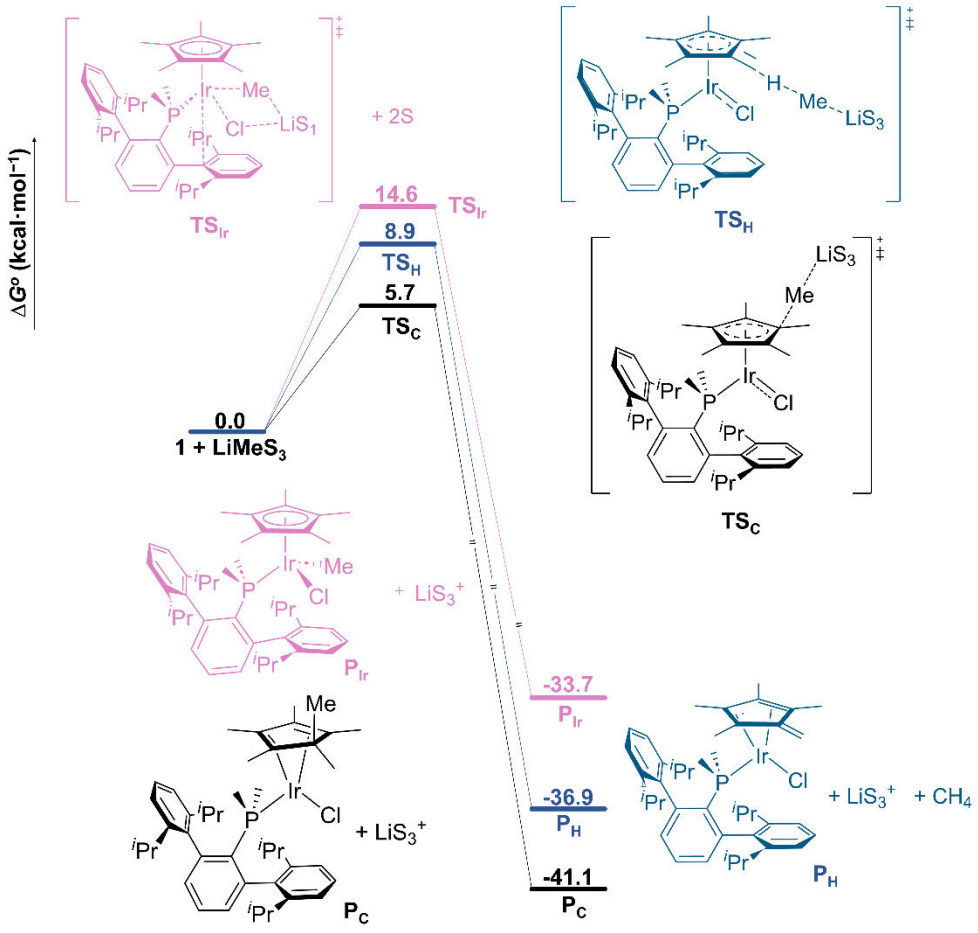

Figure 9. Free energy profile comparison of LiMe attacking the Cp (black), the metal center (pink), or acting as a base (blue). Explicit solvent molecules (Me_2O) responsible for stabilizing the Li atom included in the calculations are represented as S.*

Since the three routes of Figure 9 imply accessible barriers, the subsequent steps needed to produce the experimentally observed complex **2·Me** will be explored. In the case of LiMe directly attacking the metal, the produced intermediate would need to partake into a reductive coupling between the Cp* ligand and an Ir—Me functionality either from the Ir(I) neutral species (Figure 10) or the cationic version (product of the release of the chloride

group; Figure 11). However, both routes failed to provide energy barriers in agreement with experimental observations (Figure 10 and Figure 11).

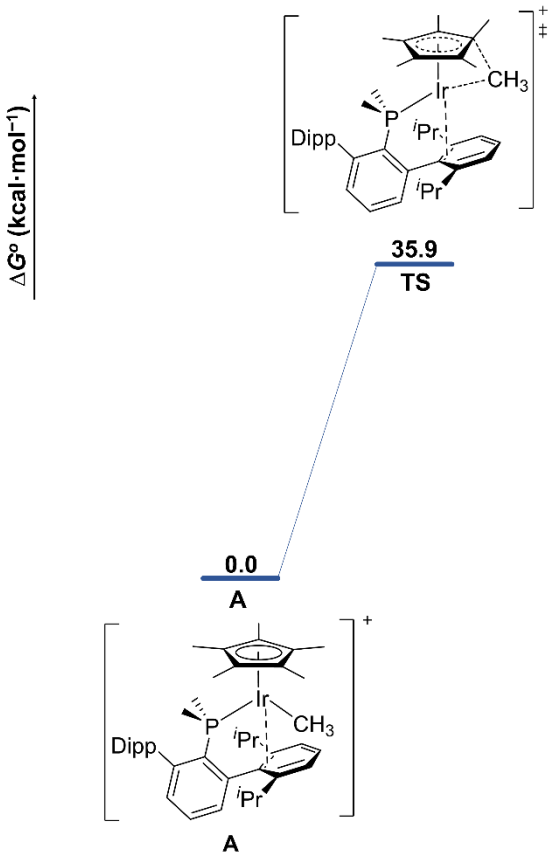

*Figure 10. Free energy profile for the reductive coupling en route to complex **2·Me**.*

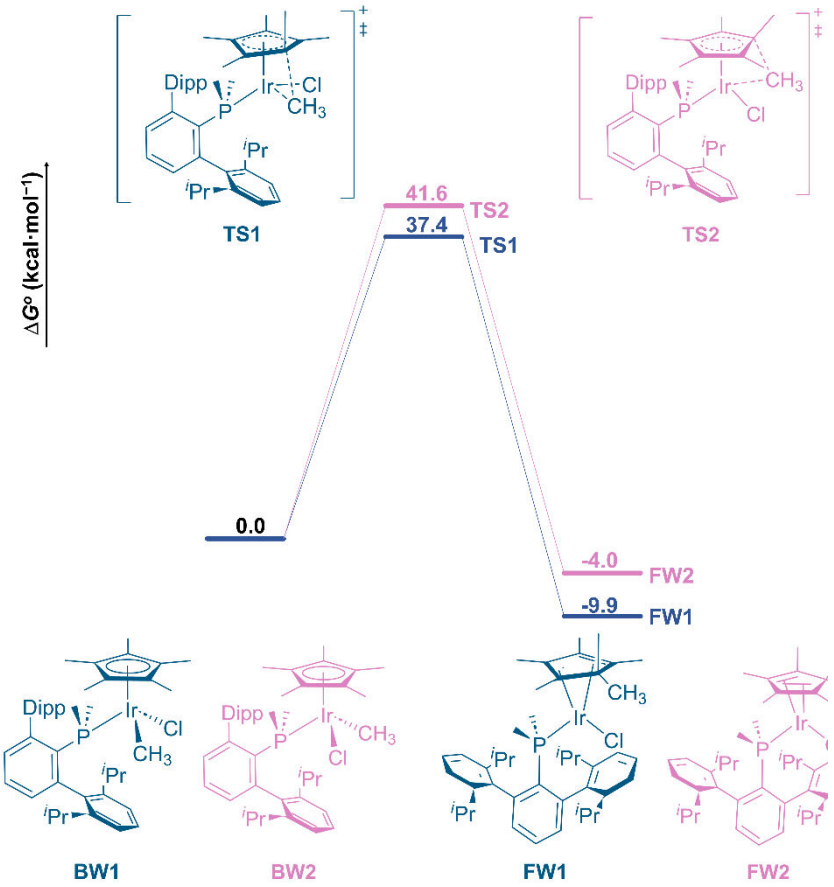

Figure 11. Free energy profile for the reductive coupling in route to complex ***2·Me****, the two routes correspond to the two possible stereochemical configurations of iridium.*

In the case of the 'proton abstraction route' (blue profile in Figure 9), although energetically accessible, products involving the formation of a fulvene intermediate would be expected. These are not observed experimentally in this case, while as they are indeed observed for the addition of LiPh and Li^{t}Bu (*vide infra*). Therefore, this route could also be ruled out.

Based on the stated above, the direct attack of the LiMe molecule on the *exo* face of the Cp* moiety is the route that takes place, without direct involvement of the metal center. The transition state of the C−C bond formation step requires surmounting a barrier of only 5.7 kcal·mol^{-1} and yields a neutral Ir(I) complex at −41.1 kcal·mol^{-1} relative to the reactants (Figure 9). Subsequent chloride release assisted by the solvated lithium atom gave complex **2·Me** through an accessible barrier of 9.2 kcal·mol^{-1} above the neutral Ir(I) complex (Figure 12).

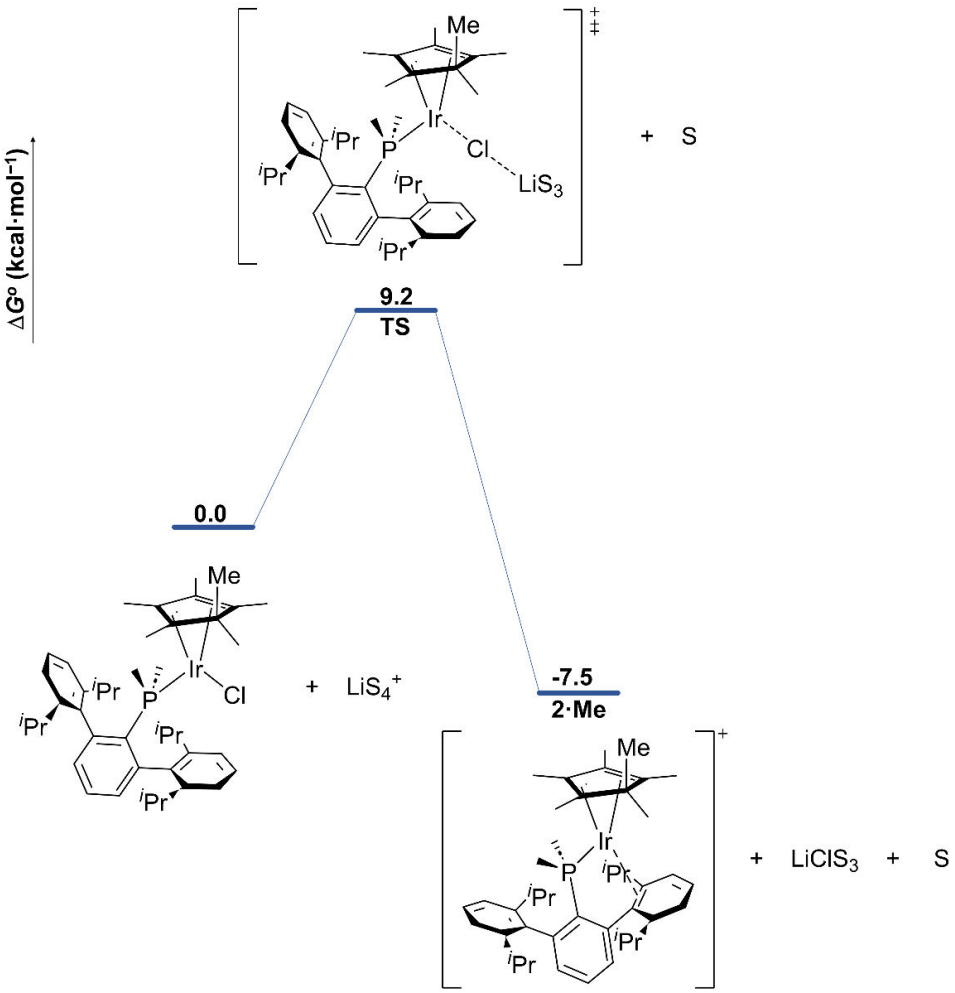

Figure 12. Free energy profile for the assisted release of chloride. Explicit solvent molecules (Me_2O) responsible for stabilizing the Li atom included in the calculations are represented as S.

I.2.1.3 Reactivity of LiPh and Li^{t}Bu toward 1

In contrast to the reactivity described in the previous subsection, the less nucleophilic lithium alkyls LiPh and Li^{t}Bu lead to a completely different outcome, acting instead as Brønsted-Lowry bases thereby deprotonating one of the methyl groups of the Cp* moiety. As shown in Scheme 8, this event triggers a complex rearrangement involving reversible C−C bond formation events between the Cp* ring and a lateral ring of the terphenyl phosphine. This is the same reactivity already discussed in section **I.1.5** and that was previously reported by our group by reaction with the much milder base NEt_3.[45] Similarly to what was observed before in those studies, this deprotonation eventually leads to a pseudoallylic structure, complex **3**, which we also observe in the reactions with Li^{t}Bu and LiPh as the major product.

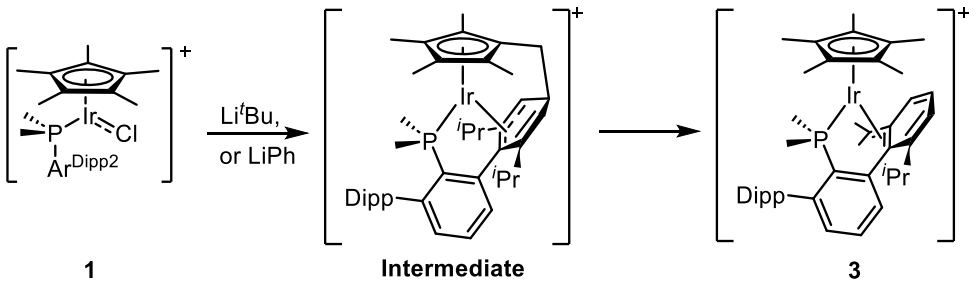

*Scheme 8. Obtention of complex **3**, final product of the reaction between complex **1** and Li^{t}Bu or LiPh. Conditions: lithium alkyls were added at −78 °C, solution was left to reach room temperature.*

It is remarkable that the unexpected electrophilicity of the internal carbon atoms of the C_5Me_5 ring outcompetes the mild, yet well-known, Brønsted-Lowry acidity of the C−H bonds, even with bases around 40 pKa units

stronger than NEt_3. To rationalize such striking divergence in reactivity, DFT studies were performed to calculate the energy profiles for LiPh acting as a nucleophile or as a base. In agreement with the experimental observations, a lower energy barrier for the deprotonation step (5.2 $kcal \cdot mol^{-1}$, Figure 13) was obtained in comparison to the attack on an internal carbon atom of the Cp* (7.9 $kcal \cdot mol^{-1}$, Figure 13), in stark contrast to the profiles calculated for LiMe (Figure 11). In these, the opposite relation operates (8.9 $kcal \cdot mol^{-1}$ vs 5.7 $kcal \cdot mol^{-1}$ energy barriers respectively for proton abstraction vs nucleophilic attack at the Cp ring by LiMe; Figure 9).

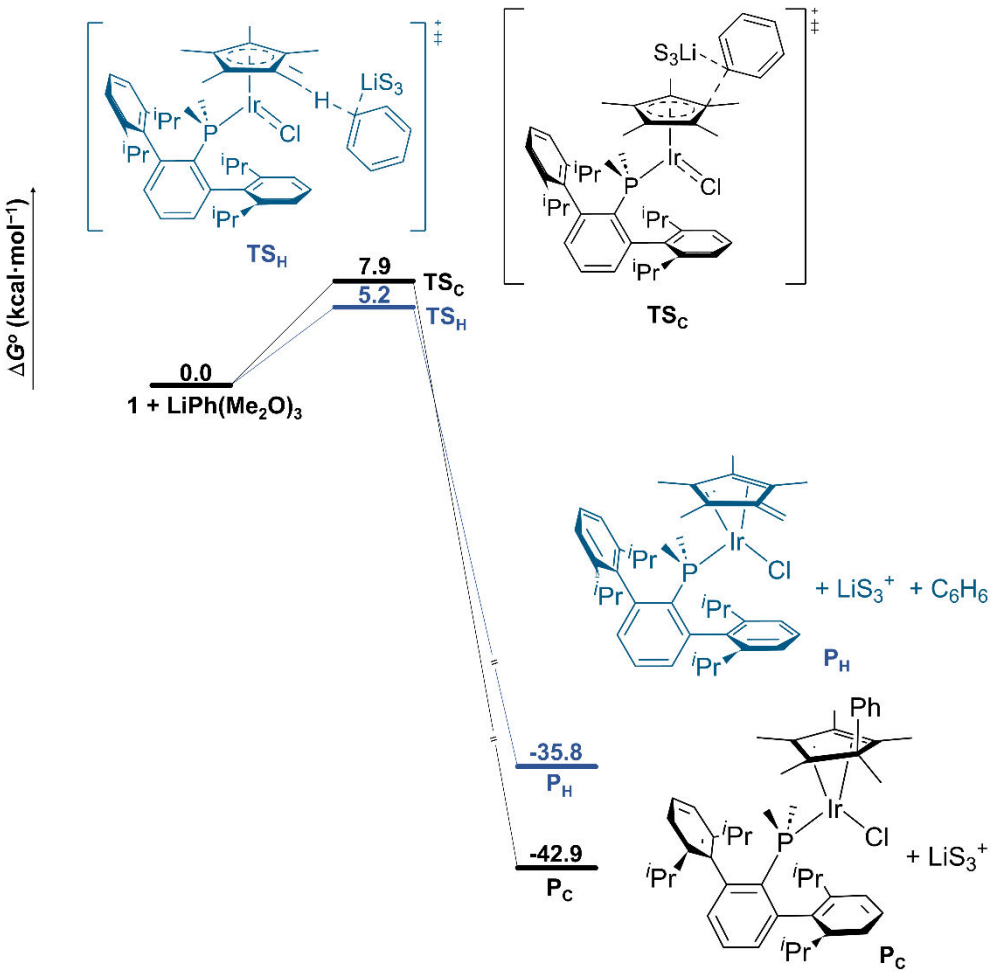

Figure 13. Free energy profiles of LiPh acting as a base (blue) or as a nucleophile (black). Explicit solvent molecules (Me_2O) responsible for stabilizing the Li atom included in the calculations are represented as S.

I.2.1.4 Reactivity of Li^{i}Pr toward 1

Bearing in mind the contrasting reactivity of alkyl lithium reagents, in particular Li^{n}Bu and Li^{t}Bu, we wondered about the outcomes of an intermediate situation in terms of steric and electronic properties of the carbon nucleophile. Thus, we examined the reactivity of **1** with one equivalent of Li^{i}Pr. Not surprisingly, *iso*-propyl lithium finds its place between the two aforementioned cases, as the reaction between complex **1** and Li^{i}Pr yields a mixture of complex **2·^{i}Pr** and complex **3** in a ca. 1:7 ratio (Scheme 9).

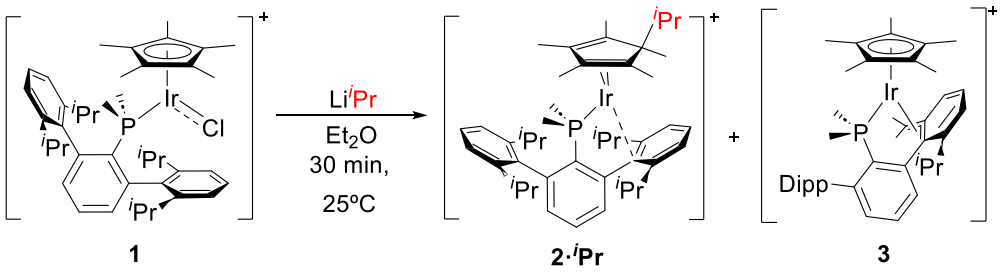

*Scheme 9. Result of the reaction between complex **1** and Li^{i}Pr. Complexes **2·^{i}Pr** and **3** are obtained in ca. 1:7 ratio.*

The spectroscopic signature of **2·^{i}Pr** was comparable to prior compounds **2** and does not require further discussion. In fact, although complex **2·^{i}Pr** could not be isolated in pure form, we could monitor its formation, along with that of **3**, by ^{31}P NMR spectroscopy and authenticate its nature by X-ray diffraction studies (Figure 14).

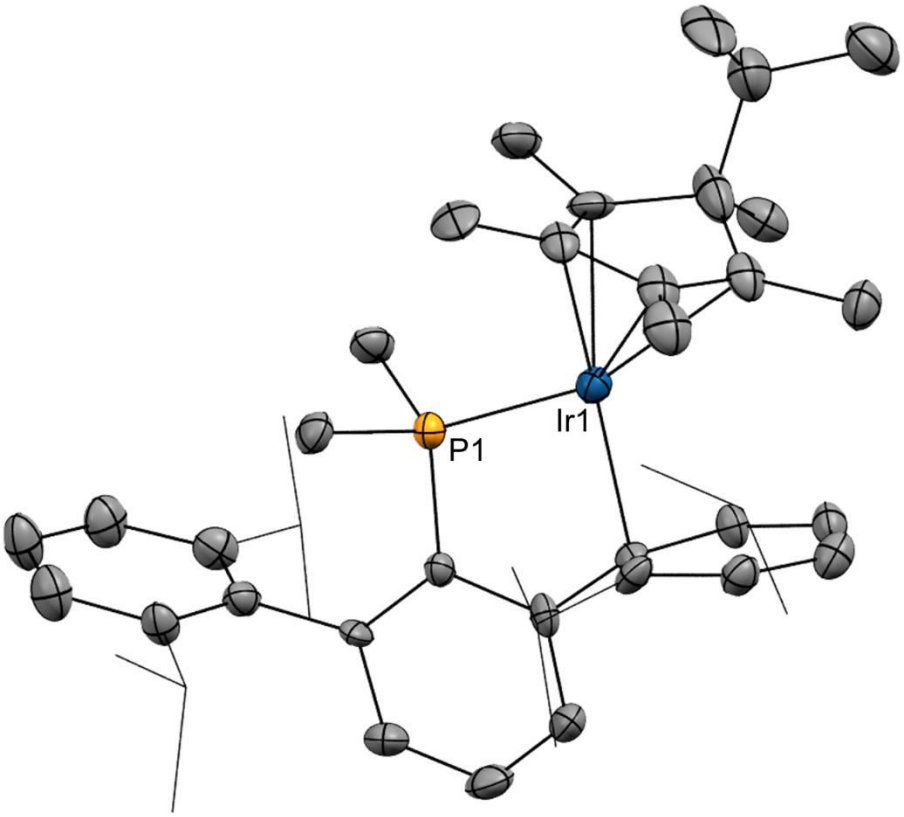

Figure 14. ORTEP diagram of the cation of ***2·^{i}Pr*** *(top right). Hydrogen atoms are excluded for clarity and thermal ellipsoids are set at 50 % probability. Wireframe is used to represent the iso-propyl groups.*

To complete our studies, we also carried out computational analyses to ascertain whether the two pathways could indeed be operative in the case of Li^{i}Pr. Although the DFT calculated barriers do not exactly match the experimentally observed ratio between the two products, the results are fully consistent with the fact that the two isomers are produced taking into consideration the DFT error range (Figure 15). Indeed, our calculations suggest that there is only around 1 kcal·mol^{-1} difference between the two key transition states that govern the formation of compounds **2·^{i}Pr** vs **3**.

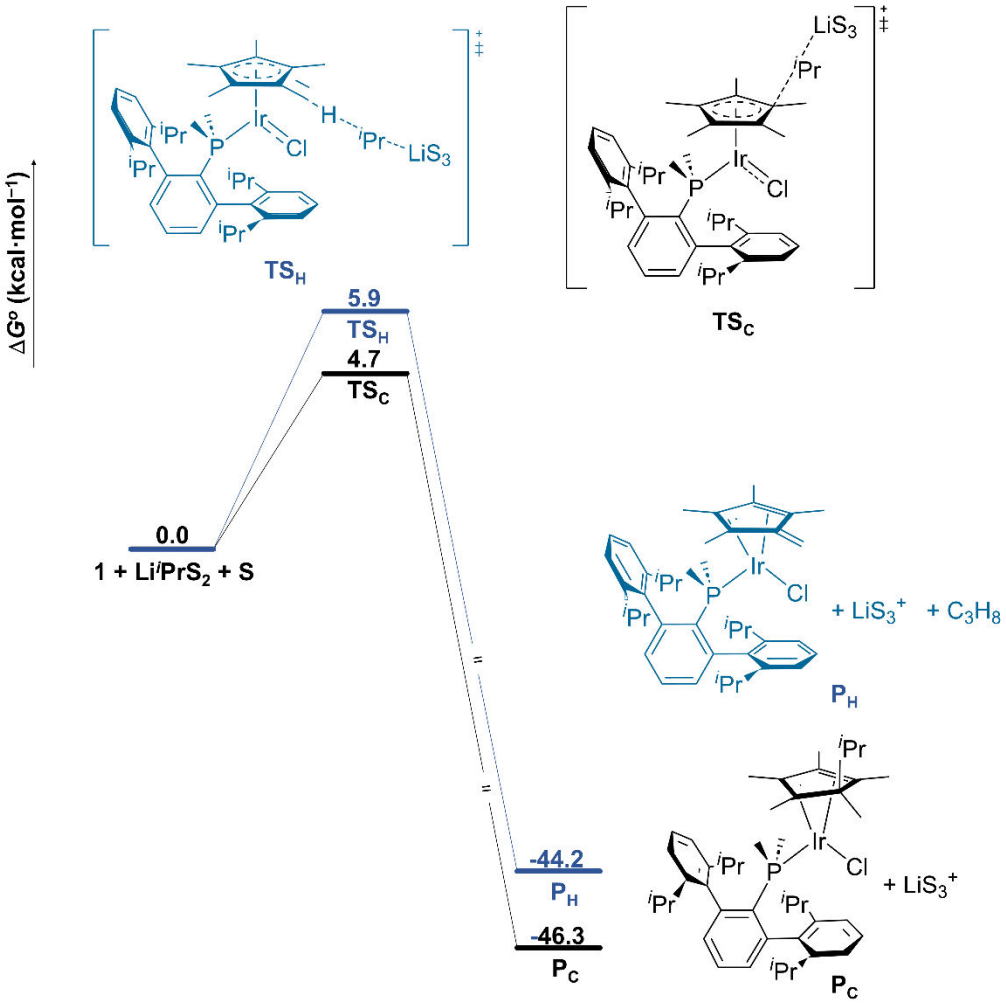

Figure 15. Free energy profile comparison of Li^{i}Pr attacking the Cp ligand (black) or acting as a base (blue). Explicit solvent molecules (Me_2O) responsible for stabilizing the Li atom included in the calculations are represented as S.*

I.2.1.5 Reactivity of Grignard reagents toward 1

As introduced earlier, organolithium reagents have been widely used in the chemistry of Cp*-containing complexes. Nonetheless, the weaker alkylating Grignard reagents have been even more commonly used and their implications in catalysis are broader.[69] Therefore, we explored the reactivity of complex **1** toward less polarized Grignard reagents. Addition of equimolar amounts of EtMgBr to diethyl ether solutions of the cationic chloride complex **1** resulted in an instantaneous color change from dark to orange due to the formation of a new species, complex **4** (Scheme 10). In stark contrast to the reactivity exhibited by organolithium reagents, the integrity of the Cp* ligand remains intact when milder Grignard reagents are used. This represents a remarkable divergent reactivity associated with common chemicals that are on many occasions used indistinctly. The coordinatively saturated complex **4** features a $^{31}P\{^{1}H\}$ NMR resonance at −27.0 ppm, therefore showing a large δ shift relative to that of complex **1** (6.6 ppm) and closer to free PMe_2Ar^{Dipp2} (−41.3 ppm), supporting the absence of the aforementioned Ir−C_{arene} π-interactions. A distinctive low-frequency doublet in the ^{1}H NMR spectrum (δ −14.9 ppm, $^{2}J_{HP}$ = 30.2 Hz) indicates the presence of an iridium hydride, while a coordinated ethylene molecule gives rise to two resonances at 2.18 and 1.88 ppm.

[69] a) Yanlong, Q.; Lu; Jiaqui; Weihua, X. *J. Mol. Catal.* **1986**, *34*, 31−38. b) Tao, X.; Qian, F.; Yong, L.; Qian, Y. *J. Mol. Catal. A: Chem.* **2000**, *156*, 121−126.

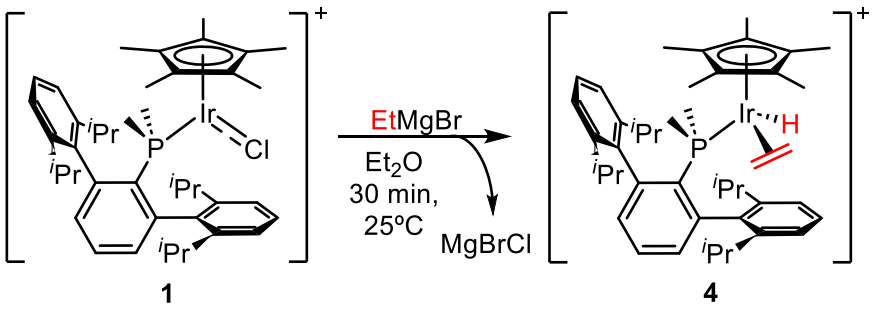

*Scheme 10. Synthesis of complex **4** from **1** and EtMgBr.*

X-ray diffraction studies confirmed the proposed formulation and revealed a C−C bond length of 1.426(1) Å (Figure 16) for the ethylene ligand, longer, as expected, than that of non-coordinated ethylene (1.332(2) Å).[70]

[70] Craig, N. C.; Groner, P.; McKean, D. C. *J. Phys. Chem. A* **2006**, *110*, 7461−7469.

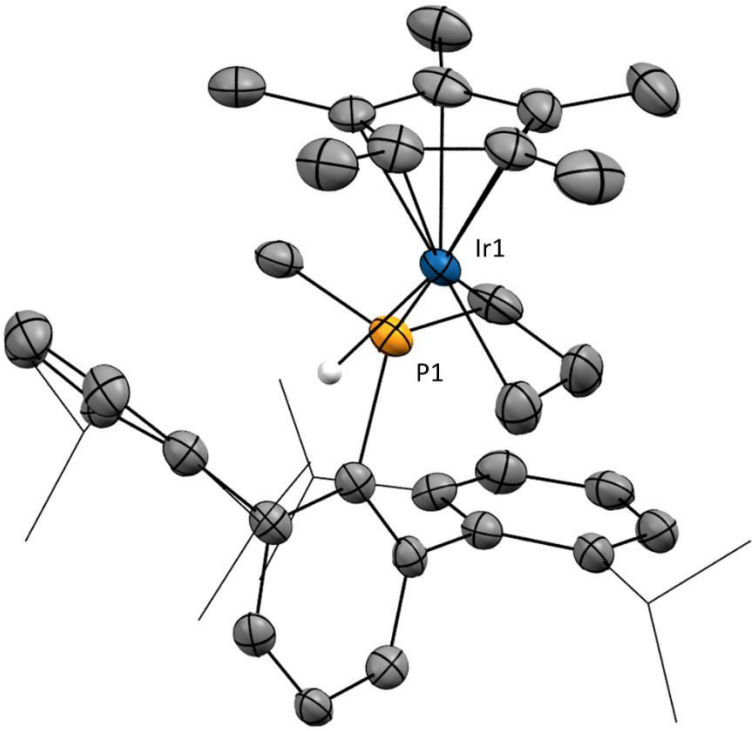

*Figure 16. ORTEP diagram of the cation of complex **4**. All hydrogen atoms but that of the hydride are excluded for clarity and thermal ellipsoids are set at 50 % probability. Wireframe is used to represent the iso-propyl groups.*

A reasonable proposal for the mechanism of the reaction leading to complex **4** is the substitution of the chloride ligand by an ethyl group with concomitant precipitation of LiCl, followed by a β-hydride elimination. Further insight into this proposed mechanism was obtained by DFT studies (Figure 17). These revealed a low barrier (2.9 kcal·mol^{-1}) for the formation

of an agostic interaction[71] between a C−H bond of the CH_3 end of the ethyl group and the Ir atom, followed by an almost barrierless β-hydride elimination ($\Delta G^{\ddagger}$ = 0.1 kcal·mol^{-1}, relative to the agostic complex). These low barriers are congruent with experimental observations, as attempts to spectroscopically detect the Ir−Et intermediate were unsuccessful even at low temperatures.

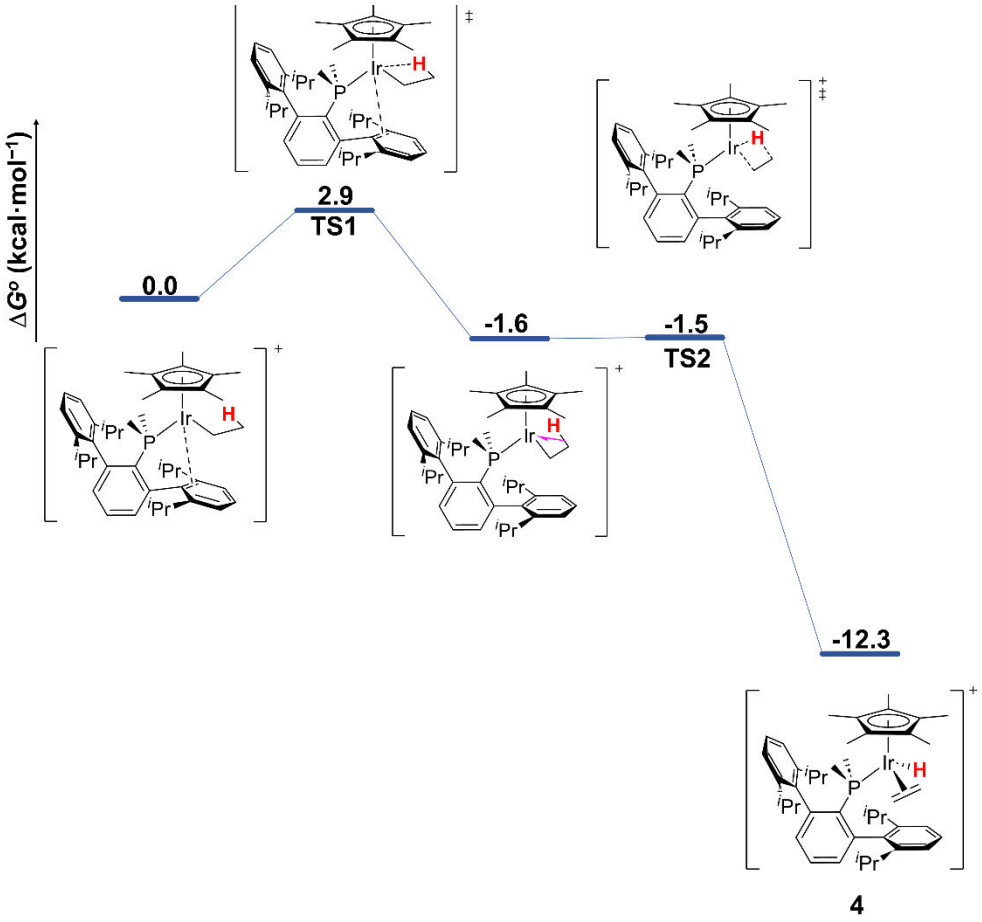

*Figure 17. Free energy profile of the proposed β-hydride elimination leading to complex **4**.*

[71] Brookhart, M.; Green, M. L. H.; Parkin, G. *Proc. Natl. Acad. Sci. U. S. A.* **2007**, *104*, 6908–6914.

The results described above promised the obtention of the analogue of Bergman's complex reacting MeMgBr with complex **1**, due to the lack of hydrogen atoms in β-position in the expected Ir−Me complex. Once more, the use of an organomagnesium reagent circumvented the direct nucleophilic attack to the Cp* ring, which remained unaltered. Yet, the observed product of this reaction was complex **5**, derived from the remote and selective activation of a non-benzylic C(sp^3)−H bond of one *iso*-propyl group of a lateral terphenyl ring (Scheme 11). At variance with the analogous ethyl reagent, the methyl fragment does not remain at the structure of **5** and instead evolves as methane, which could be observed by careful NMR monitoring (singlet in the ^{1}H NMR spectrum at 0.23 ppm). This reactivity also contrasts with the cyclometallation selectivity previously shown by this system, where the benzylic methine C−H bond is more amenable to activation.[45] Complex **5** was fully characterized by multinuclear NMR spectroscopy. Three distinctive ^{1}H multiplets, centered at 3.35, 0.73, and 0.22 ppm, each with relative intensity corresponding to 1 H, were assigned to the CH and the diastereotopic protons of the CH_2 of the Ir−CH_2CHCH_3 moiety, respectively. The structure of **5** was also confirmed by X-ray diffraction studies (Figure 18).

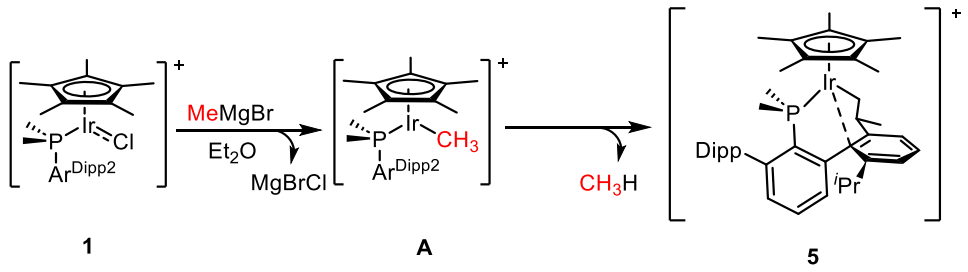

*Scheme 11. Synthesis of complex **5** from **1** and MeMgBr, through proposed intermediate complex **A**.*

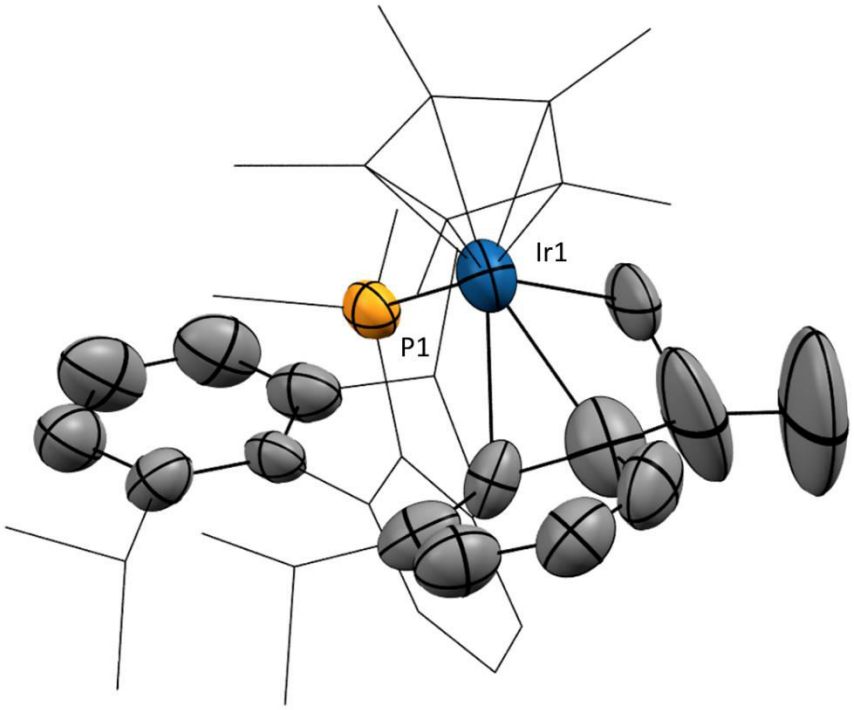

*Figure 18. ORTEP diagram of the cation of complex **5**. Hydrogen atoms are excluded for clarity and thermal ellipsoids are set at 50 % probability. Wireframe used to represent the Cp* ligand, the central aryl group of the phosphine and the iso-propyl groups.*

The mechanism of the reaction depicted in Scheme 11 was also studied through DFT methods. The direct attack of MeMgCl to the iridium center yielding a neutral Ir(I) complex was found to be inaccessible (Figure 19), which led us to explore an alternative mechanism.

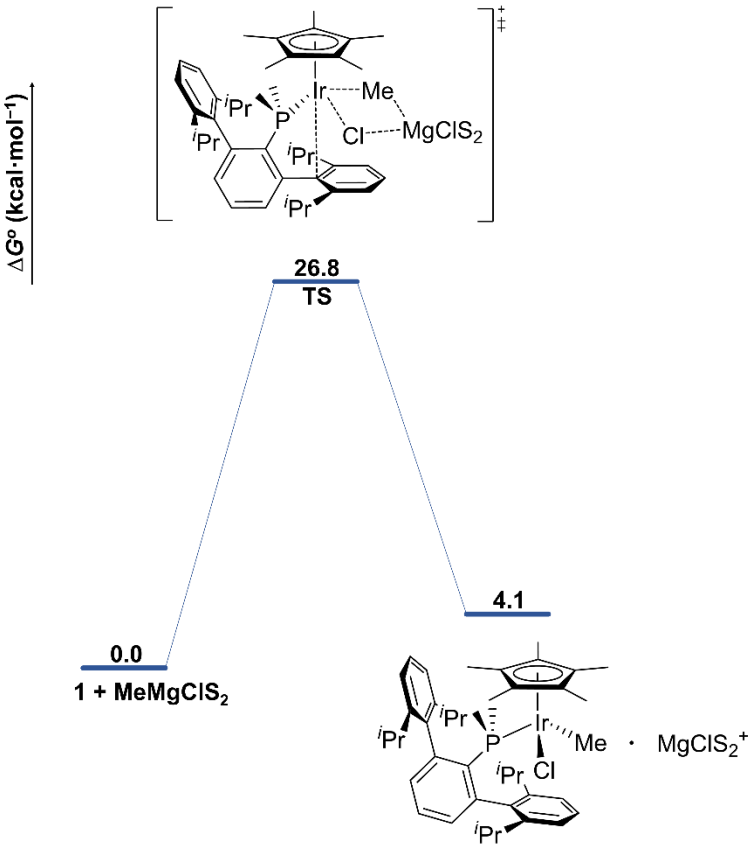

*Figure 19. Free energy profile of an inaccessible alternative route to obtain **A**.*

The formation of the Bergman's type Ir–CH_3 complex[30] (**A** in Scheme 11) commences through the magnesium-assisted chloride release ($\Delta G^{\ddagger}$ = 21.0 kcal·mol^{-1}), yielding a dicationic Ir(III) complex at 11.4 kcal·mol^{-1}. This readily reacts with the generated ($MeMgCl_2$) moiety, alkylating the metal center with concomitant release of $MgCl_2$ ($\Delta G^{\ddagger}$ = 19.7 kcal·mol^{-1}) and leading to intermediate **A** at −19.3 kcal·mol^{-1} relative to the reactants

(Figure 20). For comparison, the reaction pathway of MeMgCl attacking one of the internal carbon atoms of the Cp* was also calculated. This route involves a higher-in-energy TS (28.1 kcal·mol^{-1}), which explains the selectivity of the reaction between **1** and MeMgCl (Figure 20), that contrasts with the more powerful lithiated version where the nucleophilic attack was favored.

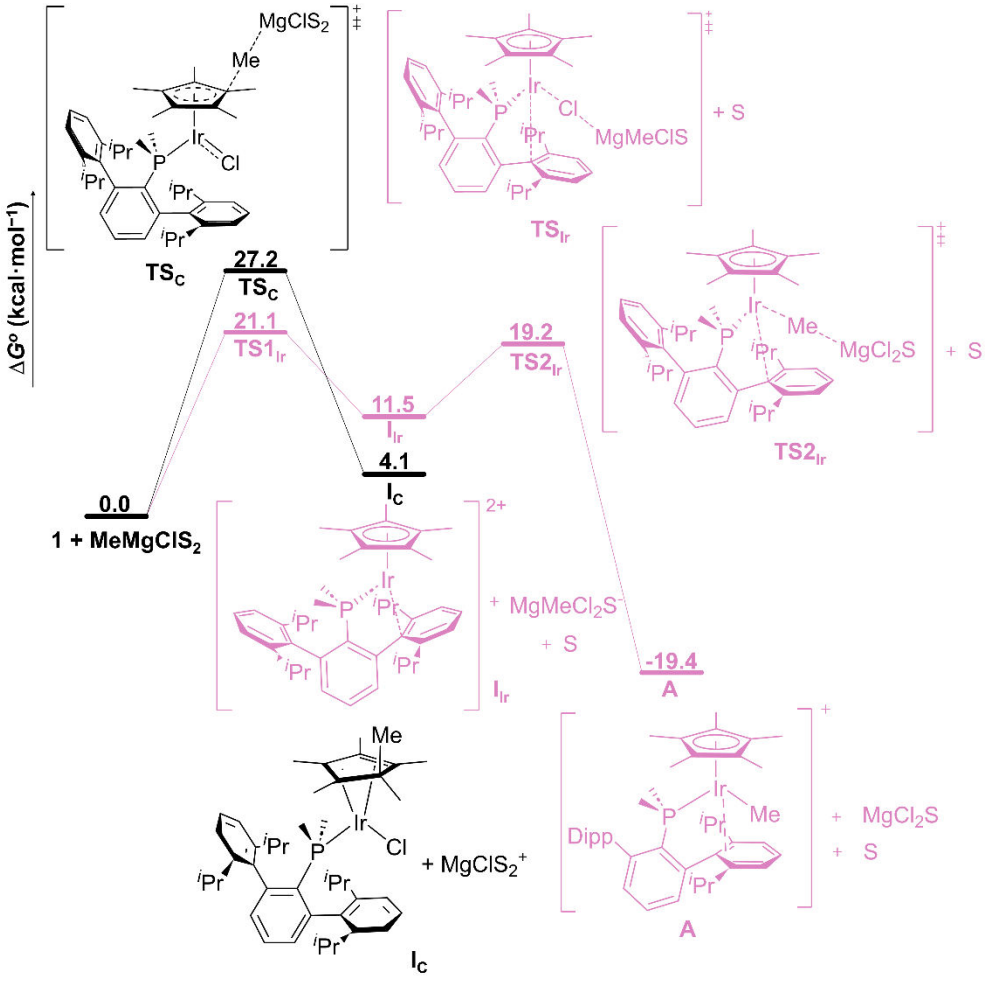

Figure 20. Free energy profile comparison of MeMgCl attacking the Cp (black) or the metal center (pink). The pink pathway leads to proposed intermediate **A**. Explicit solvent molecules (Me_2O) responsible for stabilizing the Mg atom included in the calculations are represented as S.*

We then evaluated three different pathways for the release of methane from intermediate **A**, comprising the activation of either one of the two methyl termini of an *iso*-propyl group or the methine CH. Despite benzylic C−H bonds being usually more prone to metalate, the connectivity of **5** points in a different direction, as supported by our computational studies (Figure 21). As observed experimentally, the activation of the methyl groups is kinetically favored relative to the benzylic methine, despite the latter yielding the most stable product. Notably, the activation of the two methyl groups susceptible to reacting follows different mechanisms, namely a σ-bond metathesis (black pathway in Figure 21) versus an oxidative addition mechanism (blue pathway in Figure 21).

In the σ-bond metathesis mechanism, the key intermediate (**B3** in Figure 21) exhibits an agostic interaction[71] characterized by an Ir–H distance of 1.937 Å and an Ir–H–C angle of 122.0º, both within the range expected for such an interaction.[71] This intermediate is followed by a transition state characteristic of a σ-bond metathesis process as determined by topological studies[72] (Figure 22 and Table 2). This transition state features a bond critical point (bcp) between the iridium center and the nascent CH_2 fragment as well as between the metal center and the migrating hydrogen atom. Both bcp feature characteristics belonging to a metal-ligand interaction (Table 2). The migrating hydrogen atom also exhibits a bcp with the nascent CH_2 group and another with the nascent CH_4 moiety. While the latter exhibits characteristics typical of a covalent interaction (negative Laplacian, $|V|/G > 2$; V = potential energy; G = kinetic

[72] Popelier, P. L. A. The QTAIM Perspective of Chemical Bonding. In *The Chemical Bond*; Frenking, G., Shaik, S., Eds.; Wiley, 2014. Pp. 271–308.

energy),[73] the former features an intermediate character between an ionic and covalent interaction (positive Laplacian, $1<|V|/G<2$). This fact together with the absence of a bcp between the metal center and the nascent methane molecule denotes a late-character for this transition state.

In contrast, the activation of the other methyl group, as well as that of the methine, involve the formation of Ir(V) hydride complexes as intermediates (**B1** and **B2** in Figure 21), i.e. the oxidative addition of the corresponding C–H bonds. From these intermediates, the reductive elimination of methane leads to compound **5** (or a diastereoisomer which would be hard to differentiate with the available spectroscopic data, but that naturally results from the two chiral centers in the molecule).

[73] a) Varadwaj, P. R.; Cukrowski, I.; Marques, H. M. *J. Phys. Chem. A* **2008**, *112*, 10657–10666. b) Varadwaj, P. R.; Varadwaj, A.; Marques, H. M. *J. Phys. Chem. A* **2011**, *115*, 5592–5601. c) Espinosa, E.; Alkorta, I.; Elguero, J.; Molins, E. *J. Chem. Phys*. **2002**, *117*, 5529–5542.

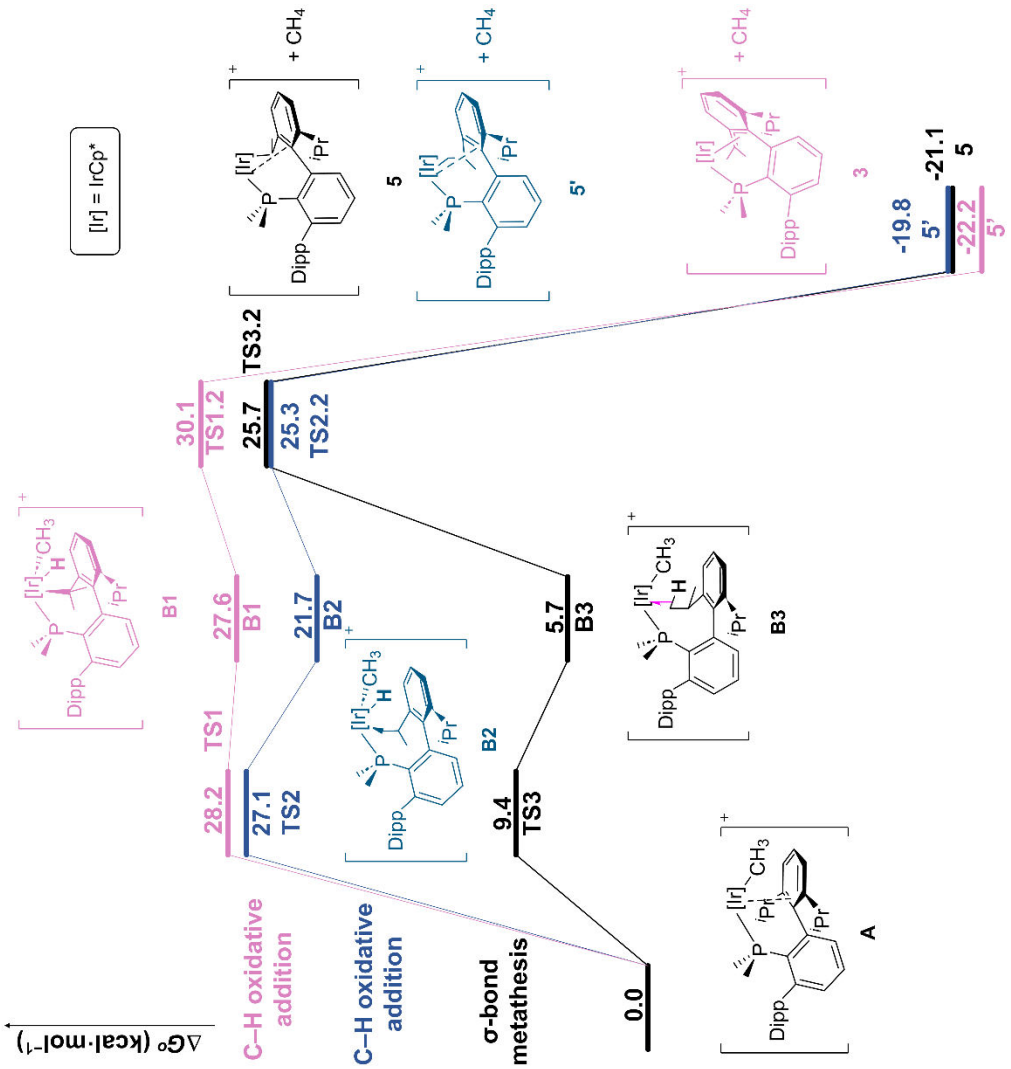

*Figure 21. Three different reaction pathways to account for the elimination of methane from the proposed Ir(III) intermediate **A**. **5'** is a diastereoisomer of **5**.*

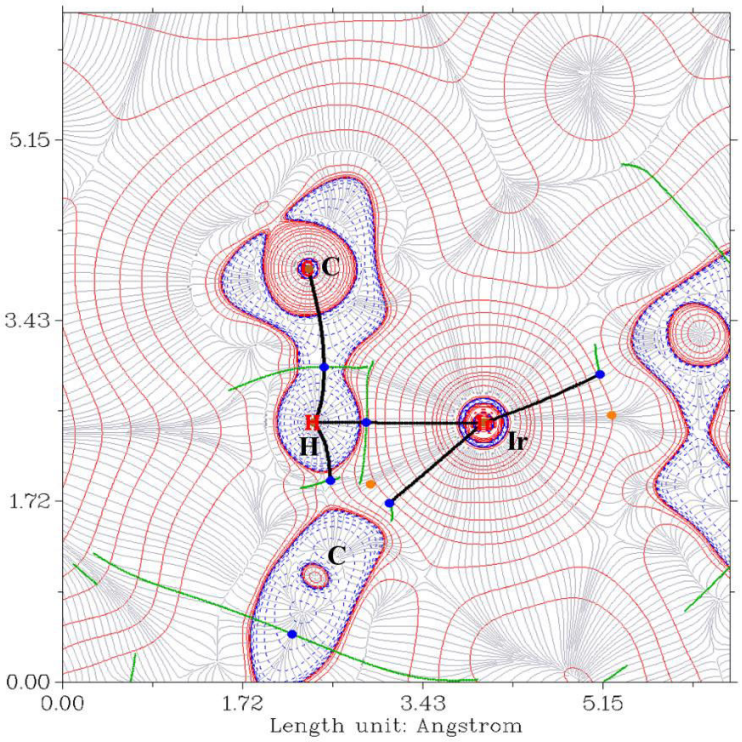

Figure 22. Plot of the Laplacian of the electron density, $\nabla^2\rho$, of the ***TS3.2*** *(Figure 21) in the C(methyl), H(agostic), Ir plane. The solid and dashed lines correspond to positive and negative values of $\nabla^2\rho$ respectively. Interatomic basins are represented in green. In plane bcps and bond paths of the electron density are superimposed. The C atom of the nascent CH_2 fragment is partially out of the plane, but the bcp and part of the bond paths connecting this atom with the H and Ir centers are shown.*

Table 2. Selected properties of the electron density at relevant bcps shown in the previous figure.

bond	ρ^b	G_a^c	V_a^c	H_a^c	$\lvert V_a \rvert / G_a$	$\nabla^2\rho^d$
Me-H	0.1191	0.0438	−0.0996	− 0.0575	2.273	− 0.0562
Ir-H	0.1321	0.1056	−0.1721	− 0.0719	1.688	0.l443
CH_2-H	0.0993	0.0408	−0.0781	− 0.0388	1.914	0.0063
CH_2-Ir	0.0942	0.0637	−0.0941	− 0.0318	1.477	0.1333

[a] average values, [b] e·bohr^{-3}, [c] Hartree, [d] e·bohr^{-5}, e = elementary charge.

When a solution of complex **5** was able to evolve at room temperature for 5 days, its $^{31}P\{^1H\}$ NMR spectrum revealed the emergence of two new peaks at 9.4 and 8.2 ppm. After heating this solution at 80 ºC for 5 hours, conversion to the species resonating at 9.4 ppm, identified as the thermodynamically more stable complex **3**, was complete. As the reaction between **1** and MeMgBr was originally carried out in a closed *J. Young* tube, one possible isomerization mechanism would be the reaction of **5** with CH_4 leading to obtaining the most stable compound **3**. Yet, DFT calculations showed that the energy barrier would be too high ($\Delta G^{\ddagger}$ = 45.3 kcal·mol^{-1}) (Figure 21) and experimentally we found that the isomerization also took place in the absence of CH_4. Although the complex resonating at 8.2 ppm could not be isolated, its multinuclear NMR pattern perfectly fits with its assignment as a diastereoisomer of **5** (compound **5'** in Figure 21) resulting from the activation of the alternative methyl group.

I.2.2 C−H activation by an unsaturated Ir(III)-Me complex

I.2.2.1 Introductory remarks

As described in section **I.1.5**, one of our goals when introducing a rather bulky terphenyl phosphine was accessing an analogue of the iconic Bergman complex $[(\eta^5\text{-}C_5Me_5)Ir(Me)(PMe_3)(ClCH_2Cl)]^+$ that has revealed an outstanding capacity to activate even the most inert C–H bonds. In the previous section, we have described in detail our previous attempts to synthesize such kind of systems by the reaction of an unsaturated cationic Cp*Ir(III) complex bearing a terphenyl phosphine with a variety of carbon nucleophiles. Contrary to our initial expectations, these reactions did not result in the anticipated methylation (or alkylation) of the vacant site at iridium and instead led to a series of activation reactions at the Cp* ligand or to a series of cyclometallation processes with the PMe_2Ar^{Dipp2} ligand.

These results prompted us to explore two alternative and complementary strategies to enhance the reactivity of Cp*Ir fragments containing bulky terphenyl phosphines towards intermolecular C–H bond activation. In the first, we considered substituting the PMe_2Ar^{Dipp2} ligand by an alternative terphenyl phosphine, namely PMe_2Ar^{Dtbp2} (Ar^{Dtbp2} = C_6H_3-2,6-(C_6H_3-3,5-$^t Bu_2$)$_2$).[74] The latter exhibits an even greater steric profile (V_{Bur} = 39.8 *vs* 41.6 % for PMe_2Ar^{Dipp2} *vs* PMe_2Ar^{Dtbp2}, respectively)[75] while maintaining comparable electronic properties, but more importantly, it locates the substituents of the lateral aryl rings at the 3,5-positions instead of the 2,6-

[74] Marín, M.; Moreno, J. J.; Navarro-Gilabert, C.; Álvarez, E.; Maya, C; Peloso, R.; Nicasio, M. C.; Carmona, E. *Chem. Eur. J.* **2019**, *25*, 260–272.
[75] Marín, M.; Moreno, J. J.; Alcaide, M. M.; Álvarez, E.; López-Serrano, J.; Campos, J.; Nicasio, M. C.; Carmona, E. *J. Organomet. Chem.* **2019**, *896*, 120–128.

positions. We anticipated that this longer distance from the alkyl groups to the binding phosphorus center may hamper the kind of intramolecular C–H bond activation processes described in prior work from the group[45] and also in the previous section **I.2.1** of this Thesis.

Besides, we envisioned a second complementary strategy to enhance the reactivity of our Cp*Ir fragments consisting of the reduction of the Ir(III) complexes to possibly more reactive Ir(I) species. These targeted compounds could be stabilized by π-type interactions with aryl rings of the terphenyl phosphines, at variance with the highly reactive analogous Ir(I) fragments photochemically accessed *in situ* by Bergman and Graham in 1982 (see Scheme 3 in the introductory section **I.1.3**),[29,30] which exhibited remarkable C–H bond activation reactivity. From the targeted Ir(I) compounds we aimed to explore not only the direct reactivity with other substrates including C–H bonds, but also to explore the reaction with carbon-based electrophiles that would lead to Bergman' compounds of type $[(\eta^5\text{-}C_5Me_5)Ir(R)(PR_3)(ClCH_2Cl)]^+$ but circumventing side reactions associated to the activation of the Cp* ligand by reaction with nucleophiles, as described in the previous section. Moreover, the two previously mentioned strategies, using ligand PMe_2Ar^{Dtbp2} and accessing reduced Ir(I) analogues, can also be combined, as will be described in detail across the present section.

I.2.2.2 Synthesis and characterization of complexes 6* and 1*

We started our studies by synthesizing the analogous Cp*Ir precursor described before but based on PMe_2Ar^{Dtbp2}. Complexes bearing the PMe_2Ar^{Dtbp2} phosphine will hereafter be denoted with an asterisk, while the absence of such will denote instead the presence of the PMe_2Ar^{Dipp2} phosphine, as it has been so far along this Chapter. Treatment of $[(\eta^5\text{–}C_5Me_5)IrCl_2]_2$ with PMe_2Ar^{Dtbp2} in CH_2Cl_2 yielded compound $[(\eta^5\text{-}C_5Me_5)IrCl_2PMe_2Ar^{Dtbp2}]$, **6*** (Scheme 12). This complex is characterized by a $^{31}P\{^1H\}$ resonance at –19.1 ppm, shifted by 19.4 ppm compared to the free phosphine (–38.5 ppm). The flanking aryl rings of the terphenyl phosphine ligand appear equivalent in the ^1H and $^{13}C\{^1H\}$ NMR spectra, suggesting either fast exchange or a symmetrical disposition.

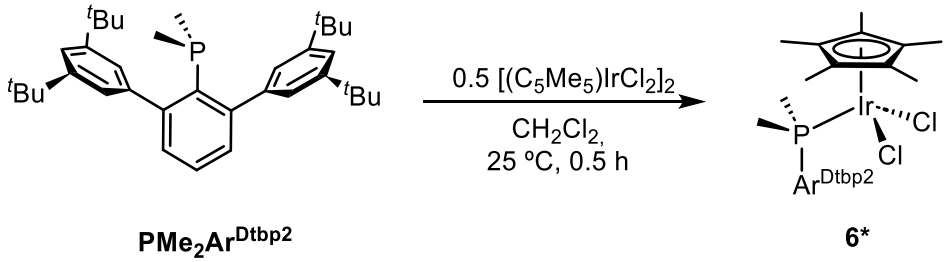

*Scheme 12. Synthesis of complex **6***.*

The formation of complex **6*** was somewhat surprising. The analogous neutral dichloride complex could not be obtained in the case of PMe_2Ar^{Dipp2}, as the reaction between the iridium Cp* dimer precursor and PMe_2Ar^{Dipp2} does not occur unless $Na[BAr^F]$ is added. In this case, the cationic compound **1** is formed.[45] Despite the bulkier character of phosphine PMe_2Ar^{Dtbp2}, we attribute its higher ability to coordinate to

iridium without the need of chloride abstraction to the less steric congestion in very close proximity to the metal center. This is indeed a very appealing feature of terphenyl phosphines, which allows to tune the steric effects not only in the first coordination sphere but also at longer range.

As in the PMe_2Ar^{Dipp2} system, chloride abstraction by $Na[BAr^F]$ was also straightforward and allowed isolation of the cationic complex $[(\eta^5\text{–}C_5Me_5)IrCl(PMe_2Ar^{Dtbp2})]^+$ (**1***) as its BAr^F salt (Scheme 13), analogous to complex **1**.[45] In the same fashion as complex **6***, the flanking aryl rings of the terphenyl phosphine ligand appear equivalent in the ^1H and $^{13}C\{^1H\}$ NMR spectra, which rules out a permanent metal-arene interaction in the unsaturated complex **1***. The existence and nature of a metal-arene interaction in this complex will be discussed further considering the X-ray diffraction and computational studies.

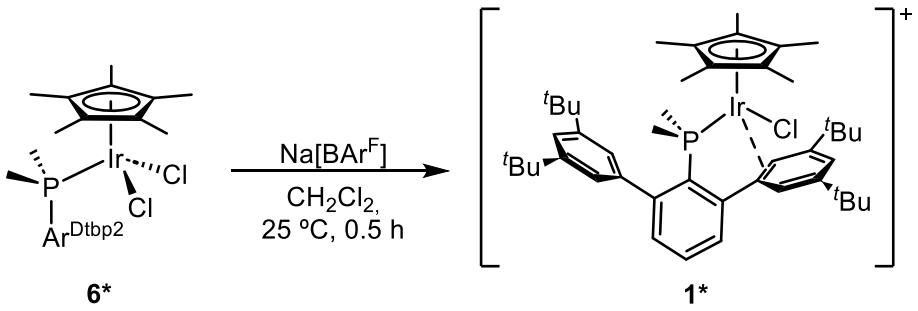

6* **1***

*Scheme 13. Synthesis of complex **1*** from **6***.*

The structures of the two new complexes were confirmed using crystallographic analysis (Figure 23). The long distances between the iridium center and the *ipso*-carbons of the lateral rings (5.222(4) and 4.046(4) Å) in complex **6*** are in agreement with the lack of a secondary interaction between the iridium center and any of the flanking aryl rings, as

expected for this saturated and neutral complex. In contrast, the structure of complex **1*** exhibits a pyramidalization of one of the *ipso*-carbons of one of the lateral rings of the phosphine, which exhibits a short Ir–C_{ipso} distance of 2.464(3) Å (*cf*. 5.400(3) Å for the non-interacting *ipso*-carbon). This agrees with the existence of a metal-arene interaction. An interesting difference that we found with respect to the PMe_2Ar^{Dipp2}-based compound **1**, is the longer Ir−Cl bond distance measured for complex **1*** (Ir−Cl = 2.428(8) Å; *cf*. (2.347(1) Å) for **1**) which seems to indicate that the chloride ligand is not acting as a π donor in the solid state, as it was proposed before for the latter compound.[45]

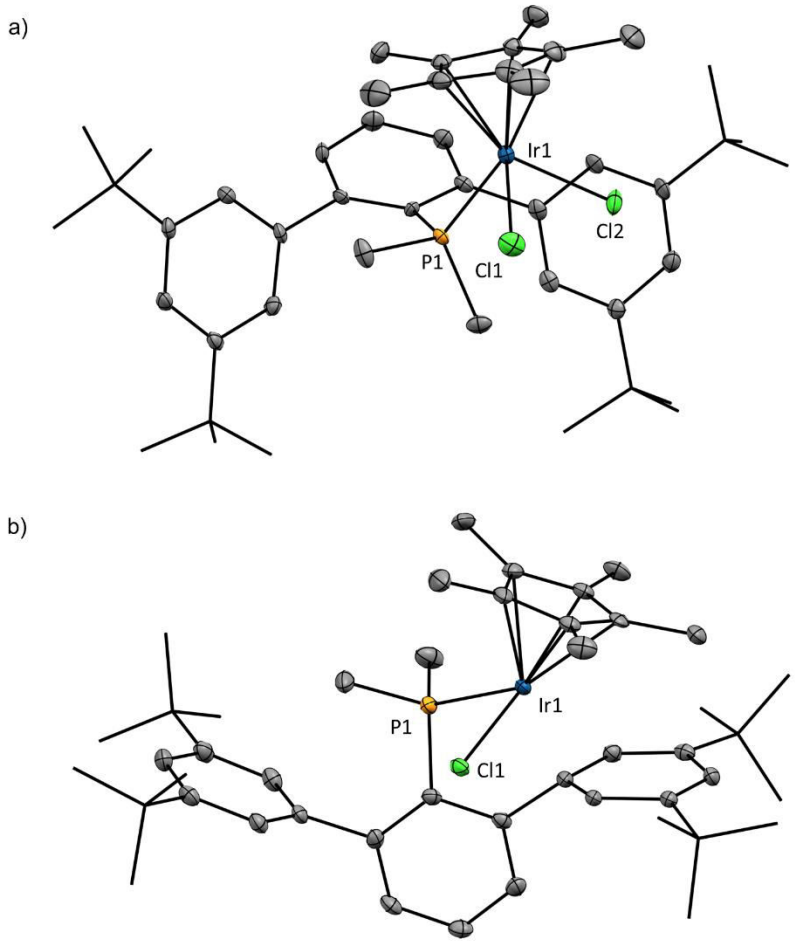

Figure 23. ORTEP diagram of complexes a) ***6****, and b)* ***1**** *([BAr^F]$^-$ counterion omitted for clarity). All hydrogen atoms are excluded for clarity and thermal ellipsoids are set at 50% probability. Wireframe is used to represent the tert-butyl groups.*

Topological studies[72] revealed a lack of bcp between the iridium atom and any of the carbon atoms of the lateral aryl rings for complex **6***, as expected. In contrast, the existence of a metal-arene interaction in complex **1*** was confirmed by the location of a bcp between the metal center and one of the lateral *ipso*-carbons (Figure 24 and Table 3), characterized by typical parameters for a metal ligand interaction.[73]

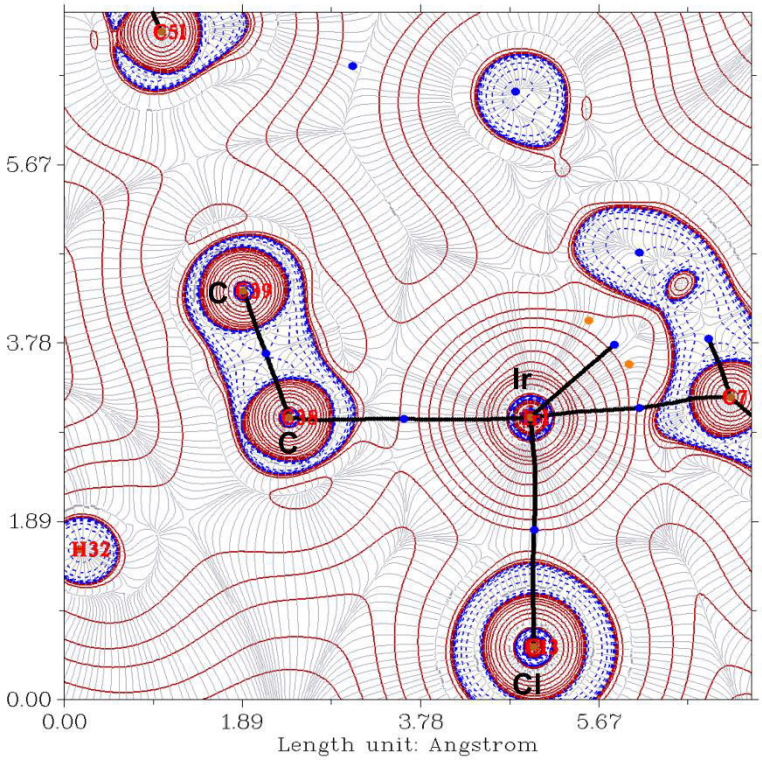

*Figure 24. Plot of the Laplacian of the electron density, $\nabla^2\rho$, of complex **1*** in the plane containing the Ir, C_{ipso}, and one of the C_{ortho} atoms. The Ir and C_{ipso} are connected by a bcp. Both C atoms belong to the Dtbp group which features an interaction with the metal center. The solid and dashed lines correspond to positive and negative values of $\nabla^2\rho$ respectively.*

Table 3. Selected properties of the electron density at relevant bcps shown in the previous figure.

bond	ρ^b	G_a^c	V_a^c	H_a^c	$\lvert V_a \rvert / G_a$	$\nabla^2\rho^d$
Ir–C_{ipso}	0.0442	0.0296	– 0.0372	– 0.0076	1.256	0.0890

[a] average values, [b] e·bohr^{-3}, [c] Hartree, [d] e·bohr^{-5}, e = elementary charge.

The contrasting difference in the interaction between the metal center and the phosphine moiety in complexes **6*** and **1*** was also explored by EDA-NOCV analysis. For complex **6***, the main contributions to the orbital interaction between the [Cp*IrCl$_2$] and phosphine fragments are depicted in Figure 25. These consist of the σ-donation of the HOMO of the phosphine moiety to an empty d orbital of the iridium center and a second, and weaker, backdonation from the metal center to the LUMO of the phosphine fragment.

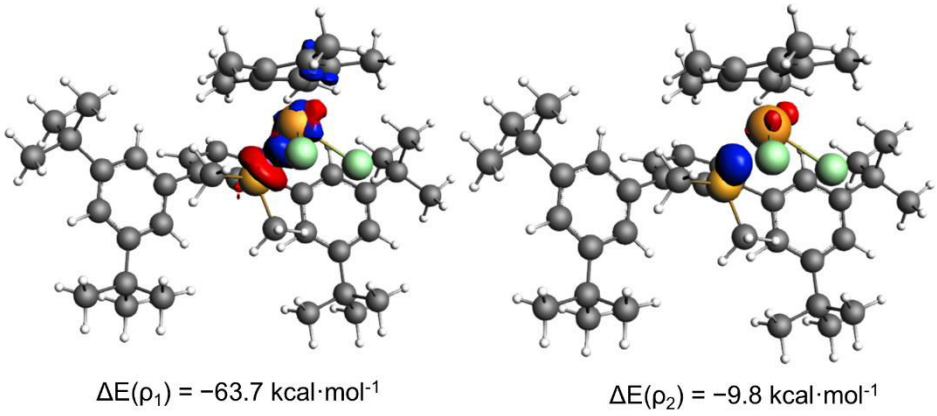

*Figure 25. Contour plots of NOCV deformation densities Δρ and associated energies ΔE(ρ) (computed at the ZORA-BP86-D3/TZ2P/PBE0-D3/SDD(Ir)/6-31(d,p)(all other atoms) level) in **6***.The fragments are defined as the phosphine moiety and the rest of the complex. Electron-density charge flows in the direction red→blue.*

In comparison, the EDA-NOCV analysis of the cationic complex **1*** revealed that the main contributions to the orbital interaction between the [Cp*IrCl$_2$] and phosphine fragments are the σ-donation of the phosphorous atom to an empty d orbital of the iridium center and the donation from the aryl ring to the metal center (Figure 26).

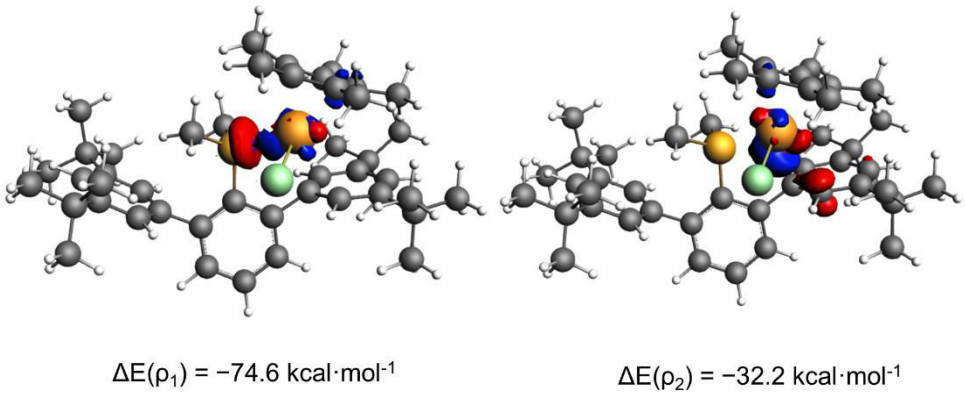

*Figure 26. Contour plots of NOCV deformation densities Δρ and associated energies ΔE(ρ) (computed at the ZORA-BP86-D3/TZ2P/PBE0-D3/SDD(Ir)/6-31(d,p)(all other atoms) level) in **1***.The fragments are defined as the phosphine moiety and the rest of the complex. Electron-density charge flows in the direction red→blue.*

All the aforementioned information points toward the existence of a metal-arene interaction in complex **1***. Nonetheless, lateral rings of the phosphine appear as equivalent by NMR spectroscopy, thereby this interaction must be weak and allow fast exchange in solution between the two flanking arenes of the terphenyl moiety.

I.2.2.3 Synthesis and characterization of complexes 7* and 7

With the cationic precursors, complexes **1** and **1***, in hand we explored the possibility to access their Ir(I) reduced versions, anticipating sufficient stabilization to the unsaturated compounds provided by the π-interactions with the terphenyl phosphines. Indeed, both complex **6*** and complex **1*** can be chemically reduced by reaction with 2 equiv. of $CoCp_2$ in dichloromethane yielding complexes **7** and **7*** (Scheme 14), respectively, in moderate yields (~ 45%) after 3h. The formation of the reduced compounds was clearly monitored by $^{31}P\{^1H\}$ NMR spectroscopy, where signals at 3.4 (for **7**) and –1.6 (for **7***) appear shifted to low frequencies compared to their cationic monochloride oxidized parent precursors (6.6 and 9.0 ppm for **1** and **1***, respectively). The ^1H NMR spectrum of complex **7*** revealed a doublet ($^3J_{HP}$ = 8.5 Hz) at 3.08 ppm for the proton in the *ortho*-position of one of the lateral rings of the phosphine ligand. This multiplicity is indicative of a strong interaction between the iridium center and the *ortho*-carbon as it is characteristic of a 3-bond-length coupling constant between hydrogen and phosphorous. This low frequency chemical shift is the result of a strong interaction between the metal center and the aryl ring, which is also supported by the $^{13}C\{^1H\}$ NMR spectrum. This shows a low frequency chemical shift of the *ipso*- and one of the *ortho*- carbons (49.5 and 40.9 ppm, respectively). Similarly, the $^{13}C\{^1H\}$ NMR spectrum of complex **7** exhibits a low frequency shift of 61.2 and 51.9 ppm for the *ipso* and *ortho* carbons of the aryl ring featuring an interaction with the metal center. This interaction is the cause of the absence of symmetry in complexes **7** and **7*** which results in high complexity of the ^1H NMR spectra, in contrast to that of their Ir(III) precursors **1**, **1*** and **6***. For the latter complexes, the flanking aryl rings of

the terphenyl phosphine ligand appear equivalent in the ^{1}H and $^{13}C\{^{1}H\}$ NMR spectra, suggesting either fast exchange or a symmetrical disposition, as discussed earlier.

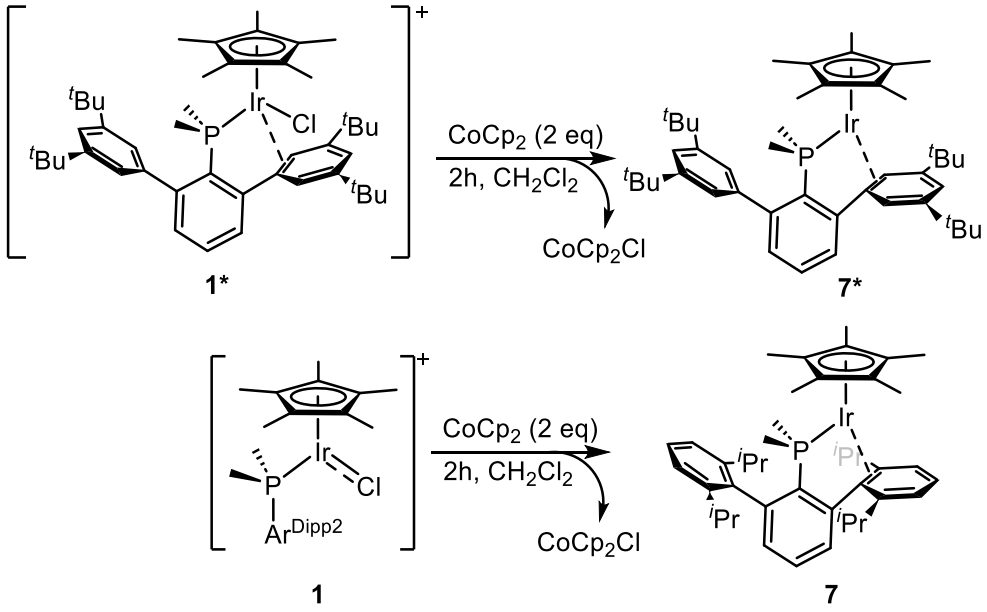

*Scheme 14. Chemical reduction of Ir(III) complexes **1** and **1*** toward Ir(I) compounds **7** and **7***, respectively.*

Single-crystals of complexes **7** and **7*** were grown from a concentrated pentane solution at –30 ºC and subjected to X–ray diffraction studies (Figure 27). These confirmed the proposed reduced formulation and the existence of interactions between the metal center and one of the lateral rings of the phosphine (**7***: Ir–C_{ipso} = 2.139(4) , Ir–C_{ortho} = 2.130(5) Å; **7**: Ir–C_{ipso} = 2.143(5), Ir–C_{ortho} = 2.157(5) Å).

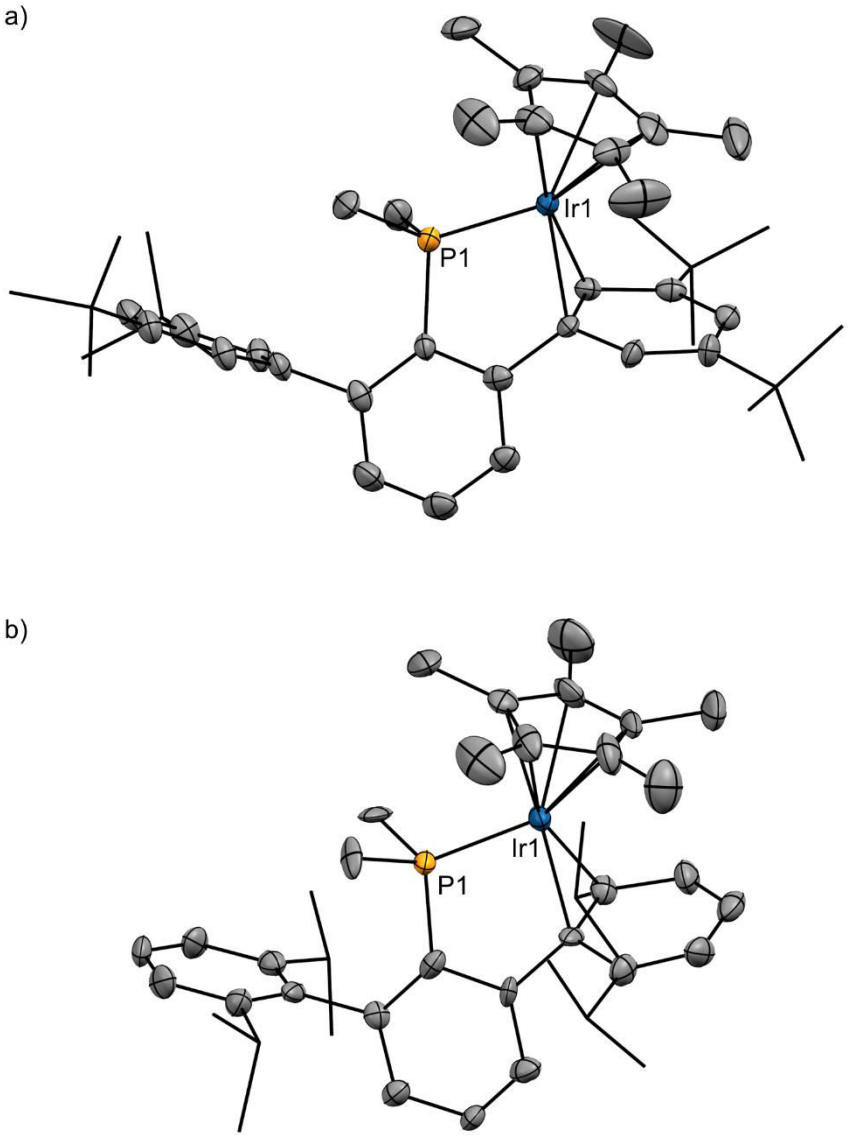

*Figure 27. ORTEP diagram of complexes a) **7***, and b) **7**. All hydrogen atoms are excluded for clarity and thermal ellipsoids are set at 50% probability. Wireframe is used to represent the tert-butyl and iso-propyl groups.*

These results indicate that the aryl ring is indeed acting as a π-donor in a η^2-fashion stabilizing the otherwise highly unsaturated metal complexes.

The comparison between the current Ir(I) complex and previously studied Ir(III) systems reveals an intriguing dichotomy. In the case of Ir(III), the metal center required a strong π-donor to stabilize the vacant coordination site. However, the current Ir(I) complex presents a more reduced oxidation state and neutral character. On one hand, this reduction might imply a decreased need for electron density donation from the aryl ring. On the other hand, the high unsaturation of the complex suggests that it would still favor interaction with a strong ligand. These opposing factors raise important questions about the relative donor/acceptor capacity of the aryl ring in this system compared to the Ir(III) complexes. To address this notion, we performed Energy Decomposition Analysis (EDA), which provides quantitative insights into the strength of the π-donation. These studies revealed that the interaction energy between the phosphine and Cp*Ir moiety is significantly higher in complexes **7** and **7*** than in complexes **6*** and **1*** (Table 4).

*Table 4. EDA-NOCV results of different Cp*Ir complexes. Fragments are defined as the phosphine and the rest of the complex. An oxidation state of III is assumed for complexes **1*** and **6***, while I is assumed for **7** and **7***. All values in kcal·mol^{-1}.*

Entry	Complex	ΔE^{int}	ΔE^{elec}	ΔE^{orb}	ΔE^{Pauli}	ΔE^{disp}
1	**1***	– 136.4	– 231.0	– 163.1	298.2	– 40.6
2	**6***	– 121.2	– 179.5	– 84.8	234.6	– 35.3
3	**7**	– 175.5	– 435.5	– 324.7	620.9	– 36.1
4	**7***	– 192.0	– 472.8	– 395.1	709.6	– 33.6

In fact, while the main contribution to the orbital term in complexes **6*** and **1*** is the σ-donation from the HOMO of the phosphine fragment atom to

the iridium center, this interaction is only the second most important one in complex **7*** (Figure 28), where the donation from the aryl to the metal center and the backdonation of the latter to the former represents the most important contribution. In a similar way, in complex **7**, the main orbital contribution consists of a mixture of σ-donation from the HOMO of the phosphine and backdonation from the iridium center to the aryl group, while the second contribution consists of the π-donation from the arene to the metal. The importance of the interaction with the lateral aryl ring in complexes **7** and **7*** may indicate that the oxidation state of the iridium center may actually be higher than +1 and somewhat approaching a metalacyclopropane-type structure.

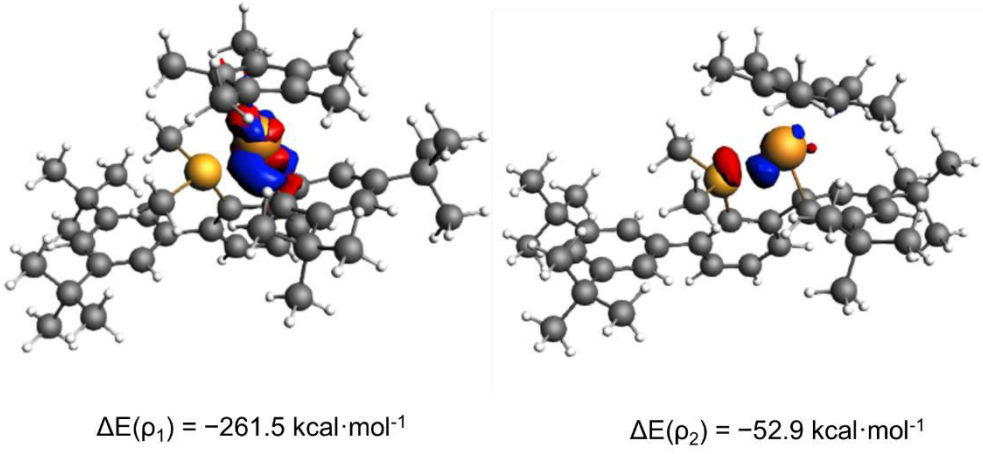

*Figure 28. Contour plots of NOCV deformation densities Δρ and associated energies ΔE(ρ) in **7***. The fragments are defined as the phosphine moiety and the rest of the complex. Electron-density charge flows in the direction red→blue.*

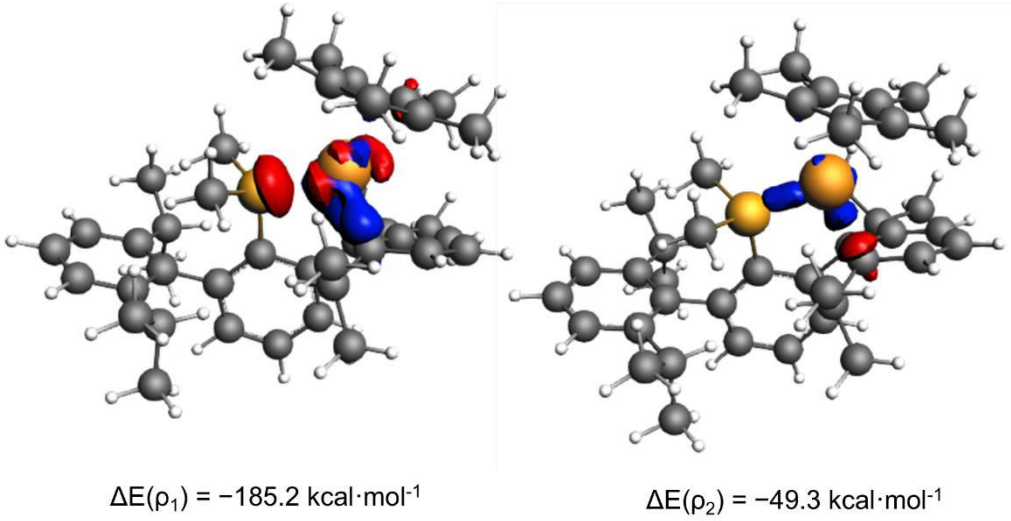

Figure 29. Contour plots of NOCV deformation densities Δρ and associated energies ΔE(ρ) in 7. The fragments are defined as the phosphine moiety and the rest of the complex. Electron-density charge flows in the direction red→blue.

Additionally, topological analysis offers a complementary perspective on the nature of the metal-ligand interaction. In complex **1*** only a single bcp between the metal center and any of the carbon atoms of the lateral aryl ring, namely a bcp between the Ir and C_{ipso} atom, was found (Figure 24). In contrast, complexes **7** and **7*** feature both a bcp involving the Ir and the C_{ipso} and a bcp involving the Ir and the C_{ortho} of one of the lateral rings (Figure 30 and Figure 31).

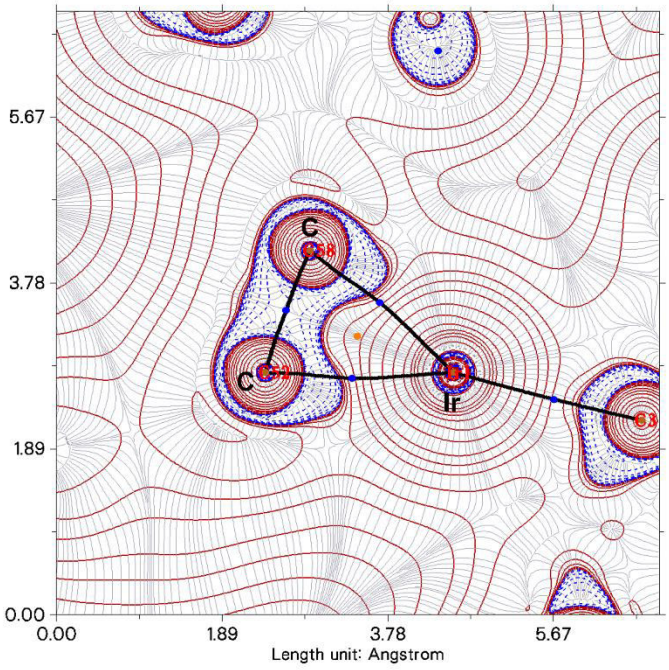

*Figure 30. Plot of the Laplacian of the electron density, $\nabla^2\rho$, of complex **7*** in the plane containing the Ir, C_{ipso}, and one of the C_{ortho} atoms. Both C atoms belong to the Dtbp group which features an interaction with the metal center. The solid and dashed lines correspond to positive and negative values of $\nabla^2\rho$, respectively.*

Table 5. Selected properties of the electron density at relevant bcps shown in the previous figure.

bond	ρ^b	$G_a{}^c$	$V_a{}^c$	$H_a{}^c$	$\lvert V_a \rvert / G_a$	$\nabla^2\rho^d$
Ir–C_{ipso}	0.10744	0.07928	– 0.12337	– 0.04409	1.5561	0.14669
Ir–C_{ortho}	0.10572	0.07937	– 0.12189	– 0.04252	1.5357	0.15328
C–C	0.26248	0.08132	– 0.30878	– 0.22746	3.7971	– 0.58457

[a] average values, [b] e·bohr^{-3}, [c] Hartree, [d] e·bohr^{-5}, e = elementary charge.

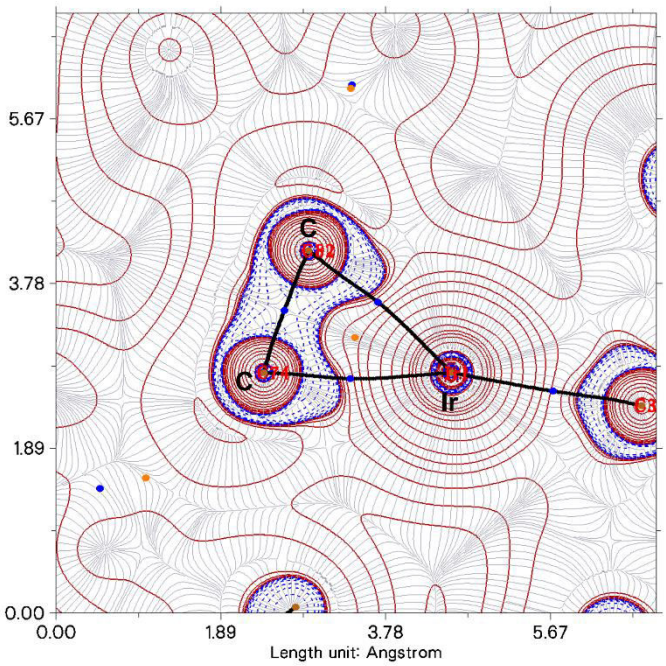

*Figure 31. Plot of the Laplacian of the electron density, $\nabla^2\rho$, of complex **7** in the plane containing the Ir, C_{ipso}, and one of the C_{ortho} atoms. Both C atoms belong to the Dipp group which features an interaction with the metal center. The solid and dashed lines correspond to positive and negative values of $\nabla^2\rho$ respectively.*

Table 6. Selected properties of the electron density at relevant bcps shown in the previous figure.

bond	ρ^b	G_a^c	V_a^c	H_a^c	$\lvert V_a \rvert / G_a$	$\nabla^2\rho^d$
Ir–C_{ipso}	0.1057	– 0.0782	– 0.1211	– 0.0428	1.548	0.1477
Ir–C_{ortho}	0.1060	– 0.0760	– 0.1192	– 0.0431	1.568	0.1371
C–C	0.2557	0.0792	– 0.2956	– 0.2163	3.732	– 0.5486

[a] average values, [b] e·bohr^{-3}, [c] Hartree, [d] e·bohr^{-5}, e = elementary charge.

I.2.2.4 Reactivity of complexes 7* and 7 toward MeOTf

As discussed in section **I.1.3**, Cp*Ir(I) complexes, such as Graham's complex illustrated in Scheme 4, have demonstrated the ability to successfully activate C–H bonds of external substrates. To investigate similar reactivity from the newly synthesized complexes **7** and **7***, we attempted reactions with various alkanes, including pentane, hexane, and methane; however, these reactions proved unsuccessful. Similarly, no reaction was observed with alkenes such as ethylene and styrene. Furthermore, these complexes showed no reactivity toward small molecules like H_2, CO, NH_3, or H_2O, which reflects the great stabilizing capacity provided by coordination to the flanking aryl rings of the phosphine. However, despite this lack of reactivity, the complexes are highly oxidation-sensitive and decompose upon exposure to air.

Surprisingly, although compounds **7** and **7*** are apparently equivalent, they showed contrasting reactivity towards MeOTf (OTf^- = trifluoromethanesulfonate). Thus, **7*** reacted rapidly with the carbon electrophile to afford cleanly a new cationic species, complex **8***, as the triflate salt (Scheme 15). At variance, complex **7** did not react even when heated at 80 °C for 24 h. The formation of **8*** was confirmed by $^{31}P\{^1H\}$ NMR spectroscopy (**7***, –1.6; **8***, 8.6 ppm), while the ^1H NMR spectrum of **8*** evinced the incorporation of a methyl group on the metal center, featuring a doublet with intensity corresponding to 3 H at 0.56 ppm ($^3J_{HP}$ = 6.4 Hz). The corresponding carbon resonates as a doublet at –14.9 ppm ($^2J_{CP}$ = 14 Hz). Complex **8*** can also be synthesized with $[BAr^F]^-$ as counteranion by directly reacting **1*** with methyl magnesium bromide (Scheme 15). However, the latter method led to variable amounts of

bismethylation, as will be discussed further in this Chapter, and therefore the route involving MeOTf was preferred for synthetic purposes.

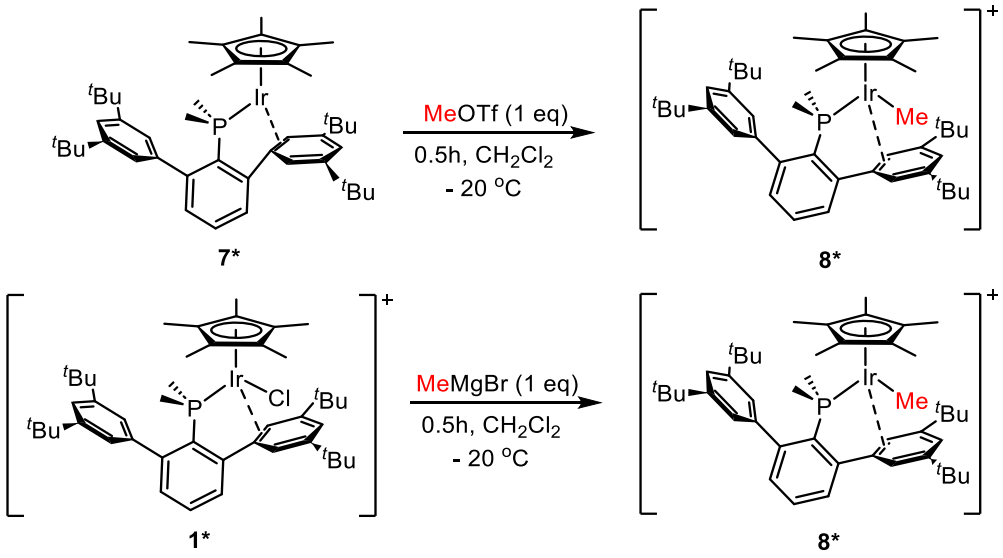

*Scheme 15. Synthesis of complex **8*** from **7*** or **1***.*

DFT studies confirmed the contrasting reactivity of complexes **7** toward MeOTf. While for both species the electrophilic attack of MeOTf is thermodynamically favored (**7***, ΔG = −17.8 kcal·mol^{-1}; **7**, ΔG = −13.2 kcal·mol^{-1}), the energy barrier for complex **7** is inaccessible (**7***, $\Delta G^{\ddagger}$ = 18.6 kcal·mol^{-1}; **7**, $\Delta G^{\ddagger}$ = 35.6 kcal·mol^{-1}) (Figure 32).

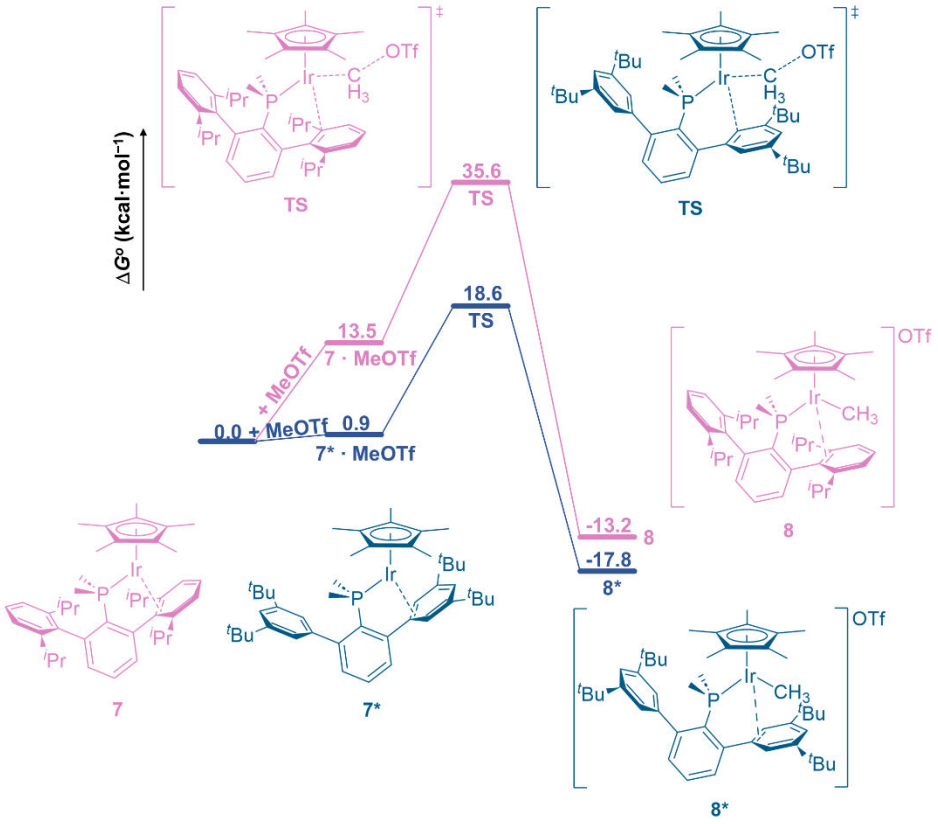

*Figure 32. Free energy profile of the proposed mechanism for the formation of **8*** and **8** in blue and pink, respectively.*

Considering the surprisingly high difference in energy for the two aforesaid transition states ($\Delta\Delta G^{\ddagger}$ = 17.0 kcal·mol^{-1}), we decided to explore this difference in reactivity through Activation Strain Analysis. The Activation Strain Model (ASM) provides a fragment-based approach to understanding reaction barriers by decomposing the potential energy surface (ΔE^{total}) along the reaction coordinate into two key contributions: the strain energy

(ΔE^{strain}) and the interaction energy (ΔE^{int}).[76] The strain energy reflects the structural deformation required for reactants to progress along the reaction pathway and is generally destabilizing, while the interaction is related to the bonding capabilities and mutual interaction between the increasingly deformed reactants along the same pathway, typically stabilizing. The interplay between these components determines the reaction barrier. This type of analysis can be used to determine the reason behind differences in energy barriers among similar systems.[77]

As can be seen in Figure 33a, while the ΔE^{int} remains quite similar for both systems along the reaction coordinate (i.e. the Ir–C bond under formation), there is an important difference between the ΔE^{strain} that is maintained along the reaction coordinate. The strain term can be broken down into the contribution from the iridium complex and that of the MeOTf moiety, as shown in Figure 33b. This study exposes that the elevated difference in the strain energy term relies on the higher deformation that the complex in the PMe_2Ar^{Dipp2}-system must undergo. In summary, the difference between the energy barriers is caused by the steric hindrance of the *iso*-propyl groups in the positions 2- and 6- of the flanking aryl rings which prevents the formation of the corresponding Ir–Me species for the PMe_2Ar^{Dipp2} phosphine (Figure 33).

[76] For reviews on this topic see: a) Bickelhaupt, F. M.; Houk, K. N. *Angew. Chem. Int. Ed.* **2017**, *56*, 10070–10086. b) Wolters, L. P.; Bickelhaupt, F. M. *WIREs Comput. Mol. Sci.* **2015**, *5*, 324–343.
[77] Fernández, I.; Bickelhaupt, F. M. *Chem. Soc. Rev.* **2014**, *43*, 4953–4967

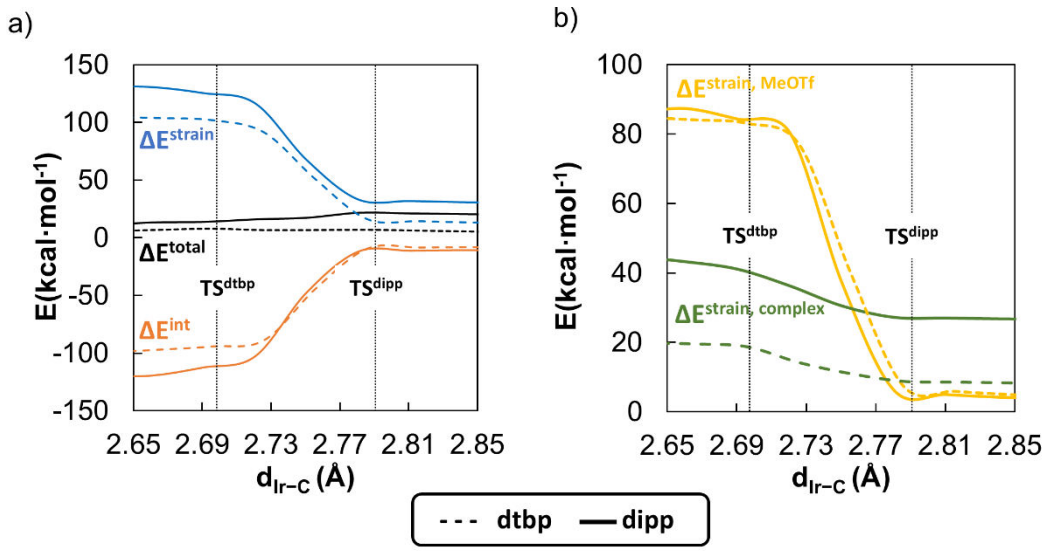

Figure 33. Activation strain analyses of the electrophilic attack of MeOTf to ***7*** *(solid lines) or* ***7**** *(dashed lines) projected onto the Ir-C bond-forming distance. a) Comparative activation strain analyses; b) Comparative strain energies of the [Ir] and MeOTf fragments. The Ir–C distance at which the transition states take place is indicated with dotted vertical lines.*

I.2.2.5 Intramolecular C–H bond activation of complex 8*

As a result of the highly reactive nature of complex **8***, this species reacts rapidly with one of the *tert*-butyl groups to eliminate methane, observed as a singlet at 0.24 ppm in the ^{1}H NMR spectrum, yielding complex **9*** (Scheme 16). This complex features two distinctive doublets at 2.36 and 1.81 ppm ($^{2}J_{HH}$ = 8.5 Hz) with intensity corresponding to 1 H each due to the two diastereotopic protons of the metalated methylene unit, which was corroborated by a correlation of the two resonances in the HSQC NMR spectrum with the same carbon resonance (^{13}C{^{1}H} NMR resonance at –2.2 ppm, $^{2}J_{CP}$ = 14 Hz).

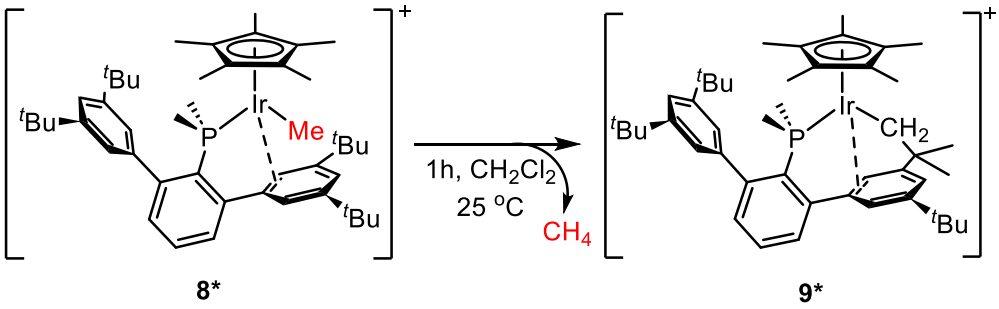

8* **9***

*Scheme 16. Formation of complex **9*** from complex **8***.*

The mechanism of the intramolecular activation of one of the *tert*-butyl groups leading to the elimination of methane was investigated by DFT studies. The formation of **9*** was found to be endothermic (ΔG = 11.9 kcal·mol^{-1}), yet the elimination of methane gas is likely the driving force of the process (Figure 34). Our studies rule out an oxidative addition pathway, as it proceeds through a highly energetic Ir(V) (ΔG = 60.8 kcal·mol^{-1}) intermediate (**C** in Figure 28) which features a slipped Cp* ligand to

alleviate steric hindrance. Although we have been unable to find a suitable transition state, we believe that the release of methane proceeds instead through a σ-bond metathesis mechanism, which would not be surprising considering that the same was proposed for the elimination of methane in the case of the PMe_2Ar^{Dipp2} system for the analogous methyl compound (see compound **A** and intermediate **B3** in Figure 21).

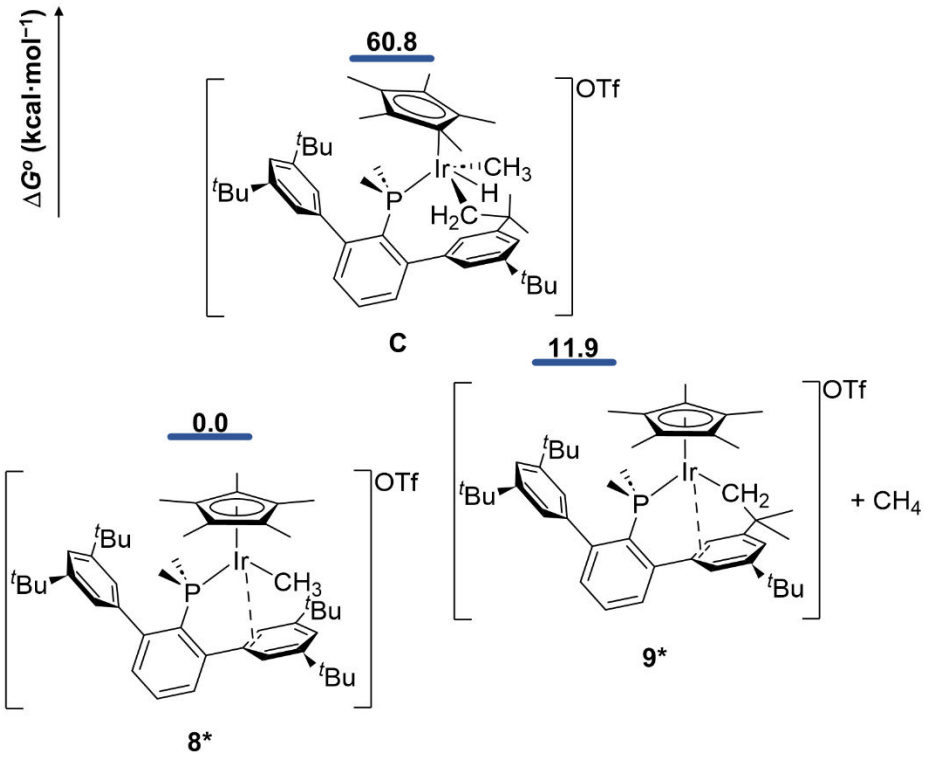

*Figure 34. Relative free energies between compounds **8*** and its evolution product **9***, including a potential oxidative addition intermediate **C** at too high energy.*

I.2.2.6 Reactivity of complexes 8* and 9* toward dihydrogen

The evolution of compound **8*** towards **9*** at room temperature ($t_{1/2} \approx 15$ min) forced us to characterize the former at low temperature to avoid the formation of **9***. At –20 ºC compound **8*** remained stable in solution, which allowed us to preliminary explore its reactivity. Indeed, it reacts rapidly with H_2 with concomitant release of methane and formation of the corresponding iridium hydride species **10*** (Scheme 17). This is evidenced by the ^{1}H NMR spectrum, which features a low-frequency doublet with intensity corresponding to 1 H that resonates at –16.6 ppm ($^2J_{HP}$ = 31.9 Hz). Interestingly, complex **10*** can also be formed by reacting complex **9*** with H_2 (Scheme 17), which further supports the proposed structure of **9*** for which we could not obtain definitive authentication through X-ray crystallography. Moreover, the reaction between **1*** and $PhSiH_3$ also yields the hydride complex **10***, corroborating its proposed structure (Scheme 18).

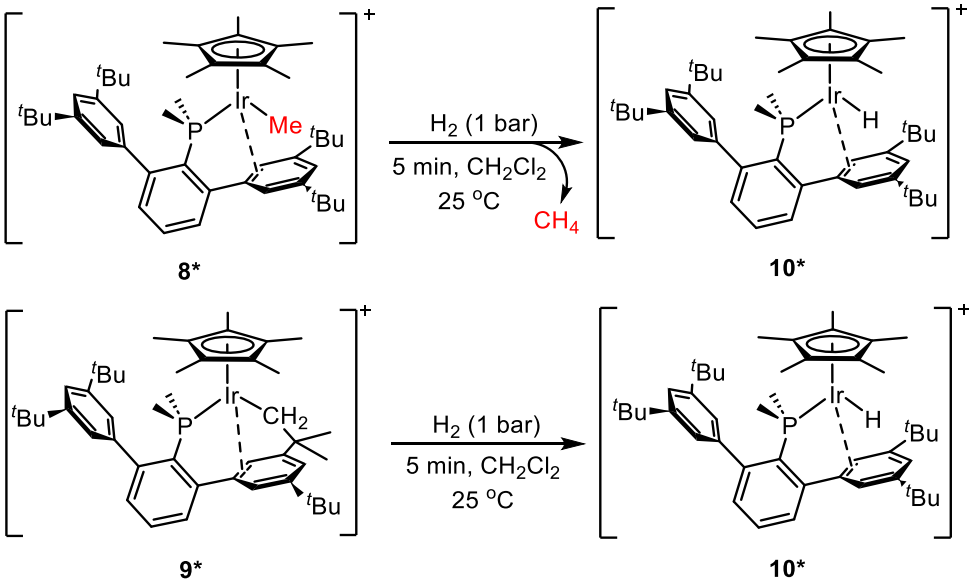

*Scheme 17. Synthesis of complex **10*** from **8*** or **9***.*

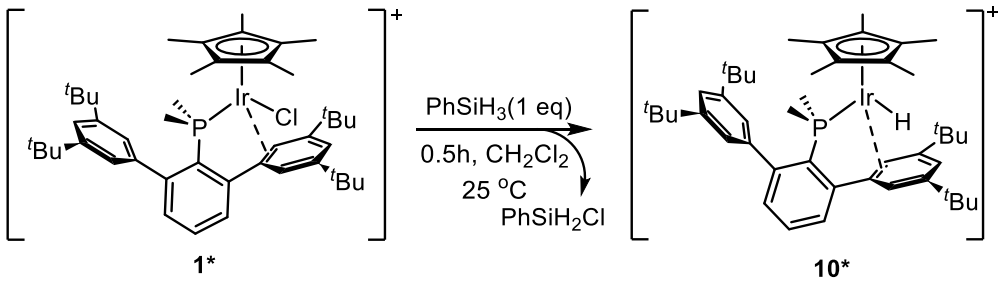

*Scheme 18. Synthesis of complex **10*** from **1***.

Next, we investigated the mechanisms of formation of the hydride complex **10***, by DFT studies, to explore whether different mechanisms might be taking place depending on the Ir(III) precursor. In the case of the reaction between **9*** and H_2, our analysis supports an oxidative addition pathway (Figure 35).

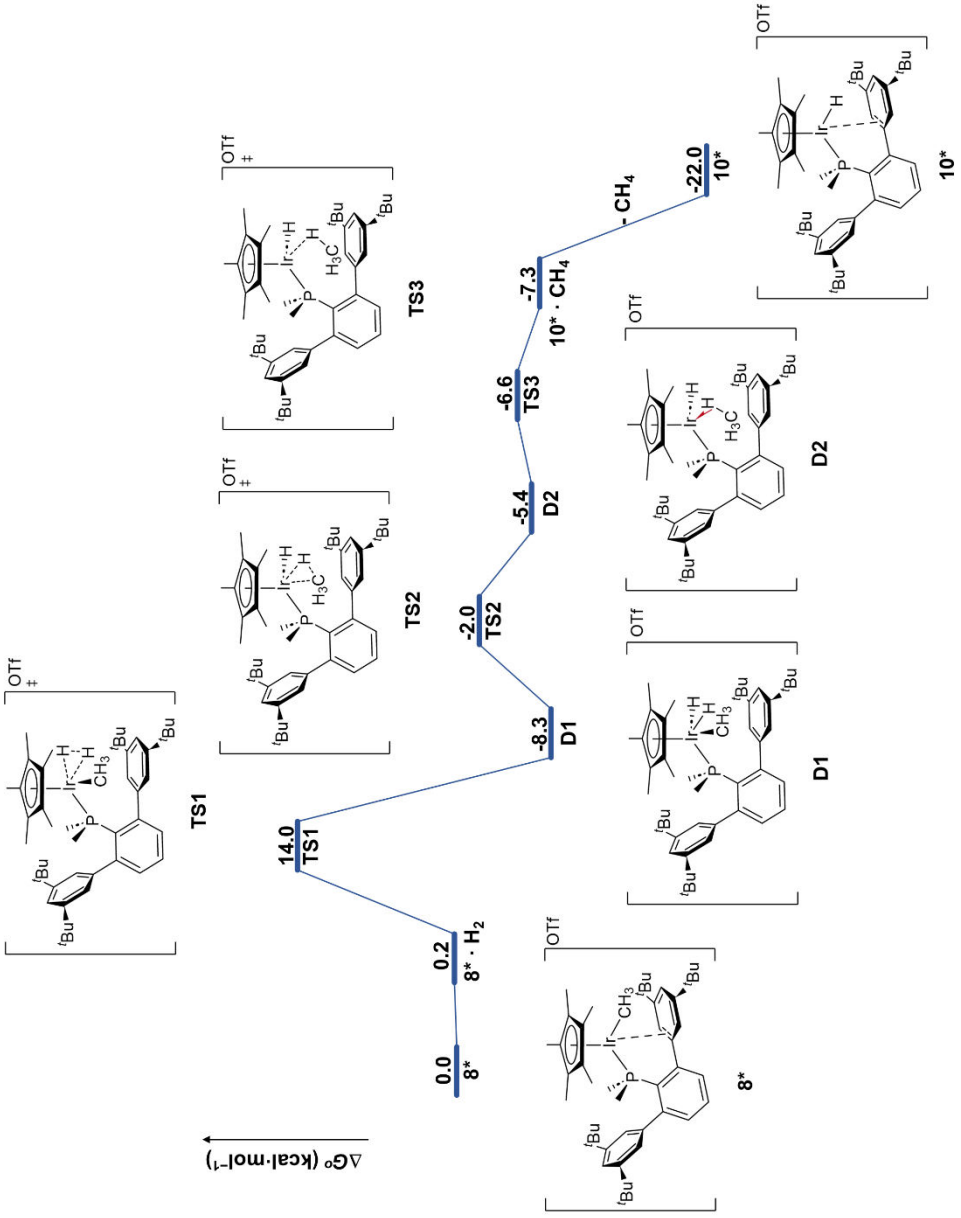

Figure 35. Free energy profile for the formation of ***10**** *from* ***8**** *and* H_2.

The mechanism depicted in Figure 35 consists of a first transition state (TS1, $\Delta G^{\ddagger}$ = 14.0 kcal·mol^{-1}) that leads to a dihydride Ir(V) intermediate (**D1**, ΔG = –8.3 kcal·mol^{-1}). This step is followed by the formation of an agostic interaction (**D2**)[71] between the newly formed CH_4 group and the metal center (TS2, $\Delta G^{\ddagger}$ = 6.3 kcal·mol^{-1}). Intermediate **D2** was characterized topologically[72] (Figure 36) showing the presence of a bcp connecting the hydrogen and iridium atoms. This bcp features parameters expected for a metal-ligand interaction (Table 7).[73]

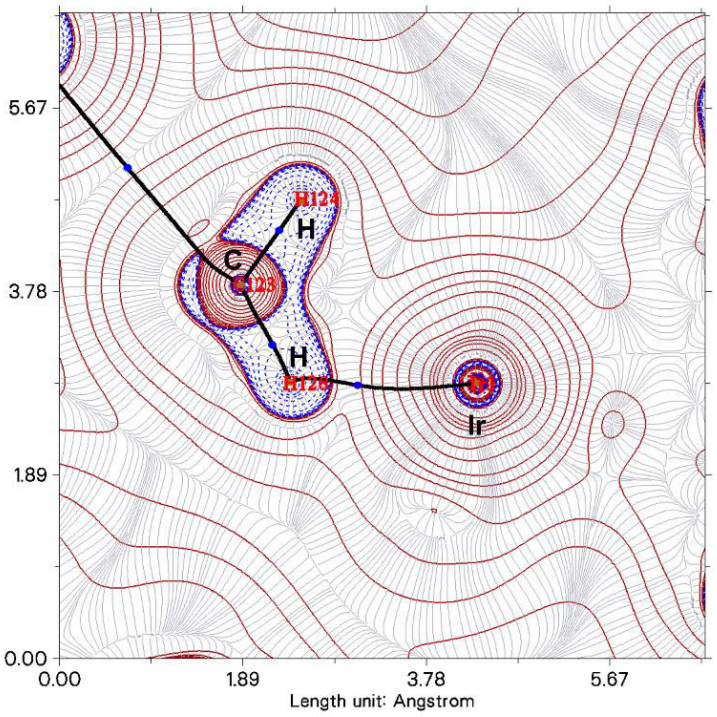

*Figure 36. Plot of the Laplacian of the electron density, $\nabla^2\rho$, of intermediate **D2** of Figure 35 in the plane containing the Ir atom and the H and C atoms of the forming CH_4. The solid and dashed lines correspond to positive and negative values of $\nabla^2\rho$ respectively.*

Table 7. Selected properties of the electron density at relevant bcps shown in the previous figure.

bond	ρ^b	$G_a{}^c$	$V_a{}^c$	$H_a{}^c$	$\lvert V_a \rvert / G_a$	$\nabla^2\rho^d$
Ir–H	0.0595	0.0546	– 0.0698	– 0.0152	1.279	0.1599
H–C	0.2357	0.0502	– 0.2649	– 0.2147	5.276	– 0.6579

[a] average values, [b] e·bohr^{-3}, [c] Hartree, [d] e·bohr^{-5} , e = elementary charge.

Finally, methane is release from intermediate **D2** upon overcoming a small energy barrier of 1.2 kcal·mol^{-1} leading to the thermodynamically favored monohydride species **10*** (ΔG = –22.0 kcal·mol^{-1}). At variance with the aforementioned mechanism, the reaction between compound **5** and H_2 seems to proceed through a different route (Figure 37). In this case, our computational studies back a coordination of the dihydrogen molecule resulting in a σ-complex intermediate (TS1, $\Delta G^{\ddagger}$ = 8.1; **E**, ΔG = –6.3 kcal·mol^{-1}).

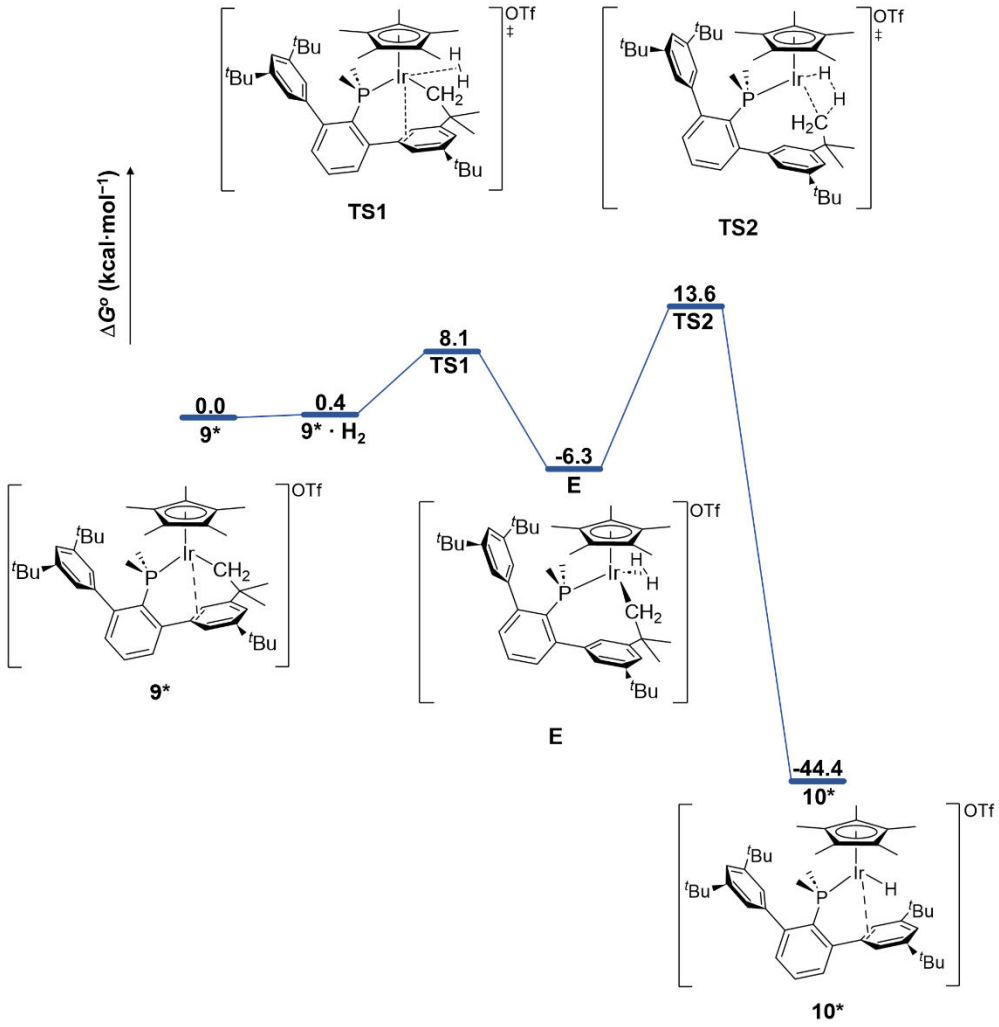

*Figure 37. Free energy profile for the formation of **10*** from **9*** and H_2.*

Topological studies[72] of **E** (Figure 38) revealed the existence of a bcp connecting the iridium center with each of the nascent hydrides, as well as a remaining bcp, of covalent character ($|V|/G > 4$)[73](Table 8), between the hydrogen atoms, as expected for a σ-complex.

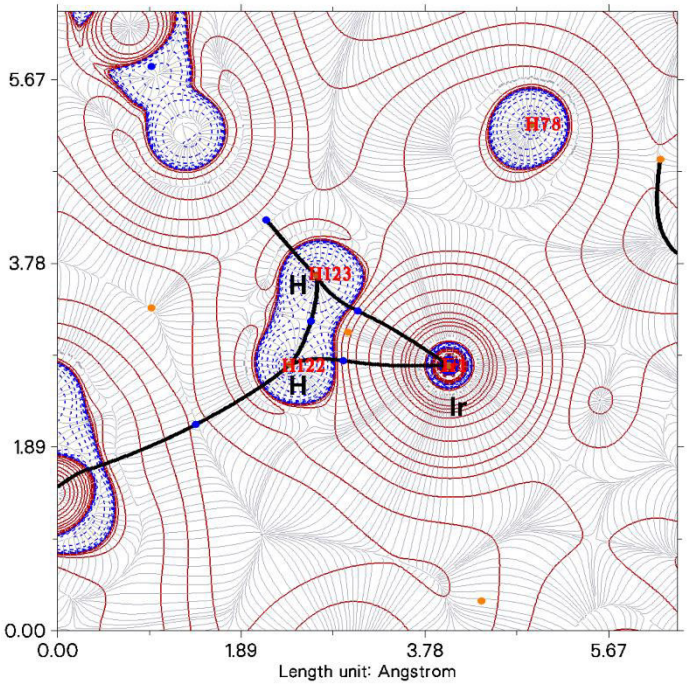

*Figure 38. Plot of the Laplacian of the electron density, $\nabla^2\rho$, of intermediate **E** of Figure 37 in the plane containing the Ir atom and the H atoms of the previous H_2. The solid and dashed lines correspond to positive and negative values of $\nabla^2\rho$ respectively.*

Table 8. Selected properties of the electron density at relevant bcps shown in the previous figure.

bond	ρ^b	$G_a{}^c$	$V_a{}^c$	$H_a{}^c$	$\lvert V_a \rvert / G_a$	$\nabla^2\rho^d$
Ir–H	0.1341	0.1224	– 0.1844	– 0.0620	1.506	0.2554
Ir–H	0.1322	0.1150	– 0.1757	– 0.0607	1.528	0.1322
H–H	0.3067	0.0998	– 0.4041	– 0.3043	4.050	– 0.8181

[a] average values, [b] e·bohr^{-3}, [c] Hartree, [d] e·bohr^{-5}, e = elementary charge.

Intermediate **E** undergoes the elimination of the newly formed methyl group with regeneration of the non-metalated phosphine via a σ-bond

metathesis transition state (TS2, $\Delta G^{\ddagger}$ = 19.9, ΔG = – 44.4 kcal·mol^{-1}) (Figure 37). Topological studies[72] performed on this transition state show that there is a bcp between the iridium and hydrogen atoms, as well between the iridium atom and the carbon atom of the nascent methyl group (Figure 39 and Table 9). The bcp between the carbon and hydrogen atoms features an intermediate character between an ionic and covalent interaction ($1 < |V|/G < 2$).[73] This fact together with the absence of a bcp between the two hydrogens denotes a late-character for this transition state.

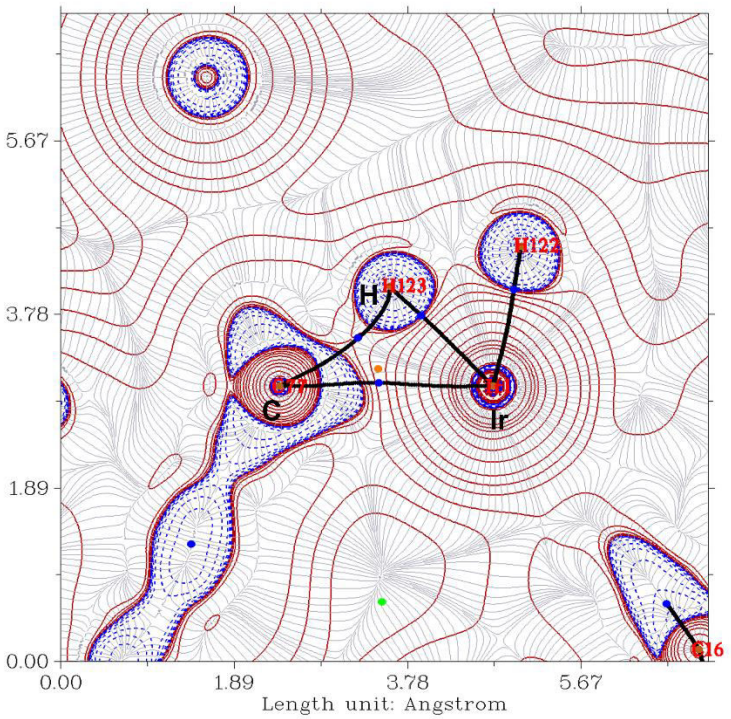

*Figure 39. Plot of the Laplacian of the electron density, $\nabla^2\rho$, of intermediate **TS2** of Figure 37 in the plane containing the Ir atom and the H atoms of the previous H_2. The solid and dashed lines correspond to positive and negative values of $\nabla^2\rho$ respectively.*

Table 9. Selected properties of the electron density at relevant bcps shown in the previous figure.

bond	ρ^b	$G_a{}^c$	$V_a{}^c$	$H_a{}^c$	$\lvert V_a \rvert / G_a$	$\nabla^2\rho^d$
Ir–C	0.0821	0.0495	– 0.0728	– 0.0233	1.470	0.1073
C–H	0.0871	0.0388	– 0.0671	– 0.0283	1.730	– 0.0419
Ir–H	0.1598	0.1041	– 0.2052	– 0.1010	1.970	0.0250

[a] average values, [b] e·bohr^{-3}, [c] Hartree, [d] e·bohr^{-5} , e = elementary charge.

In relation to the oxidative addition pathway found for complex **8*** and the σ-bond metathesis one found for complex **9***, it is interesting to observe that within the same organometallic framework different mechanisms are in operation even for rather similar reactivities.

I.2.2.7 Synthesis and characterization of complex 11*

To complete these preliminary studies, we wondered whether we could access a neutral dimethyl complex from compound **8***, which would be analogous to the corresponding neutral dichloride **6*** that was only accessible in the case of the PMe_2Ar^{Dtbp2} system. Indeed, complex **8*** reacts with MeMgBr to yield a doubly methylated neutral complex, **11*** (Scheme 19). Complex **11*** features a resonance in the $^{31}P\{^1H\}$ NMR spectrum at –30.0 ppm, and thus, low-frequency-shifted with respect to that of complex **8*** (8.6 ppm) and closer to the chemical shift of the free phosphine (–38.5 ppm). This indicates a lack of interaction between the metal center and any of the lateral aryl rings, as foreseen for a saturated species (the same was observed for compound **6*** which features a resonance at –19.1 ppm in the $^{31}P\{^1H\}$ NMR spectrum). The ^1H NMR spectrum of this complex exhibits a doublet with intensity corresponding to 6 H at –0.47 ppm ($^3J_{HP}$ = 5.1 Hz) assigned to the two equivalent methyl groups coordinated to the iridium center. The associated carbon atoms resonate at –20.8 ppm in the $^{13}C\{^1H\}$ spectrum as a doublet ($^2J_{CP}$ = 10 Hz).

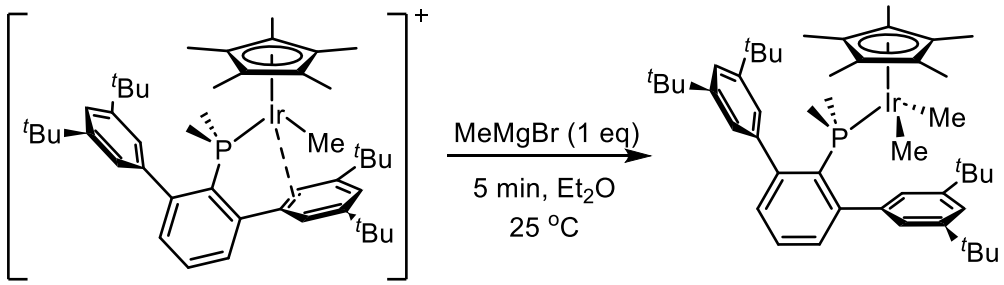

8* **11***

*Scheme 19. Synthesis of complex **11**.*

The proposed structure of complex **11*** was further corroborated by XRD analysis (Figure 40). The X-ray diffraction data of complex **11*** does not have enough quality to produce a structure of sufficiently high standards for a comprehensive geometric analysis, but connectivity is evident and bond lengths can be used for comparison purposes. The geometric parameters of complex **11*** are comparable to those of the dichlorinated neutral complex **6***. The Ir–C bond length distances are 2.081 and 2.125 Å, shorter than the Ir–Cl distances in complex **6*** (2.383(1) and 2.419(1) Å), as expected. The C–Ir–C angle is 75.35º, narrower than the Cl–Ir–Cl angle (81.85(5)º) of complex **6***. The lack of torsion of the lateral rings of the phosphine ligands (174.3 and 178.3º), closely resembling those found in complex **6*** (168.5(4) and 173.3(4)º), indicates negligible interaction with the metal center.

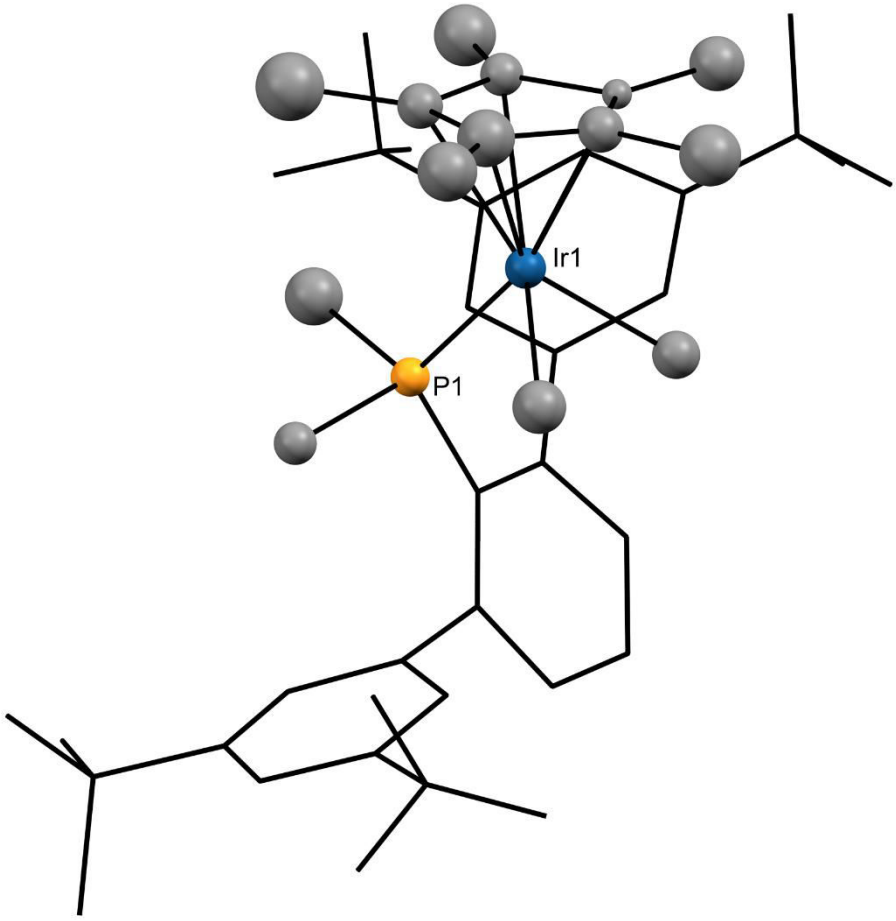

*Figure 40. X-ray diffraction structure of complex **11*** to show the connectivity, refined in isotropic mode due to the very low quality of the crystal.*

Considering the unexpected activation of the Cp^* ligand described in section **I.2.1** of this Chapter, we decided to investigate the mechanisms of the latter methylation reaction by DFT methods. In agreement with our experiments, it involves the facile ($\Delta G^{\ddagger}$ = 10.0 kcal·mol^{-1}) direct nucleophilic attack of the MeMgBr molecule on the metal center leading to the highly thermodynamically favored product **11*** (ΔG = –35.9 kcal·mol^{-1}) (Figure 41).

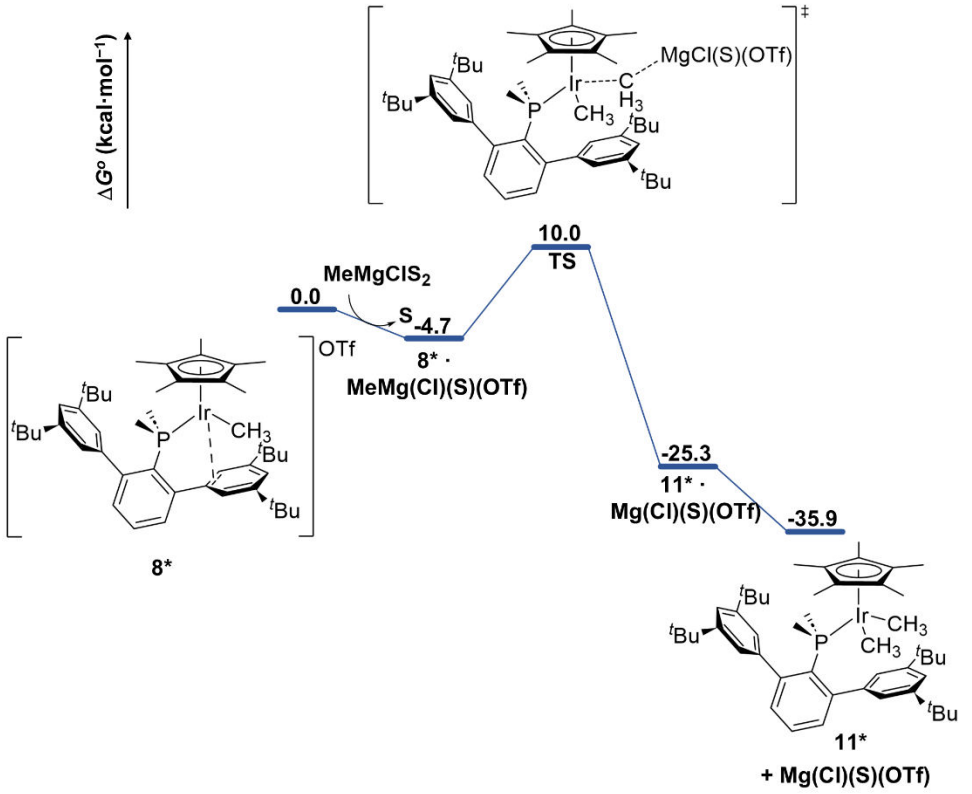

*Figure 41. Free energy profile for the formation of **11*** from **8*** and $MeMgClS_2$. Explicit solvent molecules (Me_2O) included in the calculations are represented as S.*

Since we have already proved the redox chemistry of this iridium framework, we tested the stability of the dimethyl complex under heating seeking the possibility of a reductive elimination process. However, efforts to release ethane and obtain complex **7*** from **11*** by heating proved unsuccessful in agreement with computational calculations ($\Delta G^{\ddagger}$ = 54.7 kcal·mol^{-1}) (Figure 42).

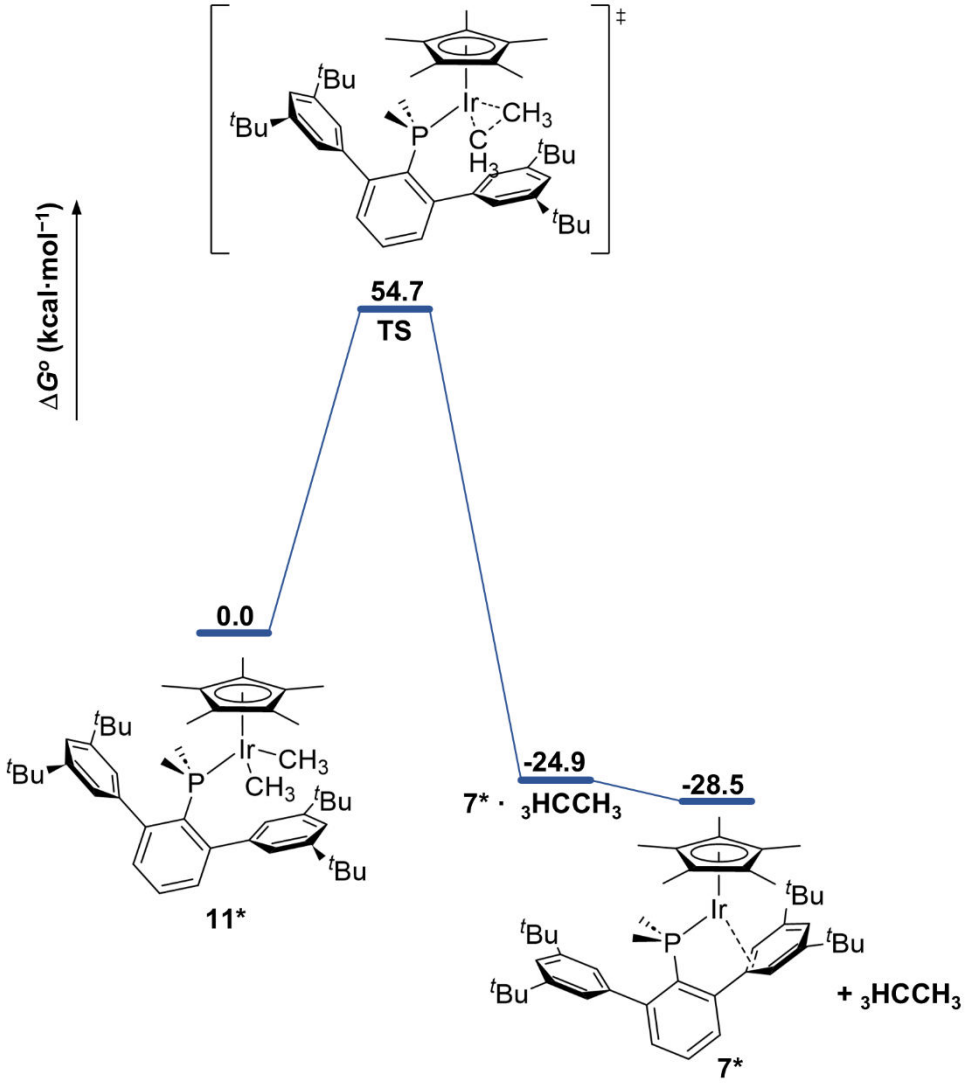

*Figure 42. Free energy profile for the potential elimination of ethane from **11***.*

I.2.2.8 Intermolecular C–H bond activation by complex 8*

As already mentioned on several occasions, Ir(III) compounds reported by Bergman, and analogous to **8*** and **9***, exhibited a remarkable capacity to activate C–H bonds of external substrates. At variance, the presence of C–H bonds within the anchored phosphine susceptible of being intramolecularly activated could preclude the observance of other C–H reactivity with external substrates in the case of **8***, while **9*** appears to be stable as well, likely due to the chelating effect of the cyclometalated phosphine. Nonetheless, to explore whether intermolecular C–H bond activation reactivity would still be accessible we tested the more electron deficient C–H bonds present in 1,2-difluorobencene as substrate. For comparison, we explored the C–H activation capabilities of both complexes **8*** and **9***.

As foreseen, only the former species was able to activate the substrate yielding complex **12***, where the methyl group has been substituted by a difluroaryl substituent with concomitant release of methane (Scheme 20).

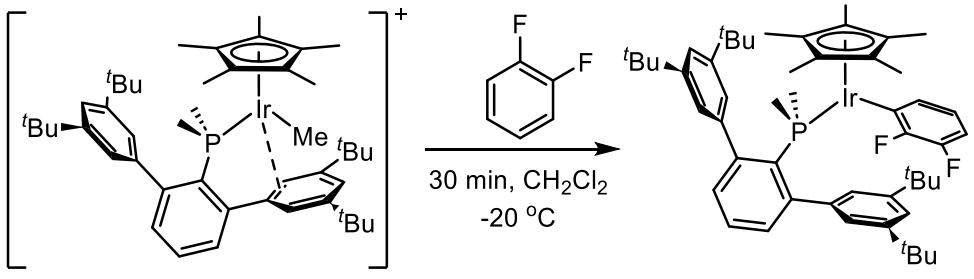

8* **12***

*Scheme 20. Synthesis of complex **12****.

Compound **12*** is characterized by a $^{31}P\{^{1}H\}$ resonance at 1.8 ppm. This new compound could not be isolated and fully characterized in pure form due to the concomitant formation of complex **9*** (spectroscopic yield for **12***, ~ 40%) even when the reaction was performed at low temperatures (–80 ºC). Nevertheless, its structure was corroborated by X-ray diffraction studies (Figure 43). In this case, the structure exhibits a slight pyramidalization of the C_{ipso} of one of the lateral rings, yet to a lesser extent than the cationic monochloride complex **1*** or the neutral Ir(I) complex **7***. The distance between the iridium center and one of the *ipso*-carbon atoms of one the lateral rings is closer (3.239(4) Å) than any of the corresponding distances in the saturated dimethylated complex **11*** (4.205 Å and 4.884 Å).

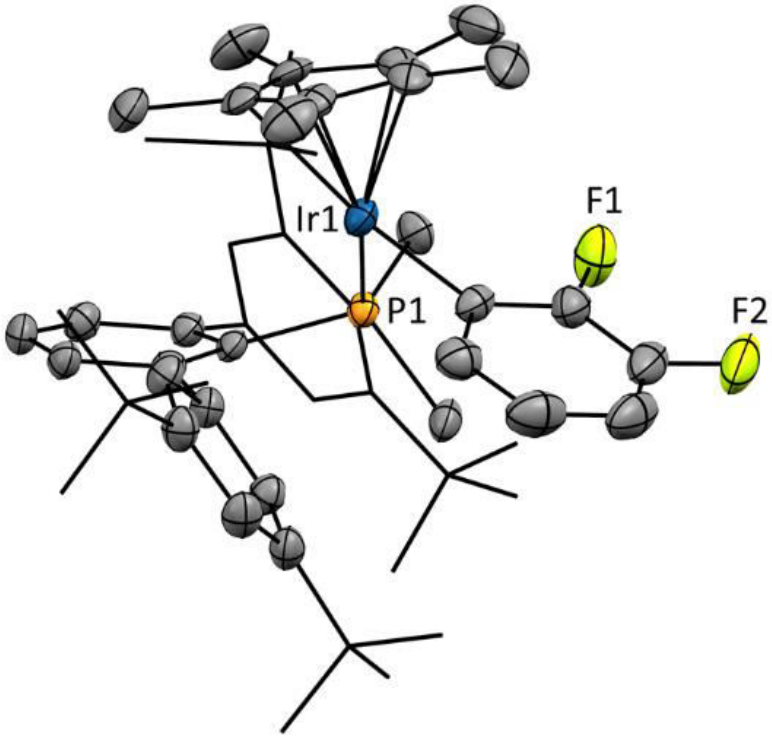

*Figure 43. ORTEP diagram of complex **12***. The triflate counterion and all hydrogen atoms are excluded for clarity. Thermal ellipsoids are set at 50% probability. Wireframe is used to represent one of the flaking aryl rings and the tert-butyl groups.*

Topological studies of complex **12*** show that there is no bcp between the iridium center and any of the carbon atoms of the lateral rings. EDA-NOCV analysis, in contrast, seems to indicate that a π-donation from the aryl ring to the iridium center, although small, is contributing to the orbital interactions. For the sake of comparison, the EDA-NOCV results of the neutral and saturated complex **11*** and those of complex **12*** are included in Table 10. The interaction energy between the phosphine and the rest of the complex is greater for complex **12***, indicating the need to stabilize this unsaturated complex. Furthermore, the main contributions to the orbital

term are depicted in Figure 44 and Figure 45 for complexes **12*** and **11***, respectively. In the case of complex **12***, the orbital term is dominated by the σ-donation of the HOMO of the phosphine to a empty d orbital of the metal center and backdonation of the metal center to the LUMO of the phosphine. A second orbital contribution consists of the donation from the aryl ring to the metal center, which is seven times weaker than the main orbital contribution (Figure 44). For complex **11***, in comparison, only the σ-donation of the phosphine and backdonation of the metal center take part in the orbital term (Figure 45).

*Table 10. EDA-NOCV results of different Cp*Ir complexes. Fragments are defined as the phosphine and the rest of the complex. All values in kcal·mol^{-1}.*

Entry	Complex	ΔE^{int}	ΔE^{elec}	ΔE^{orb}	ΔE^{Pauli}	ΔE^{disp}
1	**11***	– 81.7	– 194.4	– 102.1	249.0	– 34.1
2	**12***	– 118.2	– 187.8	– 119.0	231.7	– 43.1

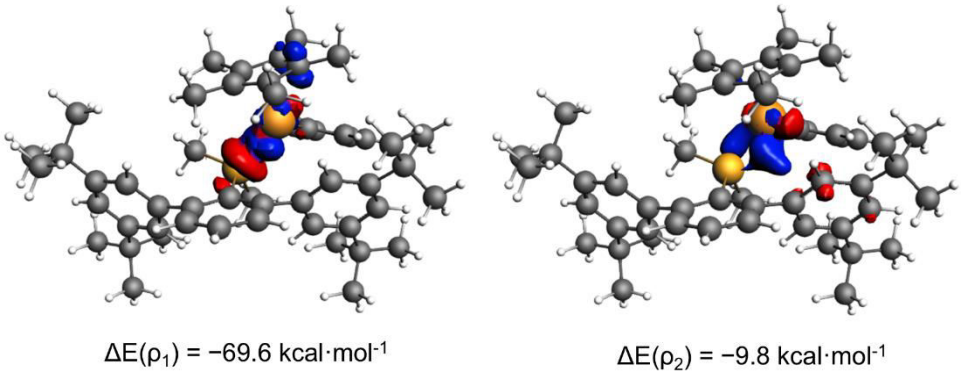

*Figure 44. Contour plots of NOCV deformation densities Δρ and associated energies ΔE(ρ) (computed at the ZORA-BP86-D3/TZ2P/PBE0-D3/SDD(Ir)/6-31(d,p)(all other atoms) level) in **12***.The fragments are defined as the phosphine moiety and the rest of the complex. Electron-density charge flows in the direction red→blue.*

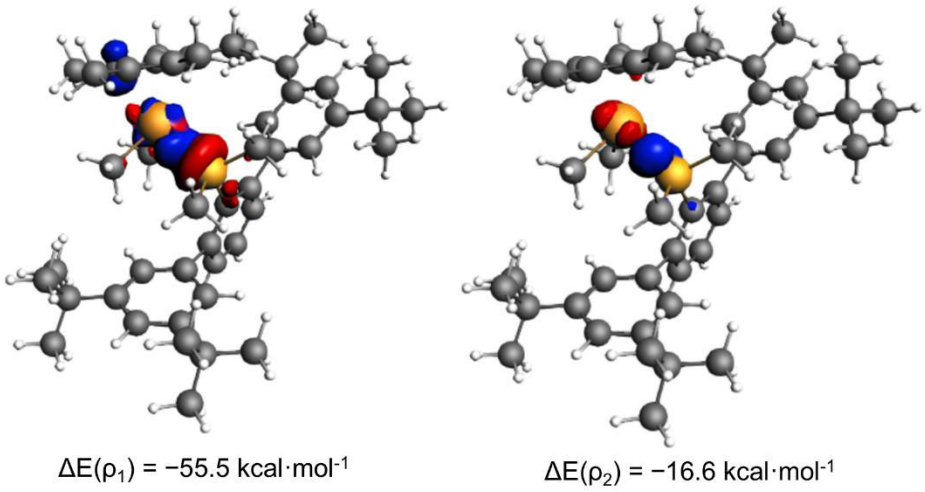

*Figure 45. Contour plots of NOCV deformation densities Δρ and associated energies ΔE(ρ) (computed at the ZORA-BP86-D3/TZ2P/PBE0-D3/SDD(Ir)/6-31(d,p)(all other atoms) level) in **11***.The fragments are defined as the phosphine moiety and the rest of the complex. Electron-density charge flows in the direction red→blue.*

I.2.2.9 Correlation between torsion angle and strength of the metal-arene interaction

Throughout the whole chapter we have recurrently discussed the existence of π-arene interactions between the iridium center and a flanking aryl ring of the terphenyl phosphine. Considering that we have also gathered sufficient structural information on those structures, we wondered whether we could correlate the geometric parameters of these compounds with the strength of the interaction between the metal center and the arene rings. In fact, the strength of that interaction can be inferred from the torsion of the interacting aryl ring relative to the central aryl ring of the phosphine. A linear correlation between the interaction energy, as calculated by the EDA-NOCV method, of the phosphine moiety and the rest of the organometallic complex is evident, with higher interaction energy resulting in greater torsion (Figure 46).

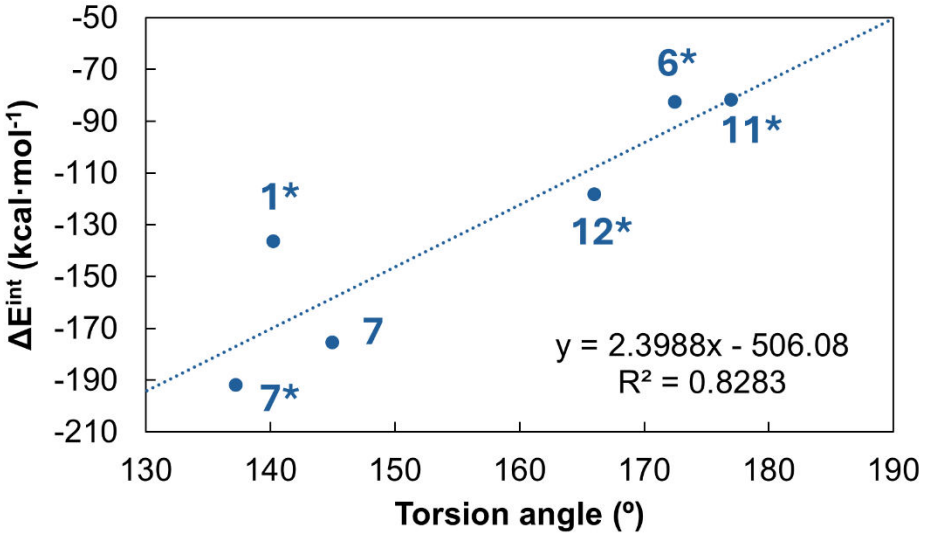

Figure 46. Plot of the interaction energy (ΔE^{int}) between the phosphine ligand and the rest of the complex versus the torsion angle of the lateral ring. In each case, the ring considered is the one that exhibits the greatest deviation from 180º.

As it has previously been commented, the somewhat ambiguous interaction between the phosphine moiety and the metal center in complex **12*** locates this complex in between the saturated ones (complex **6*** and **11***) and those featuring a clear secondary interaction with one of the lateral rings of the phosphine (complexes **1***, **7** and **7***). This type of correlation may be useful to estimate the relative energy of metal-arene interactions in this type of complexes, not only of terphenyl phosphines, but also of widespread Buchwald biaryl phosphines, as we intend to investigate further in the near future.

Summary and conclusions

*This chapter explores the synthesis and reactivity of Cp*Ir complexes bearing bulky terphenyl phosphines. In the first part, the study highlights how the reactivity of an Ir(III) precursor varies significantly with polarized alkylating reagents. Strongly nucleophilic lithium alkyls (e.g., LiMe, LiEt) induce alkylation of the Cp* ligand through direct nucleophilic attack, yielding Ir(I) complexes via formal reduction. Weaker nucleophiles, such as LiPh, act as Brønsted bases, deprotonating a methyl group on the Cp* ligand and triggering rearrangement into a pseudoallylic structure. Intermediate nucleophiles, like Li^{i}Pr, produce a mixture of these products. In contrast, Grignard reagents selectively alkylate the metal center, leaving the Cp* ligand intact and enabling subsequent C−H activation events. The second part focuses on the synthesis of two Ir(I) species and their contrasting reactivity with MeOTf. One species forms a cationic Ir−Me complex, which exhibits remarkable reactivity by undergoing intramolecular C−H bond activation. This reactivity extends to intermolecularly activating the C−H bond of 1,2-difluorobenzene as external substrate. These findings highlight the potential of Cp*Ir frameworks to investigate C−H activation reactions and to gather fundamental mechanistic knowledge.*

I.3 EXPERIMENTAL SECTION

I.3.1 General Considerations

All manipulations were carried out using standard Schlenk techniques, under a high purity nitrogen atmosphere. Solvents were dried and distilled under nitrogen prior to use. *n*-Pentane (C_5H_{12}) and *n*-hexane (C_6H_{14}) were distilled over sodium. Diethyl ether was distilled over sodium/benzophenone. CH_2Cl_2 and CD_2Cl_2 were dried over CaH_2. THF-d_8 was dried over 4 Å molecular sieves. $[Ir(C_5Me_5)Cl_2]_2$,[78] $Na[BAr^F]$,[79] PMe_2Ar'[80], and complex **1**[54] were prepared according to literature methods. All cationic complexes were isolated as salts of the $[BAr^F]^-$ anion. $PhSiH_3$ was commercially available and used as received. Solution NMR spectra were recorded on Bruker AVANCE NEO-300, AVANCE NEO-400, AVANCE III-400R and AVANCE NEO-500 spectrometers. Spectra were referenced to external $SiMe_4$ (δ: 0 ppm) using the residual proton solvent peaks as internal standards (^1H NMR experiments), or the characteristic resonances of the solvent nuclei (^{13}C NMR experiments), while ^{31}P was referenced to H_3PO_4. Spectral assignments were made by routine one- and two-dimensional NMR experiments (^1H, $^1H\{^{31}P\}$, $^{13}C\{^1H\}$, $^{31}P\{^1H\}$, COSY, NOESY, HSQC and HMBC) when appropriate. For elemental analysis a LECO TruSpec CHN elementary analyzer was utilized.

---

[78] White, C.; Yates, A.; Maitlis, P. M.; Heinekey, D. M. *Inorg. Synth.* **1992**, *29*, 228–234.
[79] Yakelis, N. A.; Bergman, R. G. *Organometallics* **2005**, *24*, 3579–3581.
[80] a) Campos, J.; Ortega-Moreno, L.; Conejero, S.; Peloso, R.; López-Serrano, J.; Maya, C.; Carmona, E. *Chem. Eur. J.* **2015**, *21*, 8883–8886; b) Ortega-Moreno, L.; Peloso, R.; Maya, C.; Suárez, A.; Carmona, E. *Chem. Commun.* **2015**, *51*, 17008–17011.

Calculations were performed at the DFT level with the Gaussian 09 (Revision E.01) program.[81] The hybrid functionals PBE0[82] was used throughout the computational study. Dispersion effects were accounted for by using Grimme's D3 parameter set with Becke−Johnson (BJ) damping.[83] Geometry optimizations were carried out without geometry constraints, using the 6-31G(d,p)[84] basis set to represent the C, H, P, Cl, Mg, O, F, S, N atoms and the Stuttgart/Dresden Effective Core Potential and its associated basis set (SDD)[85] to describe the Ir atom. Bulk solvent effects (dichloromethane, diethylether) were included at the optimization stage with the SMD continuum model.[86] The stationary points and their nature as minima or saddle points (TS) were characterized by vibrational analysis,

[81] Frisch, M. J.; Trucks, G. W.; Schlegel, H. B.; Scuseria, G. E.; Robb, M. A.; Cheeseman, J. R.; Scalmani, G.; Barone, V.; Mennucci, B; Petersson, G. A.; Nakatsuji, H.; Caricato, M.; Li, X.; Hratchian, H. P.; Izmaylov, A. F.; Bloino, J.; Zheng, G.; Sonnenberg, J. L.; Hada, M.; Ehara, M.; Toyota, K.; Fukuda, R.; Hasegawa, J.; Ishida, M.; Nakajima, T.; Honda, Y.; Kitao, O.; Nakai, H.; Vreven, T.; Montgomery, J. A. J.; Peralta, J. E.; Ogliaro, F.; Bearpark, M.; Heyd, J. J.; Brothers, E.; Kudin, K. N.; Staroverov, V. N.; Kobayashi, R.; Normand, J.; Raghavachari, K.; Rendell, A.; Burant, J. C.; Iyengar, S. S.; Tomasi, J.; Cossi, M.; Rega, N.; Millam, J. M.; Klene, M.; Knox, J. E.; Cross, J. B.; Bakken, V.; Adamo, C.; Jaramillo, J.; Gomperts, R.; Stratmann, R. E.; Yazyev, O.; Austin, A. J.; Cammi, R.; Pomelli, C.; Ochterski, J. W.; Martin, R. L.; Morokuma, K.; Zakrzewski, V. G.; Voth, G. A.; Salvador, P.; Dannenberg, J. J.; Dapprich, S.; Daniels, A. D.; Farkas, O.; Foresman, J. B.; Ortiz, J. V.; Cioslowski, J.; Fox, D. J.; Gaussian 09, Revision D.01, Gaussian, Inc.: Wallingford CT, 2013.

[82] Perdew, J. P.; Burke, K.; Ernzerhof, M. *Phys. Rev. Lett.* **1996**, *77*, 3865–3868.

[83] Grimme, S.; Antony, J.; Ehrlich, S.; Krieg, H. *J. Chem. Phys*. **2010**, *132*, 154104.

[84] a) Hehre, W. J.; Ditchfield, R.; Pople, J. A. *J. Phys. Chem.* **1972**, *56*, 2257–2261. b) Hariharan, P. C.; Pople, J. A. *Theor. Chim. Acta.* **1973**, *28*, 213–222. c) Francl, M. M.; Pietro, W. J.; Hehre, W. J.; Binkley, J. S.; Gordon, M. S.; Defrees, D. J.; Pople, J. A. *J. Chem. Phys.* **1982**, *77*, 3654–3665.

[85] Andrae, D.; Haeussermann, U.; Dolg, M.; Stoll, H.; Preuss, H. *Theor. Chim. Acta* **1990**, *77*, 123–141.

[86] Marenich, A. V.; Cramer, C. J.; Truhlar, D. G. *J. Phys. Chem. B* **2009**, *113*, 6378–6396.

which also produced enthalpy (H), entropy (S) and Gibbs energy (G) data at 298.15 K. The minima connected by a given transition state were determined by Intrinsic Reaction Coordinate (IRC) calculations or by perturbing the transition states along the TS coordinate and optimizing to the nearest minimum.

QTAIM analyses were performed with the Multiwfn[87] software on wavefunctions generated with the Gaussian 09 program. The electron density (ρ) at a bond critical point is commonly linked to the strength of the bond. For covalent interactions, the Laplacian ($\nabla^2\rho$) of the electron density at the bond critical point is negative, indicating an accumulation of charge density, while for closed shell or ionic interactions, $\nabla^2\rho$ is positive, signifying a depletion of charge density. Additionally, the total energy density (H) is typically negative in covalent interactions, whereas it tends to be positive in ionic interactions. Another way to characterize the nature of the interaction between two atoms is by examining the ratio of the local potential energy (V) to the kinetic energy (G). An ionic interaction is generally characterized by a ratio $|V|/G < 1$, while covalent interactions exhibit $|V|/G > 2$. Intermediate interactions, such as metal-metal and metal-ligand interactions, are characterized by positive $\nabla^2\rho$ values, energy densities (H) near zero, and a ratio of $1 < |V|/G < 2$.[72,73]

The computational modeling of alkyl/aryl lithium and Grignard reagents presents significant challenges due to the intricate equilibria these species undergo. These equilibria, influenced by solvent, concentration, and temperature, result in the coexistence of multiple species in solution. For example, Grignard reagents are well known to participate in dynamic

[87] Lu, T.; Chen, F. *J. Comput. Chem.* **2012**, *33*, 580–592.

equilibria involving mono- and polymetallic species (i.e. Schlenk equilibria), as emphasized by Eisenstein and Cascella.[88] Similarly, lithium reagents exhibit aggregation equilibria that depend on the nature of the R group and solvent.[89] Despite these complexities, employing simplified monomeric models for computational studies is a practical and justified approach. This methodology has been widely adopted in recent computational studies for Grignard reagents.[90] Additionally, for Grignard reagents, experimental data indicates that monomeric RMgX species predominate in diethyl ether solutions.[91] In lithium chemistry, although aggregates help stabilize the polar Li–C bond, monomeric species are generally regarded as the key reactive intermediates in solution-phase reactions.[92] Considering these experimental and computational precedents, we selected prototypical monomers as representative models for our calculations. Care was taken to accurately evaluate the solution effects, and the degree of solvation chosen corresponds to the most thermodynamically stabilized species.

---

[88] Peltzer, R. M.; Gauss, J.; Eisenstein, O.; Cascella, M. *J. Am. Chem. Soc*. **2020**, *142*, 2984–2994.

[89] Kwon, O.; Sevin, F.; McKee, M. L. *J. Phys. Chem. A* 2001, *105,* 913–922.

[90] a) Sharma, A. K.; Sameera, W. M. C.; Jin, M.; Adak, L.; Okuzono, C.; Iwamoto, T.; Kato, M.; Nakamura, M.; Morokuma, K. *J. Am. Chem. Soc.* **2017,** *139*, 16117–16125. b) Gutsev, L. G.; Gutsev, G. L.; Tibbetts, K. M.; Jena, P. *J. Phys. Chem. A* **2019,** *123*, 9693–9700. c) Ikuma, N.; Nakagawa, K.; Kokubo, K.; Oshima, T. *Org. Biomol. Chem.* **2016,** *14,* 7103–7108.

[91] Tammiku-Taul, J.; Burk, P.; Tuulmets, A. *J. Phys. Chem. A* **2004,** *108*, 133–139

[92] a) Lebon, J.; Mortis, A.; Maichle-Mössmer, C.; Manßen, M.; Sirsch, P.; Anwander, R. *Angew. Chem., Int. Ed.* **2023,** *62,* e202214599. b) Davison, N.; Falbo, E.; Waddell, P. G.; Penfold, T. J.; Lu, E. *Chem. Commun.* **2021,** *57,* 6205–6208.

The EDA-NOCV calculations were carried out with the program package ADF 2021[67,93] on the PBE0-D3/SDD(Ir)/6-31G(d,p) optimized geometries using the BP86-D3 functional in conjunction with a triple-ζ-quality basis set using uncontracted Slater-type orbitals (STOs) augmented by two sets of polarization function with a frozen-core approximation for the core electrons.[94] An auxiliary set of s, p, d, f, and g STOs were used to fit the molecular densities and to represent the Coulomb and exchange potentials accurately in each SCF cycle.[95] Scalar relativistic effects were incorporated by applying the zeroth-order regular approximation (ZORA).[96]

[93] ADF 2021.104, SCM, Theoretical Chemistry, Vrije Universiteit, Amsterdam, The Netherlands, http://www.scm.com.
[94] Snijders, J. G.; Baerends, E. J.; Vernooij, P. *At. Data. Nucl. Data Tables* **1982**, *26*, 483.
[95] Krijn, A.; Baerends, E. J. Fit *Functions in the HFS-Method, Internal Report (in Dutch),* Vrije Universiteit Amsterdam, The Netherlands, 1984.
[96] a) van Lenthe, E.; Baerends, E. J.; Snijders, J. G. *J. Chem. Phys.* **1993**, *99*, 4597–4610. b) van Lenthe, E.; Baerends, E. J.; Snijders, J. G. *J. Chem. Phys.* **1994**, *101*, 9783–9792. c) van Lenthe, E.; Ehlers, A.; Baerends, E. J. *J. Chem. Phys.* **1999**, *110*, 8943–8953.

I.3.2 Synthesis and characterization of new complexes

I.3.2.1 Preparation of complexes 2·Me, 2·Et, 2·^{i}Pr and 2·^{n}Bu

To a Et_2O solution (10 mL) of complex **1** (100.0 mg, 0.060 mmol) was added 1.1 equivalents of commercial solution of LiR (R=Me, Et, ^{i}Pr, or ^{n}Bu) at room temperature. There was an instantaneous color change to red. The solution was filtered, the solvent was evaporated under reduced pressure and the residue was washed with pentane (6 mL). Single crystals were grown from a saturated CH_2Cl_2-hexane solution at −32 °C.

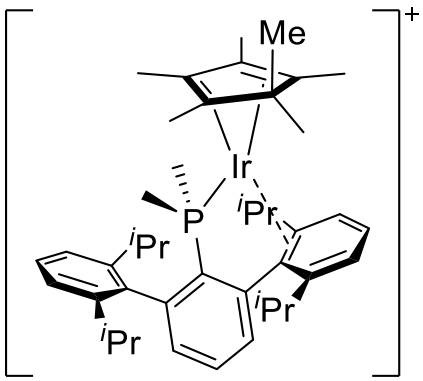

Complex 2·Me

Anal. Calcd. for $C_{74}H_{73}BF_{24}IrP$: C, 54.1; H, 4.4. **Found:** C, 54.2; H, 4.4.

^{1}H NMR (400 MHz, CD_2Cl_2, −20 °C) δ: 7.71 (m, 8H, *o*-Ar), 7.55 (s, 4H, *p*-Ar), 7.50 (td, 1H, $^{3}J_{HH}$ = 7.6 Hz, $^{5}J_{HP}$ = 2.1 Hz, *p*-C_6H_3), 7.43 (m, 2H, *p*-Dipp, *m*-Dipp'), 7.36 (d, 1H, $^{3}J_{HH}$ = 7.6 Hz, *m*-Dipp'), 7.30 (t, 1H, $^{3}J_{HH}$ = 7.6 Hz, *p*-Dipp'), 7.28 (d, 1H, $^{3}J_{HH}$ = 7.7 Hz, *m*-Dipp), 7.23 (d, 1H, $^{3}J_{HH}$ = 7.8 Hz, *m*-Dipp), 7.20 (ddd, 1H, $^{3}J_{HH}$ = 7.5 Hz, $^{4}J_{HP}$ = 2.8 Hz, $^{4}J_{HH}$ = 0.9 Hz, *m*-C_6H_3), 6.99 (ddd, 1H, $^{3}J_{HH}$ = 7.7 Hz, $^{4}J_{HP}$ = 2.0 Hz, $^{4}J_{HH}$ = 0.9 Hz, *m'*-C_6H_3), 2.64 (sept, 1H, $^{3}J_{HH}$ = 6.8 Hz, (C*H*Me$_2$)$_{Dipp'}$), 2.32 (sept, 1H, $^{3}J_{HH}$ = 6.8 Hz, (C*H*Me$_2$)$_{Dipp}$), 2.15 (sept, 1H, $^{3}J_{HH}$ = 6.8 Hz, (C*H*Me$_2$)$_{Dipp}$),

2.01 (sept, 1H, $^{3}J_{HH}$ = 6.8 Hz, (C*H*Me$_2$)$_{Dipp'}$), 1.85 (d, 3H, $^{4}J_{HP}$ = 1.1 Hz, C_5Me_6), 1.53 (s, 3H, C_5Me_6), 1.48 (d, 3H, $^{2}J_{HP}$ = 10.1 Hz, P*Me*Me), 1.35 (d, 3H, $^{3}J_{HH}$ = 7.0 Hz, Me$_{Dipp'}$), 1.30 (d, 3H, $^{3}J_{HH}$ = 7.1 Hz, Me$_{Dipp'}$), 1.24 (d, 3H, $^{2}J_{HP}$ = 10.3 Hz, PMe*Me*), 1.23 (d, 3H, $^{3}J_{HH}$ = 6.7 Hz, Me$_{Dipp}$), 1.19 (d, 3H, $^{3}J_{HH}$ = 6.7 Hz, Me$_{Dipp}$), 1.13 (s, 3H, C_5Me_6), 1.00 (d, 3H, $^{3}J_{HH}$ = 6.6 Hz, Me$_{Dipp}$), 0.90 (m, 6H, Me$_{Dipp}$, Me$_{Dipp'}$), 0.77 (s, 3H, C_5Me_6), 0.73 (s, 3H, C_5Me_6), 0.70 (d, 3H, $^{3}J_{HH}$ = 6.8 Hz, Me$_{Dipp'}$), 0.32 (d, 3H, $^{4}J_{HP}$ = 3.4 Hz, C_5Me_6).

^{13}C{^{1}H} NMR (100 MHz, CD_2Cl_2, −20 ºC) δ: 161.7 (q, $^{1}J_{CB}$ = 50 Hz, *ipso*-Ar), 146.9 (*o*-Dipp), 146.5 (*o*-Dipp), 146.3 (d, $^{2}J_{CP}$ = 27 Hz, *o*-C_6H_3), 144.2 (*o*-C_6H_3), 141.5 (*o*-Dipp'), 137.6 (d, $^{1}J_{CP}$ = 53 Hz, *ipso*-C_6H_3), 135.7 (*ipso*-Dipp), 134.7 (*o*-Ar), 133.7 (d, $^{3}J_{CP}$ = 5 Hz, *m*-C_6H_3), 133.6 (*m*-Dipp'), 132.5 (m, *m*-Dipp', *o*-Dipp'), 131.7 (d, $^{3}J_{CP}$ = 13 Hz, *m*-C_6H_3), 131.1 (*p*-C_6H_3), 129.7 (*p*-Dipp), 128.7 (q, $^{2}J_{CF}$ = 32 Hz, *m*-Ar), 127.8 (*p*-Dipp'), 124.4 (q, $^{1}J_{CF}$ = 272 Hz, CF_3), 123.1 (overlapped, *m*-Dipp), 122.9 (*m*-Dipp), 122.5 (d, $^{2}J_{CP}$ = 15 Hz, *C*$_5$Me$_6$), 120.4 (overlapped, *ipso*-Dipp'), 117.5 (m, *p*-Ar), 114.5 (*C*$_5$Me$_6$), 78.3 (*C*$_5$Me$_6$), 61.9 (*C*$_5$Me$_6$), 56.7 (*C*$_5$Me$_6$), 34.2 ((*C*HMe$_2$)$_{Dipp'}$, (*C*HMe$_2$)$_{Dipp'}$), 31.4 ((*C*HMe$_2$)$_{Dipp}$), 31.2 ((*C*HMe$_2$)$_{Dipp}$), 29.7 (C$_5$*Me*$_6$), 26.1 (Me$_{Dipp}$), 25.7 (Me$_{Dipp}$), 24.7 (Me$_{Dipp}$), 24.4 (Me$_{Dipp'}$), 24.2 (Me$_{Dipp'}$), 24.1 (Me$_{Dipp'}$), 21.4 (C$_5$*Me*$_6$), 21.2 (Me$_{Dipp}$), 21.1 (Me$_{Dipp}$), 15.7 (d, $^{1}J_{CP}$ = 39 Hz, PMe*Me*), 15.1 (d, $^{1}J_{CP}$ ≈ 39 Hz, P*Me*Me), 13.4 (C$_5$*Me*$_6$), 12.3 (C$_5$*Me*$_6$), 11.8 (C$_5$*Me*$_6$), 8.3 (C$_5$*Me*$_6$).

^{31}P{^{1}H} NMR (120 MHz, CD_2Cl_2, −20 ºC) δ: 5.1.

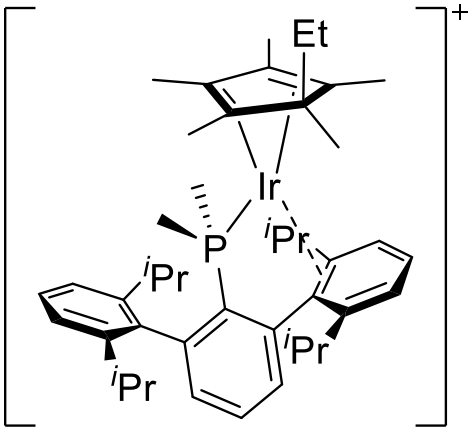

Complex 2·Et

Anal. Calcd. for $C_{76}H_{75}BF_{24}IrP$: C, 54.4; H, 4.5. **Found:** C, 54.3; H, 4.4.

^{1}H NMR (400 MHz, CD_2Cl_2, −20 ºC) δ: 7.75 (m, 8H, *o*-Ar), 7.59 (s, 4H, *p*-Ar), 7.53 (td, 1H, $^3J_{HH}$ = 7.6 Hz, $^5J_{HP}$ = 2.1 Hz, *p*-C_6H_3), 7.47 (t, 1H, $^3J_{HH}$ = 7.8 Hz, *p*-Dipp), 7.43 (d, 2H, $^3J_{HH}$ = 7.6 Hz, *m*-Dipp'), 7.31 (m, 3H, *p*-Dipp', *m*-Dipp, *m*-Dipp), 7.26 (dd, 1H, $^3J_{HH}$ = 7.5 Hz, $^4J_{HP}$ = 2.8 Hz, $^4J_{HH}$ = 0.9 Hz, *m*-C_6H_3), 7.01 (dd, 1H, $^3J_{HH}$ = 7.7 Hz, $^4J_{HP}$ = 2.0 Hz, *m*'-C_6H_3), 2.69 (m, 1H, (C*H*Me$_2$)$_{Dipp'}$), 2.39 (m, 1H, (C*H*Me$_2$)$_{Dipp}$), 2.26 (m, 1H, (C*H*Me$_2$)$_{Dipp}$), 2.07 (m, 1H, (C*H*Me$_2$)$_{Dipp'}$), 1.90 (br s, 3H, C_5*Me*$_5$Et,), 1.58 (m, 6H, C_5*Me*$_5$Et, P*Me*Me), 1.41 (d, 6H, $^3J_{HH}$ = 6.8 Hz, Me$_{Dipp}$, Me$_{Dipp}$), 1.28 (m, 11H, Me$_{Dipp'}$, Me$_{Dipp'}$, PMe*Me*, C*H*$_2$CH$_3$), 0.99 (m, 6H, Me$_{Dipp}$, Me$_{Dipp}$), 0.88 (m, 6H, Me$_{Dipp'}$, Me$_{Dipp'}$), 0.79 (s, 3H, C_5*Me*$_5$Et), 0.71 (m, 3H, C_5*Me*$_5$Et), 0.32 (br s, 3H, C_5*Me*$_5$Et), 0.17 (t, 3H, $^1J_{HH}$ = 7.3 Hz, CH_2CH_3).

^{13}C{^{1}H} NMR (100 MHz, CD_2Cl_2, −20 ºC) δ: 161.8 (q, $^1J_{CB}$ = 50 Hz, *ipso*-Ar), 147.3 (*o*-Dipp, *o*-Dipp), 146.8 (d, $^2J_{CP}$ = 27 Hz, *o*-C_6H_3), 144.5 (*o*-C_6H_3), 142.9 (*o*-Dipp'), 138.0 (d, $^1J_{CP}$ = 53 Hz, *ipso*-C_6H_3), 135.7 (*ipso*-

Dipp), 134.8 (*o*-Ar), 134.0 (d, $^{3}J_{CP}$ = 5 Hz, *m*-C_6H_3), 133.4 (*m*-Dipp'), 132.5 (m, *m*-Dipp', *o*-Dipp'), 131.9 (d, $^{3}J_{CP}$ = 13 Hz, *m*-C_6H_3), 130.9 (*p*-C_6H_3), 129.8 (*p*-Dipp), 128.9 (q, $^{2}J_{CF}$ = 32 Hz, *m*-Ar), 127.8 (*p*-Dipp'), 124.1 (m, $^{1}J_{CF}$ = 272 Hz, CF_3), 123.3 (*overlapped*, *m*-Dipp), 123.1 (*m*-Dipp), 121.6 (d, $^{2}J_{CP}$ = 15 Hz, C_5Me_5Et), 120.5 (*overlapped*, *ipso*-Dipp'), 117.5 (m, *p*-Ar), 115.8 (C_5Me_5Et), 80.0 (C_5Me_5Et), 61.4 (C_5Me_5Et), 59.4 (C_5Me_5Et), 34.2 ((CHMe$_2$)$_{Dipp'}$, (CHMe$_2$)$_{Dipp'}$), 31.3 ((CHMe$_2$)$_{Dipp}$), 30.9 ((CHMe$_2$)$_{Dipp}$), 29.7 (C_5Me_5Et), 26.4 (Me$_{Dipp}$, Me$_{Dipp'}$), 24.6 (Me$_{Dipp}$, Me$_{Dipp'}$), 23.1 (Me$_{Dipp}$, Me$_{Dipp'}$), 21.6 (Me$_{Dipp}$, Me$_{Dipp'}$), 17.8 ($C_5Me_5CH_2CH_3$), 16.1 (d, $^{1}J_{CP}$ = 39 Hz, PMe_2), 13.3 (C_5Me_5Et), 11.8 (C_5Me_5Et), 10.6 (C_5Me_5Et), 9.4 ($C_5Me_5CH_2CH_3$), 8.4 (C_5Me_5Et).

^{31}P{^{1}H} NMR (162 MHz, CD_2Cl_2 , −20 ºC) δ: 4.8.

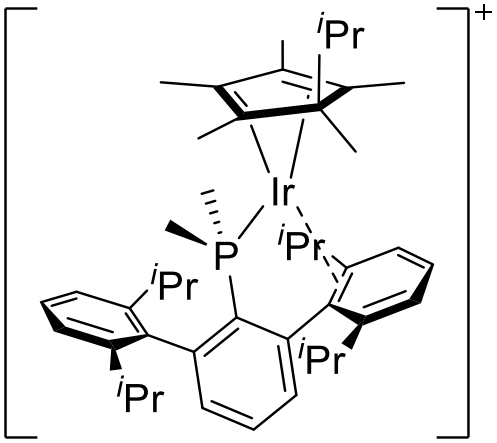

Complex 2·^{i}Pr

^{31}P{^{1}H} NMR (162 MHz, CD_2Cl_2, 25°C) δ: −0.6.

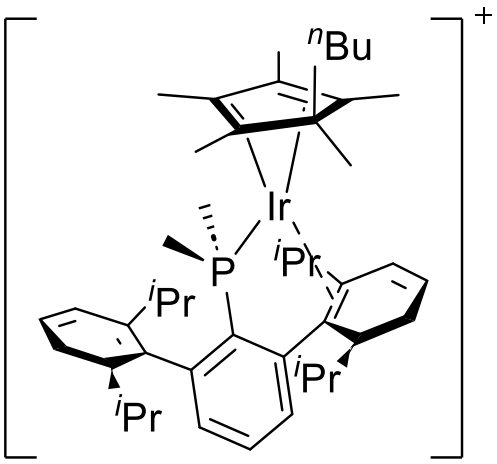

Complex 2·^{n}Bu

Anal. Calcd. for $C_{78}H_{79}BF_{24}IrP$: C, 54.9; H, 4.7. **Found:** C, 54.8; H, 4.7.

^{1}H NMR (500 MHz, CD_2Cl_2, −20 °C) δ: 7.72 (m, 8H, *o*-Ar), 7.56 (s, 4H, *p*-Ar), 7.52 (td, $^{3}J_{HH}$ = 7.7 Hz, $^{5}J_{HP}$ = 1.9 Hz, 1H, *p*-C_6H_3), 7.43 (m, 2H, *p*-Dipp, *m*-Dipp'), 7.29 (m, 2H, *p*-Dipp', *m*-Dipp'), 7.22 (m, 3H, *m*-C_6H_3, *m*-Dipp, *m*-Dipp), 6.99 (d, 1H, $^{3}J_{HH}$ = 7.7 Hz , *m*'-C_6H_3), 2.70 (m, 1H, (C*H*Me$_2$)$_{Dipp'}$), 2.35 (m, 1H, (C*H*Me$_2$)$_{Dipp}$), 2.16 (m, 1H, (C*H*Me$_2$)$_{Dipp}$), 1.99 (m, 1H, (C*H*Me$_2$)$_{Dipp'}$), 1.86 (s, $C_5Me_5{}^{n}$Bu), 1.54 (s, $C_5Me_5{}^{n}$Bu), 1.50 (d, $^{2}J_{HP}$ = 15 Hz, 3H, P*Me*Me), 1.36 (d, 3H, $^{3}J_{HH}$ = 7.0 Hz, Me$_{Dipp'}$), 1.33 (d, 3H, $^{3}J_{HH}$ = 7.2 Hz, Me$_{Dipp'}$), 1.24 (m, 11H, PMe*Me*, Me$_{Dipp}$, $C_5Me_5{}^{n}$Bu, CH$_{2n\text{Bu}}$, CH$_{2n\text{Bu}}$) 1.20 (d, 3H, $^{3}J_{HH}$ = 6.7 Hz, Me$_{Dipp}$), 1.06 (m, 2H, CH$_{2n\text{Bu}}$,CH$_{2n\text{Bu}}$), 1.01 (d, $^{3}J_{HH}$ = 6.7 Hz, 3H, Me$_{Dipp}$), 0.93 (d, $^{3}J_{HH}$ = 6.7 Hz, 3H, Me$_{Dipp}$), 0.90 (d, $^{3}J_{HH}$ = 6.7 Hz, 3H, Me$_{Dipp'}$), 0.71 (m, 9H, Me$_{Dipp'}$, $C_5Me_5{}^{n}$Bu, CH$_{3nBu}$), 0.32 (m, 2H, CH$_{2nBu}$), 0.25 (s, 3H, $C_5Me_5{}^{n}$Bu).

^{13}C{^{1}H} NMR (125 MHz, CD_2Cl_2, −20 °C) δ: 161.8 (q, $^{1}J_{CB}$ = 50 Hz, i*pso*-Ar), 147.0 (*o*-Dipp), 146.6 (*o*-Dipp), 146.4 (d, $^{2}J_{CP}$ = 27 Hz, *o*-C_6H_3), 144.3 (*o*-C_6H_3), 142.5 (*o*-Dipp'), 137.8 (d, $^{2}J_{CP}$ = 53 Hz, *ipso*-C_6H_3), 135.8

(*ipso*-Dipp), 134.8 (*o*-Ar), 133.9 (d, $^{3}J_{CP}$ = 5 Hz, *m*-C_6H_3), 133.8 (*m*-Dipp'), 132.5 (m, *m*-Dipp', *o*-Dipp'), 131.9 (d, $^{3}J_{CP}$ = 13 Hz, *m*-C_6H_3), 131.6 (*o*-Dipp), 131.1 (*p*-C_6H_3), 129.8 (*p*-Dipp), 128.8 (q, $^{2}J_{CF}$ = 32 Hz, *m*-Ar), 127.7 (*p*-Dipp'), 124.1 (m, CF_3), 123.0 (*m*-Dipp) , 121.6 (d, $^{2}J_{CP}$ = 15 Hz, $C_5Me_5{}^{n}Bu$), 120.2 (d, $^{2}J_{CP}$ = 4 Hz, *ipso*-Dipp'), 117.6 (m, *p*-Ar), 115.7 (d, $^{2}J_{CP}$ = 4 Hz, $C_5Me_5{}^{n}Bu$), 79.6 ($C_5Me_5{}^{n}Bu$), 61.0 ($C_5Me_5{}^{n}Bu$), 60.7 ($C_5Me_5{}^{n}Bu$), 37.5 (CH_2), 34.3 ((CHMe$_2$)$_{Dipp'}$, (CHMe$_2$)$_{Dipp'}$), 31.5 ((CHMe$_2$)$_{Dipp}$), 31.3 ((CHMe$_2$)$_{Dipp}$), 27.4 (CH_2), 26.2 (Me$_{Dipp}$), 25.7 (Me$_{Dipp}$), 24.7 (Me$_{Dipp}$), 24.3 ($C_5Me_5{}^{n}Bu$), 24.1 (Me$_{Dipp}$, Me$_{Dipp}$), 23.0 (Me$_{Dipp}$), 22.6 (CH_2), 22.3 (CH_3), 22.1 (Me$_{Dipp}$), 21.2 (Me$_{Dipp}$), 21.0 ($C_5Me_5{}^{n}Bu$), 15.8 (d, $^{1}J_{CP}$ = 39 Hz, PMe*Me*), 15.3 (d, $^{1}J_{CP}$ = 38 Hz, P*Me*Me), 12.1 ($C_5Me_5{}^{n}Bu$), 11.0 ($C_5Me_5{}^{n}Bu$), 8.6 ($C_5Me_5{}^{n}Bu$).

$^{31}P\{^{1}H\}$ NMR (202 MHz, CD_2Cl_2, 25°C) δ: 4.7.

I.3.2.2 Preparation of complexes 4 and 5

To a Et_2O solution (10 mL) of complex **1** (100 mg, 0.060 mmol) was added 1.1 equivalents of RMgBr (R=Me or Et) at room temperature. The resulting red solution was stirred for 20 h to ensure completion and then filtered. The solvent was evaporated under reduced pressure and the residue was washed with pentane (6 mL). Single crystals were grown from a saturated CH_2Cl_2-hexane solution at −32ºC.

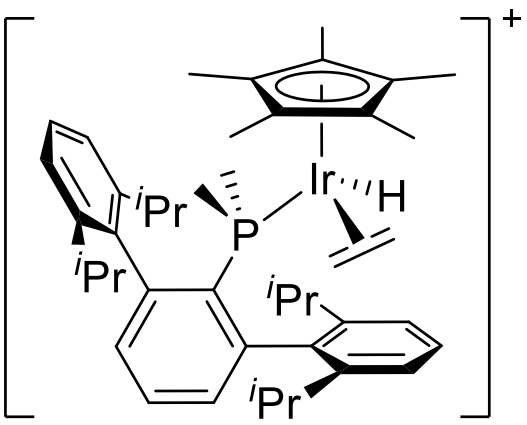

Complex 4

Anal. Calcd. for $C_{76}H_{75}BF_{24}IrP$: C, 54.4; H, 4.5. **Found:** C, 54.4; H, 4.5.

^{1}H NMR (400 MHz, CD_2Cl_2, 25 ºC) δ: 7.71 (s, 8H, *o*-Ar), 7.56 (s, 4H, *p*-Ar), 7.50 (td, 1H, $^{3}J_{HH}$ = 7.6 Hz, $^{5}J_{HP}$ = 2.1 Hz, *p*-C_6H_3), 7.46 (t, 2H, $^{3}J_{HH}$ = 7.8 Hz, *p*-Dipp), 7.28 (m, 6H, *m*-Dipp, *m*-C_6H_3), 2.55 (m, 4H, (C*H*Me$_2$)$_{Dipp}$), 2.19 (d, 2H, $^{2}J_{HP}$ = 6.7 Hz, C*H*HC*H*H), 1.88 (d, 2H, $^{2}J_{HP}$ = 6.7 Hz, CH*H*CH*H*), 1.78 (d, 3H, $^{2}J_{HP}$ = 11.1 Hz, P*Me*Me), 1.62 (s, 15H, C_5Me_5), 1.37 (m, 12H, Me$_{Dipp}$), 1.30 (d, 3H, $^{2}J_{HP}$ = 11.1 Hz, PMe*Me*), 0.97 (m, 12H, Me$_{Dipp}$), −14.9 (d, 1H, $^{2}J_{HP}$ = 30.2 Hz, IrH).

^{13}C{^{1}H} NMR (100 MHz, CD_2Cl_2, 25 ºC) δ: 162.1 (q, $^{1}J_{CB}$ = 50 Hz, i*pso*-Ar), 147.5 (*o*-Dipp), 144.9 (d, $^{2}J_{CP}$ = 10 Hz, *o*-C_6H_3), 137.1 (d, $^{3}J_{CP}$ = 5 Hz, *ipso*-Dipp), 134.8 (*o*-Ar), 133.2 (d, $^{3}J_{CP}$ = 9 Hz, *m*-C_6H_3), 132.7 (d, $^{1}J_{CP}$ = 57 Hz, *ipso*-C_6H_3), 130.6 (*p*-Dipp), 129.9 (d, $^{4}J_{CP}$ = 3 Hz, *p*-C_6H_3), 129.3 (q, $^{2}J_{CF}$ = 31 Hz, m-Ar), 125.0 (q, $^{1}J_{CF}$ = 272 Hz, CF_3), 117.5 (m, *p*-Ar), 95.7 (d, $^{2}J_{CP}$ = 3 Hz, *C*$_5$Me$_5$), 33.8 (CH_2CH_2), 31.5 ((*C*HMe$_2$)$_{Dipp}$), 25.9 (v. br., Me$_{Dipp}$), 22.5 (d, $^{1}J_{CP}$ = 39 Hz, P*Me*Me), 21.8 (br, Me$_{Dipp}$), 20.6 (d, $^{1}J_{CP}$ = 39 Hz, PMe*Me*), 9.2 (C_5*Me*$_5$).

$^{31}P\{^{1}H\}$ NMR (162 MHz, CD_2Cl_2, 25 ^{o}C) δ: −27.0.

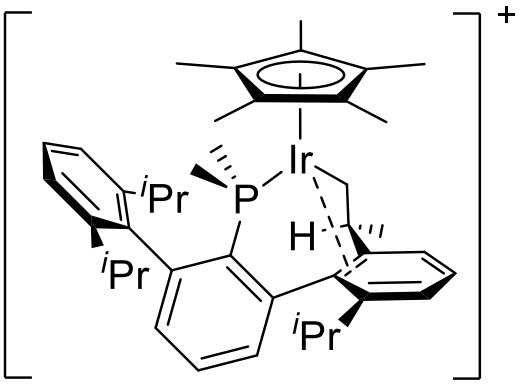

Complex 5

Anal. Calcd. for $C_{74}H_{69}BF_{24}IrP$: C, 53.9; H, 4.2. **Found:** C, 53.8; H, 4.2.

^{1}H NMR (500 MHz, CD_2Cl_2, −20 ºC) δ: 7.72 (s, 8H, *o*-Ar), 7.56 (s, 4H, *p*-Ar), 7.53 (m, 1H, *p*-Dipp'), 7.48 (t, $^3J_{HH}$ = 7.8 Hz, 1H, *p*-Dipp), 7.43 (td, $^3J_{HH}$ = 7.7 Hz, $^5J_{HP}$ = 2.3 Hz, 1H, *p*-C_6H_3), 7.34 (dd, $^3J_{HH}$ = 7.8 Hz, $^4J_{HH}$ = 1.0 Hz, 1H, *m*-Dipp), 7.29 (dd, $^3J_{HH}$ = 7.8 Hz, $^4J_{HH}$ = 1.0 Hz, 1H, *m*-Dipp), 7.19 (ddd, $^3J_{HH}$ = 7.7 Hz, $^4J_{HP}$ = 3.3 Hz, $^4J_{HH}$ = 1.1 Hz, 1H, *m*-C_6H_3), 7.14 (d, $^3J_{HH}$ = 8.5 Hz, 1H, *m*-Dipp'), 6.99 (m, 1H, *m*-Dipp'), 6.49 (ddd, $^3J_{HH}$ = 7.7 Hz, $^4J_{HP}$ = 2.5 Hz, $^4J_{HH}$ = 1.1 Hz, 1H, *m'*-C_6H_3),3.30 (m, 1H, C*H*CH_2Ir), 2.50 (m, 1H, (C*H*Me_2)$_{Dipp}$), 2.43 (m, 1H, (C*H*Me_2)$_{Dipp'}$), 2.33 (m, 1H, (C*H*Me_2)$_{Dipp'}$), 1.92 (d, $^2J_{HP}$ = 10.5 Hz, 3H, P*Me*Me), 1.36 (d, $^3J_{HH}$ = 6.7 Hz, 3H, Me_{Dipp}), 1.31 (d, $^4J_{HP}$ = 1.8 Hz, 15H, C_5Me_5), 1.24 (d, $^3J_{HH}$ = 6.7 Hz, 3H, Me_{Dipp}), 1.21 (m, 6H, $Me_{Dipp'}$, PMe*Me*), 1.07 (d, $^3J_{HH}$ = 6.7 Hz, 3H, Me_{Dipp}) 1.05 (d, $^3J_{HH}$ = 6.7 Hz, 3H, Me_{Dipp}), 1.02 (d, $^3J_{HH}$ = 6.7 Hz, 3H, $Me_{Dipp'}$) 1.00 (d, $^3J_{HH}$ = 6.7 Hz, 3H, $Me_{Dipp'}$), 0.69 (m, 1H, C*H*HIr), 0.18 (m, 1H, CH*H*Ir).

^{13}C{^{1}H} NMR (125 MHz, CD_2Cl_2, −20 ºC) δ: 162.1 (q, $^1J_{CB}$ = 50 Hz, i*pso*-Ar), 157.0 (*o*-Dipp), 147.9 (d, $^2J_{CP}$ = 27 Hz, *o*-C_6H_3), 147.7 (*o*-Dipp'), 146.9 (*o'*-Dipp'), 144.8 (d, $^2J_{CP}$ = 2 Hz, *o'*-C_6H_3), 138.3 (d, $^2J_{CP}$ = 59 Hz,

ipso-C_6H_3), 136.0 (d, $^3J_{CP}$ = 2 Hz, *ipso*-Dipp), 135.2 (*o*-Ar), 133.5 (d, $^3J_{CP}$ = 6 Hz, *m*-C_6H_3), 132.1 (d, $^4J_{CP}$ = 2 Hz, *p*-C_6H_3), 130.4 (*p*-Dipp'), 130.3 (*p*-Dipp), 129.9 (d,$^3J_{CP}$ = 13 Hz, *m*-C_6H_3), 129.3 (q, $^2J_{CF}$ = 32 Hz, *m*-Ar), 127.2 (m, CF_3) 124.5 (*m*-Dipp'), 123.6 (*m*-Dipp, *m*-Dipp) , 120.1 (*m*-Dipp'), 117.9 (m, *p*-Ar), 102.7 (d, $^2J_{CP}$ = 4 Hz, *ipso*-Dipp'), 97.4 (d, $^3J_{CP}$ = 3 Hz, C_5Me_5), 85.6 (*o'*-Dipp), 37.7 ((CHCH$_2$Me)$_{Dipp}$), 32.9 ((CHMe$_2$)$_{Dipp}$), 31.7 ((CHMe$_2$)$_{Dipp'}$), 31.4 ((CHMe$_2$)$_{Dipp'}$), 26.4 (Me$_{Dipp'}$), 26.3 (Me$_{Dipp'}$), 25.6 (Me$_{Dipp}$), 24.3 (Me$_{Dipp}$), 21.9 (Me$_{Dipp'}$), 21.7 (Me$_{Dipp'}$), 20.1 ((CHCH$_2$*Me*)$_{Dipp}$), 17.6 (d, $^1J_{CP}$ = 36 Hz, P*Me*Me), 11.7 (d, $^1J_{CP}$ = 45 Hz, PMe*Me*), 8.6 (C_5Me_5), −23.4 (d, $^2J_{CP}$ = 8 Hz, CHCH$_2$Me)$_{Dipp}$).

^{31}P{^{1}H} NMR (202 MHz, CD_2Cl_2, −20 ºC) δ: 6.3.

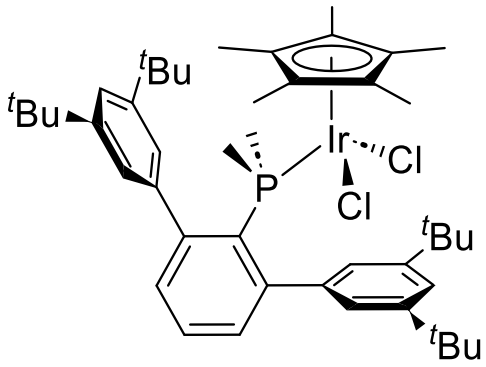

Complex 6*. To a dry CH_2Cl_2 solution (12 mL) of $[IrCp^*Cl_2]_2$ (74 mg, 0.093 mmol), a dry CH_2Cl_2 solution of PMe_2Ar^{Dtbp2} (100 mg, 0.195 mmol) was added at room temperature. There was an instantaneous color change from orange to bright orange-red. The solution was stirred for 30 min. Then, the solvent was evaporated under reduced pressure. The residue was washed with pentane (3 mL) to yield a yellow powder. Yield: 158 mg (92%).

Anal. Calcd. for $C_{46}H_{66}Cl_2IrP$: C, 60.5; H, 7.3. **Found**: C, 60.6; H, 7.3.

^{1}H NMR (500 MHz, CD_2Cl_2, 25 ºC) δ: 7.48 (s, 2H, *p*-Dtbp), 7.41 (s, 2H, *o*-Dtbp), 7.35 (td, $^3J_{HH}$ = 7.5 Hz, $^5J_{HP}$ = 1.5 Hz, 1H, *p*-C_6H_3), 7.25 (dd, $^3J_{HH}$ = 7.5 Hz, $^4J_{HP}$ = 2.1 Hz, 2H, *m*-C_6H_3), 7.03 (s, 2H, *o*-Dtbp'), 1.63 (d, $^2J_{HP}$ = 10.9 Hz, 6H, PMe_2), 1.46 (s, 18H, $(CH_3)_3C_{Dtbp}$), 1.37 (s, 18H, $(CH_3)_3C_{Dtbp}$), 1.35 (d, $^4J_{HP}$ = 1.9 Hz, 15H, C_5Me_5).

^{13}C{^{1}H} NMR (100 MHz, CD_2Cl_2, 25 ºC) δ: 151.4 (d, $^2J_{CP}$ = 26 Hz, *o*-C_6H_3), 150.4 (*m*-C_6H_3), 149.9 (*m'*-C_6H_3), 148.0 (*o*-C_6H_3), 142.5 (d, $^3J_{CP}$ = 3 Hz, *ipso*-Dtbp), 132.1 (d, $^1J_{CH}$ = 8 Hz, *m*-C_6H_3), 128.4 (d, $^1J_{CP}$ = 41 Hz, *ipso*-C_6H_3), 128.5 (d, $^4J_{CP}$ = 3 Hz, *p*-C_6H_3), 127.9 (*o*-Dtbp), 124.0 (*o*-Dtbp), 122.5 (*p*-Dtbp), 91.2 (d, $^2J_{CP}$ = 3 Hz, C_5Me_5), 35.3 ($(CH_3)_3C_{Dtbp'}$),

35.0 ($(CH_3)_3C_{Dtbp}$), 31.8 ($(CH_3)_3C_{Dtbp}$), 31.5 ($(CH_3)_3C_{Dtbp'}$), 18.9 (d, $^1J_{CP}$ = 36.0 Hz, PMe_2), 8.9 (C_5Me_5).

$^{31}P\{^1H\}$ NMR (120 MHz, CD_2Cl_2, 25 ºC) δ: –19.1.

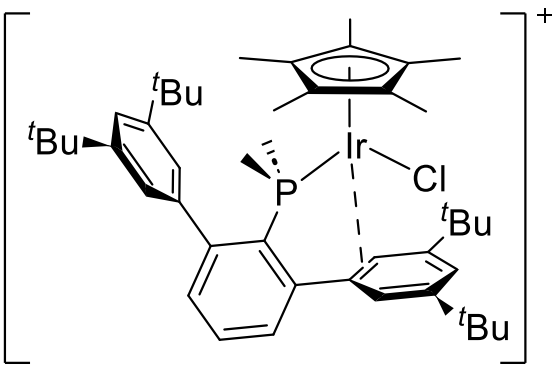

Complex 1*. A dry CH_2Cl_2 solution (12 mL) of **6*** (120 mg, 0.133 mmol) and Na[BAr^F] (118 mg, 0.133 mmol) was stirred at room temperature for 30 min. The solution boasts a dark brown-red color. The solvent was evaporated under reduced pressure and the residue was washed with pentane (3 mL) to yield an orange powder. Yield: 215 mg (93%).

Anal. Calcd. for $C_{78}H_{79}BF_{24}IrP$: C, 54.9; H, 4.7. **Found**: C, 54.9; H, 4.6.

^{1}H NMR (500 MHz, CD_2Cl_2, 25 ºC) δ: 7.85 (s, 2H, *p*-Dtbp), 7.76 (m, 8H, *o*-Ar), 7.59 (s, 4H, *p*-Ar), 7.35 (td, $^3J_{HH}$ = 7.6 Hz, $^5J_{HP}$ = 2.0 Hz, 1H, *p*-C_6H_3), 7.21 (s, 4H, *o*-Dtbp), 6.81 (dd, $^3J_{HH}$ = 7.6 Hz, 2.7 Hz, 2H, *m*-C_6H_3), 1.74 (d, $^2J_{HP}$ = 11.0, 6H, PMe_2), 1.40 (s, 36H, $(CH_3)_3C$), 1.21 (d, $^4J_{HP}$ = 1.6 Hz, 15H, C_5Me_5).

^{13}C{^{1}H} NMR (100 MHz, CD_2Cl_2, 25 ºC) δ: 162.3 (q, $^1J_{CB}$ = 50 Hz, *ipso*-Ar), 151.7 (br., *m*-Dtbp), 147.1 (d, $^2J_{CP}$ = 13 Hz, *o*-C_6H_3), 135.3 (d, $^1J_{CP}$ = 47 Hz, *ipso*-C_6H_3), 132.0 (*p*-C_6H_3), 131.7 (d, *m*-C_6H_3), 129.4 (q, $^2J_{CF}$ = 32 Hz, *m*-Ar), 125.3 (q, $^1J_{CF}$ = 272 Hz, CF_3), 127.14 (*ipso*-Dtbp), 125.5 (m, *o*-Dtbp, *p*-Dtbp), 125.1 (q, $^1J_{CF}$ = 272 Hz, CF_3), 117.9 (m, *p*-Ar), 95.7

(C_5Me_5), 35.8 ($(CH_3)_3C$), 31.4 ($(CH_3)_3C$), 15.9 (d, $^1J_{CP}$ = 36 Hz, PMe_2), 8.6 (C_5Me_5).

$^{31}P\{^1H\}$ NMR (120 MHz, CD_2Cl_2, 25 ºC) δ: 9.0.

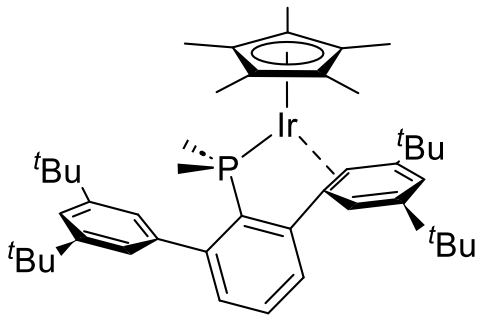

Complex 7*. A dry CH_2Cl_2 solution (12 mL) of **6*** (120 mg, 0.133 mmol) and $CoCp_2$ (51 mg, 0.270 mmol) was stirred at room temperature for 30 min, observing the formation of orange-yellow cobaltocenium salts that precipitated. The solvent was evaporated and the residue was extracted with pentane (3x5 mL). A final evaporation under reduced pressure gave a dark yellow solid. Yield: 46 mg (42 %).

Anal. Calcd. for $C_{46}H_{66}IrP$: C, 65.6; H, 7.9. **Found**: C, 65.7; H, 7.8.

^{1}H NMR (500 MHz, CD_2Cl_2, 25 ºC) δ: 7.41 (s, 1H, *o*-Dtbp), 7.03 (m, 4H, *p*-C_6H_3, *p*-Dtbp, *o*-Dtbp, *m*-C_6H_3), 6.66 (d, $^4J_{HP}$ = 6.7 Hz, 1H, *m*-C_6H_3), 6.44 (s, 1H, *o*-Dtbp'), 6.22 (s, 1H, *p*-Dtbp'), 3.08 (d, $^4J_{HP}$ = 8.5 Hz, 1H, *o*-Dtbp'), 1.67 (d, $^2J_{HP}$ = 10.5 Hz, 6H, PMe_2), 1.55 (s, 15H, C_5Me_5), 1.29 (s, 18H, $(CH_3)_3C_{Dtbp}$), 1.22 (s, 9H, $(CH_3)_3C_{Dtbp'}$), 1.19 (s, 9H, $(CH_3)_3C_{Dtbp'}$).

^{13}C{^{1}H} NMR (100 MHz, CD_2Cl_2, 25 ºC) δ: 165.1 (d, $^2J_{CP}$ = 30 Hz, *o*-C_6H_3), 150.2 (*m*-Dtbp), 150.2 (*o*-C_6H_3), 147.3 (*m*-Dtbp), 141.9 (*ipso*-Dtbp'), 137.6 (*m*-Dtbp), 132.9 (d, $^1J_{CP}$ = 48 Hz, *ipso*-C_6H_3), 128.6 (*p*-C_6H_3), 127.2 (*m*-C_6H_3), 126.4 (d, $^2J_{CP}$ = 13 Hz, *m*-C_6H_3), 124.8 (*o*-Dtbp), 124.3 (*p*-Dtbp), 122.9 (*o*-Dtbp), 121.2 (*o*-Dtbp'), 109.3 (*p*-Dtbp'), 89.9 (C_5Me_5), 49.5 (*ipso*-Dtbp'), 40.9 (*o'*-Dtbp'), 35.7 ($(CH_3)_3C_{Dtbp}$), 35.2 (br., $(CH_3)_3C_{Dtbp'}$, $(CH_3)_3C_{Dtbp}$), 34.4 ($(CH_3)_3C_{Dtbp'}$), 31.2 ($(CH_3)_3C$), 30.9

((CH$_3$)$_3$C), 30.6 ((CH$_3$)$_3$C$_{Dtbp'}$), 29.9 ((CH$_3$)$_3$C$_{Dtbp'}$), 19.7 (d, $^1J_{CP}$ = 42 Hz, PMe), 14.8 (d, $^1J_{CP}$ = 39 Hz, PMe), 9.5 (C$_5$*Me$_5$*).

^{31}P{^{1}H} NMR (120 MHz, CD_2Cl_2, 25 ºC) δ: –1.6.

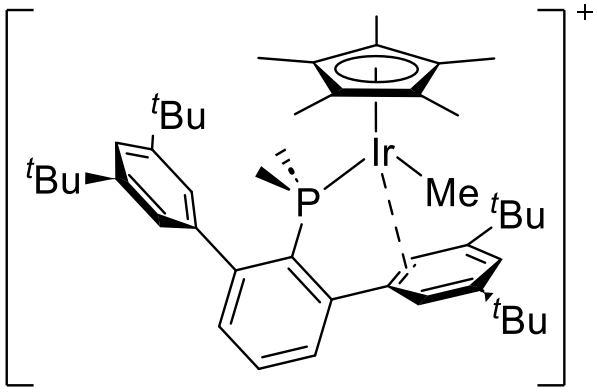

Complex 8*. Complex **7*** (50 mg, 0.059 mmol) was dissolved in 5 mL of dichloromethane. To this solution, 1.1 eq of MeOTf was added (7.6 μL, 0.065 mmol). The solution was stirred for 5 min at –20 ºC. The solvent was evaporated and the residue was washed with cold pentane (3x5 mL) and dried under reduced pressure.

Although pure by $^{31}P\{^{1}H\}$ NMR spectroscopy, the product never offered a clean ^{1}H NMR spectra, this is why only some limited characteristic resonances can be undoubtedly assigned while the rest remain ambiguous due to overlapping signals, impurities, or dynamic behavior. Lowering the temperature (–80 ºC) did not result in improved resolution. The following are the assigned resonances:

^{1}H NMR (500 MHz, CD_2Cl_2, –20 ºC) δ: 7.53 (s, 2H, *p*-Dtbp), 7.03 (s, 4H, *o*-Dtbp), 1.33 (s, 18H, $(CH_3)_3C$), 1.28 (s, 18H, $(CH_3)_3C$), 1.26 (d, $^{4}J_{HP}$ = 1.6 Hz, 15H, C_5Me_5), 0.56 (d, $^{2}J_{HP}$ = 6.4 Hz, 3H, CH_3).

^{13}C{^{1}H} NMR (100 MHz, CD_2Cl_2, –20 ºC) δ: –14.9 (d, $^{2}J_{CP}$ = 14 Hz, CH_3)

^{31}P{^{1}H} NMR (120 MHz, CD_2Cl_2, –20 ºC) δ: 8.6

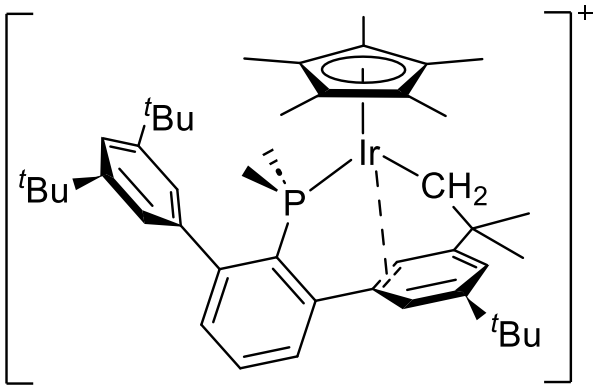

Complex 9*. Complex **7*** (50 mg, 0.059 mmol) was dissolved in 5 mL of dichloromethane. To this solution, 1.1 eq of MeOTf was added (7.6 μL, 0.065 mmol). The solution was stirred for 3h at room temperature. The solvent was evaporated and the residue was washed with pentane (3x5 mL) and dried under reduced pressure to yield a yellow-brown powder. Yield: 16 mg (27 %).

Anal. Calcd. for $C_{47}H_{65}F_3O_3SIrP$: C, 57.0; H, 6.6; S, 3.2. **Found**: C, 57.1; H, 6.5; S, 3.2.

^{1}H NMR (500 MHz, CD_2Cl_2, 25 ºC) δ: 7.62 (s, 1H, *p*-Dtbp), 7.51 (td, $^3J_{HH}$ = 7.7 Hz, $^5J_{HP}$ = 2.5 Hz, 1H, *p*-C_6H_3), 7.38 (m, overlapped, 3H, *m*-C_6H_3, *o*-Dtbp), 7.11 (s, 1H, *p*-Dtbp'), 6.86 (s, 1H, *o*-Dtbp'), 6.83 (ddd, $^3J_{HH}$ = 7.5 Hz, $^4J_{HP}$ = 2.7 Hz, $^4J_{HH}$ = 0.9 Hz, 1H, *m'*-C_6H_3), 3.98 (s, 1H, *o'*-Dtbp'), 2.36 (d, $^2J_{HH}$ = 8.5 Hz, 1H, CH_2), 1.81 (dd, $^2J_{HH}$ = 8.5 Hz, $^3J_{HP}$ = 2.7 Hz, 1H, CH_2), 1.50 (d, $^4J_{HP}$ = 0.9 Hz, 15H, C_5Me_5), 1.43 (s, 9H, $((CH_3)_3C)_{Dtbp'}$), 1.41 (s, 18H, $((CH_3)_3C)_{Dtbp}$), 1.26 (s, 6H, $(CH_3)_2C_{Dtbp'}$), 1.23 (d, $^2J_{HP}$ = 14.7 Hz, 6H, PMe_2).

$^{13}C\{^1H\}$ NMR (100 MHz, CD_2Cl_2, 25 ºC) δ: 157.9 (d, $^2J_{CP}$ = 26 Hz, *o*-C_6H_3), 152.3 (*m*-Dtbp), 152.1 (*m*-Dtbp'), 147.7 (*o*-C_6H_3), 147.1 (*m'*-Dtbp'), 138.7 (*m*-C_6H_3), 133.4 (*p*-C_6H_3), 130.7 (*m*-C_6H_3), 129.5 (*m'*-C_6H_3), 129.0 (*ipso*-Dtbp), 124.8 (*o*-Dtbp), 123.6 (*o*-Dtbp'), 123.4 (br., *o*-Dtbp), 123.1 (*p*-Dtbp), 122.2 (d, $^1J_{CP}$ = 47 Hz, *ipso*-C_6H_3), 122.1 (*ipso*-Dtbp') 117.9 (*p*-Dtbp'), 98.0 (C_5Me_5), 70.8 (*o'*-Dtbp'), 36.2 ($(Me_2CH_2C)_{Dtbp'}$), 35.1 ($(Me_3C)_{Dtbp'}$), 31.2 ($(Me_3C)_{Dtbp}$, $(Me_3C)_{Dtbp}$), 30.2 ($(Me_3C)_{Dtbp}$), 29.7 (Me_2C), 8.2 (C_5Me_5), 1.4 (d, $^1J_{CP}$ = 36 Hz, PMe_2), –2.2 (d, $^2J_{CP}$ = 14 Hz, CH_2)

$^{31}P\{^1H\}$ NMR (120 MHz, CD_2Cl_2, 25 ºC) δ: – 6.9.

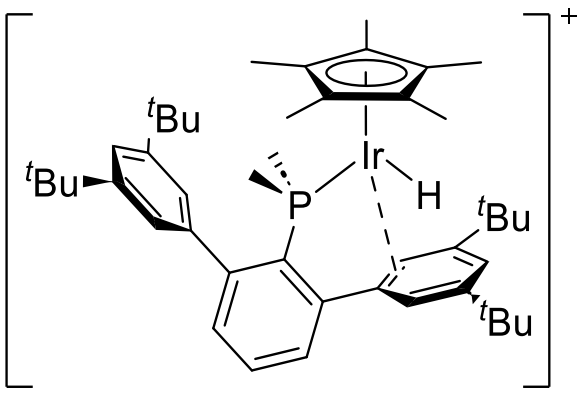

Complex 10*. A dry CH_2Cl_2 solution (12 mL) of **1*** (100 mg, 0.057 mmol) and $PhSiH_3$ (10.4 μL, 0.114 mmol) was stirred at room temperature for 30 min. The solvent was evaporated. The residue was dissolved in Et_2O (4 mL) and precipitated with pentane (15 mL). The solvent was filtered off and the precipitate was dried under reduced pressure to afford a yellow solid. Yield: 94 mg (97 %)

Anal. Calcd. for $C_{78}H_{79}BF_{24}IrP$: C, 54.9; H, 4.7. **Found**: C, 54.9; H, 4.7.

^{1}H NMR (500 MHz, CD_2Cl_2, 25 ºC) δ: 7.72 (m, 8H, *o*-Ar), 7.56 (s, 4H, *p*-Ar), 7.54 (s, 1H, *p*-Dtbp), 7.38 (td, $^3J_{HH}$ = 7.7 Hz, $^5J_{HP}$ = 2.3 Hz 1H, *p*-C_6H_3), 7.16 (m, 1H, *p*-Dtbp'), 7.14 (t, 1H, *o*-Dtbp'), 7.10 (ddd, $^3J_{HH}$ = 7.5 Hz, 3.3 Hz, 1.1 Hz, 1H, *m*-C_6H_3), 7.01 (t, $^3J_{HH}$ = Hz, 1H, *o*-Dtbp'), 6.93 (ddd, $^3J_{HH}$ = 8.0 Hz, $^4J_{HP}$ = 2.7 Hz, $^4J_{HH}$ = 1.1 Hz, 1H, *m*-C_6H_3), 6.90 (m, 1H, *o*-Dtbp), 5.06 (s, 1H, *o*-Dtbp'), 1.88 (d, $^2J_{HP}$ = 11.1 Hz, 3H, P*Me*Me), 1.60 (d, $^2J_{HP}$ = 11.4 Hz, 3H, PMe*Me*), 1.55 (d, $^4J_{HP}$ = 1.6 Hz, 15H, C_5Me_5), 1.44 (s, 9H, Me_3C), 1.36 (s, 9H, Me_3C), 1.33 (s, 18H, Me_3C), –16.6 (d, $^2J_{HP}$ = 31.9 Hz, 1H, IrH).

$^{13}C\{^1H\}$ NMR (100 MHz, CD_2Cl_2, 25 ºC) δ: 162.2 (q, $^1J_{CB}$ = 50 Hz, *ipso*-Ar), 154.1 (d, $^2J_{CP}$ = 25.76 Hz, *o*-C_6H_3), 151.4 (*m*-Dtbp), 150.67 (*m*-Dtbp), 150.37 (*m*-Dtbp), 148.6 (*o*-C_6H_3), 147.3 (*m*-Dtbp), 138.75 (*ipso*-Dtbp), 132.3 (*m*-C_6H_3), 131.9 (*p*-C_6H_3), 131.3 (*m*-C_6H_3), 129.3 (*ipso*-C_6H_3), 129.0 (q, $^2J_{CF}$ = 32 Hz, *m*-Ar), 125.0 (q, $^1J_{CF}$ = 272 Hz, CF_3), 124.8 (*o*-Dtbp), 124.4 (*o*-Dtbp), 122.9 (*p*-Dtbp'), 119.9 (*p*-Dtbp), 117.9 (m, *p*-Ar), 99.3 (C_5Me_5), 86.5 (d, *ipso*-Dtbp), 62.7 (*o*-Dtbp), 36.6 (Me_3C), 35.7 (Me_3C), 35.3 (Me_3C), 31.5 (Me_3C), 30.6 (Me_3C), 30.7 (Me_3C), 26.7 (P*Me*Me), 15.7 (PMe*Me*), 9.4 (C_5Me_5).

$^{31}P\{^1H\}$ NMR (120 MHz, CD_2Cl_2, 25 ºC) δ: – 4.4

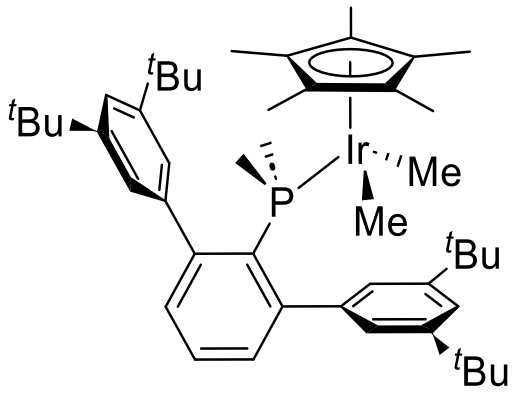

Complex 11*. To a CH_2Cl_2 solution (12 mL) of **1*** (100 mg, 0.057 mmol) in an NMR tube was added 1.5 eq. of MeMgBr (0.028 mL, 0.086 mmol), observing a change of color from red to bright yellow. The product was characterized *in situ* by multinuclear NMR spectroscopy. Crystals can be obtained from slow diffusion of hexane into a concentrated dichloromethane solution.

^{1}H NMR (500 MHz, CD_2Cl_2, 25 ºC) δ: 7.41 (s, 2H, *p*-Dtbp), 7.37 (s, 2H, *o*-Dtbp), 7.14 (td, $^{3}J_{HH}$ = 7.5 Hz, $^{5}J_{HP}$ = 1.5 Hz, 1H, *p*-C_6H_3), 7.06 (m, 4H, *m*-C_6H_3, *o*-Dtbp'), 1.41 (s, 18H, (CH_3)$_3$C)), 1.37 (d, $^{4}J_{HP}$ = 1.9 Hz, 15H, C_5Me_5), 1.35 (s, 18H, (CH_3)$_3$C), 1.29 (d, $^{2}J_{HP}$ = 10.9 Hz, 6H, PMe_2), – 0.47 (d, $^{3}J_{HP}$ = 5.1 Hz, 3H, $IrMe_2$).

^{13}C{^{1}H} NMR (125 MHz, CD_2Cl_2, 25 ºC) δ: 150.8 (*m*-C_6H_3), 148.9 (*m'*-C_6H_3), 148.8 (*o*-C_6H_3), 143.6 (d, $^{3}J_{CP}$ = 3 Hz, *ipso*-Dtbp), 132.0 (d, $^{1}J_{CH}$ = 8 Hz, *m*-C_6H_3), 127.4 (*o*-Dtbp), 126.4 (d, $^{1}J_{CP}$ = 38 Hz, *ipso*-C_6H_3), 126.1 (*p*-C_6H_3), 123.9 (*o*-Dtbp), 121.8 (*p*-Dtbp), 91.4 (d, $^{2}J_{CP}$ = 4 Hz, C_5Me_5), 35.3 ((CH_3)$_3$*C*), 35.0 ((CH_3)$_3$*C*), 31.8 ((CH_3)$_3$C), 31.5 ((CH_3)$_3$C), 20.7 (d, $^{1}J_{CP}$ = 36.0 Hz, PMe_2), 8.6 (C_5Me_5), – 20.6 (d, $^{2}J_{CP}$ = 10 Hz, $IrMe_2$).

^{31}P{^{1}H} NMR (120 MHz, CD_2Cl_2, 25 ºC) δ: – 30.0.

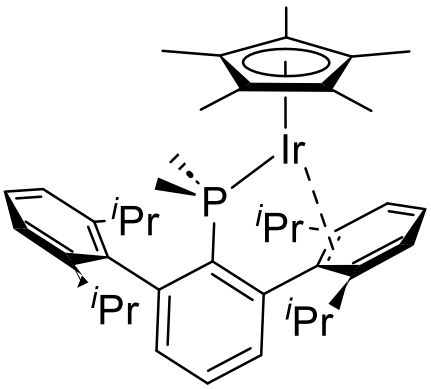

Complex 7. A dry CH_2Cl_2 solution (12 mL) of **1** (100 mg, 0.059 mmol) and $CoCp_2$ (22 mg, 0.121 mmol) was stirred at room temperature for 30 min, observing the formation of orange-yellow cobaltocenium salts that precipitated. The solvent was evaporated and the residue was extracted with pentane (3x5 mL). A final evaporation under reduced pressure gave a dark yellow solid. Yield: 21 mg (51 %).

Anal. Calcd. for $C_{43}H_{61}IrP$: C, 64.5; H, 7.7. **Found**: C, 64.5; H, 7.7.

^{1}H NMR (500 MHz, CD_2Cl_2, –20 ºC) δ: 7.34 (t, 1H, $^3J_{HH}$ = 7.8 Hz *p*-Dipp), 7.22 (d, 1H, $^3J_{HH}$ = 7.8 Hz, *m*-Dipp), 7.17 (d, 1H, $^3J_{HH}$ = 7.8 Hz, *m*-Dipp), 7.16 (t, 1H, $^3J_{HH}$ = 7.6 Hz *p*-C_6H_3), 7.06 (d, 1H, $^3J_{HH}$ = 7.6 Hz *m*-C_6H_3), 6.76 (ddd, 1H, $^3J_{HH}$ = 7.6 Hz, $^4J_{HP}$ = 2.9 Hz, $^4J_{HH}$ = 1.0 Hz, *m*-C_6H_3), 6.25 (d, $^3J_{HH}$ = 8.3 Hz, 1H, *m*-Dipp'), 6.10 (d, 1H, $^3J_{HH}$ = 6.5 Hz, *m*-Dipp'), 6.01 (dd, 1H, $^3J_{HH}$ = 8.3 Hz, $^3J_{HH}$ = 6.5 Hz, *m*-Dipp'), 2.98 (sept, 1H, $^3J_{HH}$ = 6.8 Hz, (C*H*Me$_2$)$_{Dipp'}$), 2.55 (sept, 1H, $^3J_{HH}$ = 6.8 Hz, (C*H*Me$_2$)$_{Dipp}$), 2.05 (sept, ^{1}H, $^3J_{HH}$ = 6.7 Hz, (C*H*Me$_2$)$_{Dipp'}$) 1.46 (d, 6H, $^2J_{HP}$ = 10.2 Hz, PMe$_2$), 1.43 (s, 15H, C_5*Me$_5$*), 1.22 (m, overlapped, 6H, (CH*Me*$_2$)$_{Dipp}$), 1.15 (m, 6H, (CH*Me*)$_{Dipp}$, PMe), 1.10 (m, overlapped, 6H, (CH*Me*$_2$)$_{Dipp}$), 0.99 (m, overlapped, 6H, (CH*Me*$_2$)$_{Dipp}$), 0.80 (d, 3H, $^3J_{HH}$ =

6.7 Hz, (CH*Me*$_2$)$_{Dipp}$), 0.51(sept, 1H, $^3J_{HH}$ = 6.8 Hz, (C*H*Me$_2$)$_{Dipp'}$), 0.19 (d, 3H, $^3J_{HH}$ = 6.7 Hz, (CH*Me*$_2$)$_{Dipp'}$).

^{13}C{^{1}H} NMR (100 MHz, CD_2Cl_2, 25 ºC) δ: 148.1 (*o*-Dipp'), 150.2 (*m*-Dipp), 147.8 (*o*-Dipp), 146.6 (*o*-Dipp), 140.3 (*m*-Dipp), 138.1 (*o*-Dipp), 136.6 (d, $^1J_{CP}$ = 50 Hz, *ipso*-C_6H_3), 133.2 (*m*-C_6H_3), 131.2 (d, $^2J_{CP}$ = 13 Hz, *m*-C_6H_3), 126.4 (*m*-Dipp), 128.4 (*p*-Dipp), 127.3 (*p*- C_6H_3), 122.3 (*o*-C_6H_3, *ipso*-Dipp), 114.8 (*p*-Dipp'), 107.8 (*m*-Dipp'), 90.9 (*C*$_5$Me$_5$), 61.2 (*ipso*-Dipp'), 51.9 (*o*-Dipp'), 36.7 (*C*HMe$_2$), 31.6 (*C*HMe$_2$), 30.9 (*C*HMe$_2$), 30.5 (*C*HMe$_2$), 26.5 (CH*Me*$_2$), 25.8 (CH*Me*$_2$), 24.8 (CH*Me*$_2$), 23.0 (CH*Me*$_2$), 21.4 (CH*Me*$_2$), 21.3, (CH*Me*$_2$), 21.2 (CH*Me*$_2$), 21.0 (CH*Me*$_2$), 18.2 (d, $^1J_{CP}$ = 38 Hz, P*Me*Me), 15.4 (d, $^1J_{CP}$ = 36 Hz, PMe*Me*), 9.1 (C$_5$*Me*$_5$).

^{31}P{^{1}H} NMR (120 MHz, CD_2Cl_2, 25 ºC) δ: 3.4.

REFERENCES

1. a) Goldberg, K. I.; Goldman, A. S. *Activation and Functionalization of C−H bonds*. ACS Symposium Series 885, American Chemical Society, Washington DC, 2004; b) Bergman, R. G. *Nature* **2007**, *446*, 391–393.

2. a) Hill, C. L. *Activation and functionalization of alkanes*. John Wiley & Sons, New York, 1989; b) Pérez, P. J. *Alkane C−H Activation by Single-Site Metal Catalysis*. Springer, Dordrecht, 2012; c) Labinger, J. A.; Bercaw, J. E. *Nature* **2002**, *417*, 507–514.

3. Caballero, A.; Pérez, P. J. *Chem. Soc. Rev.* **2013**, *42*, 8809–8820.

4. Gunsalus, N. J.; Koppaka, A.; Park, S. H.; Bischof, S. M.; Hashiguchi, B. G.; Periana, R. A. *Chem. Rev.* **2017**, *117*, 8521–8573.

5. a) Belgued, M., Pareja, P., Amariglio, A., Amariglio, H. *Nature* **1991**, *352*, 789–790. b) Guo, X.; Fang, G.; Li, G.; Ma, H.; Fan, H.; Yu, L.; Ma, C.; Wu, X.; Deng, D.; Wei, M.; Tan, D.; Si, R.; Zhang, S.; Li, J.; Sun, L.; Tang, Z.; Pan, X.; Bao, X. *Science* **2014**, *344*, 616–619. c) Morejudo, S. H.; Zanon, R.; Escolastico, S.; Yuste-Tirados, I.; Malerod-Fjeld, H.; Vestre, P. K.; Coors, W. G.; Martinez, A.; Norby, T.; Serra, J. M.; Kjølseth, C. *Science* **2016**, *353*, 563–566.

6. a) Lin, M.; Sen, A. *Nature* **1994**, *368*, 613–615. b) Periana, R. A., Mironov, O., Taube, D., Bhalla, G., Jones, C. J. *Science* **2003**, *301*, 814–818. c) Cui, X.; Li, H.; Wang, Y.; Hu, Y.; Hua, L.; Li, H.; Han, X.; Liu, Q.; Yanf, F.; He, L.; Chen, X.; Li, Q.; Xiao, J.; Deng, D.; Bao, X. *Chem* **2018**, *4*, 1902–1910.

7. a) Periana, R. A.; Taube, D. J.; Gamble, S.; Taube, H.; Satoh, T.; Fujii, H. *Science* **1998**, *280*, 560–564. b) Caballero, A.; Despagnet-Ayoub, E.; Díaz-Requejo, M. M.; Díaz-Rodríguez, A.; Gonzalez-Núñez, M. E.; Mello, R.; Muñoz, B. K.; Ojo, W.-S.; Asensio, G.; Etienne, M.; Pérez, P. J. *Science* **2011**, *332*, 835–838.

8. a) Periana, R. A.; Taube, D. J.; Evitt, E. R.; Löffler, D. G.; Wentrcek, P. R.; Voss, G.; Masuda, T. *Science* **1993**, *259*, 340–343. b) Hammond, C.; Forde, M. M.; Rahim, M. H. A.; Thetford, A.; He, Q.; Jenkins, R. L.; Dimitratos, N.; Lopez-Sanchez, J. A.; Dummer, N. F.; Murphy, D. M.;

Carley, A. F.; Taylor, S. H.; Willock, D. J.; Stangland, E. E.; Kang, J.; Hagen, H.; Kiely, C. J.; Hutchings, G. J. *Angew. Chem., Int. Ed.* **2012**, *51*, 5129–5133. c) Sushkevich, V.L.; Palagin, D.; Ranocchiari, M.; van Bokhoven, J.A.; *Science* **2017**, *356*, 523–527. d) Agarwal, N.; Freakley, S. J.; McVicker, R. U.; Althahban, S. M.; Dimitratos, N.; He, Q.; Morgan, D. J.; Jenkins, R. L.; Willock, D. J.; Taylor, S. H.; Kiely, C. J.; Hutchings, G. J. *Science* **2017**, *358*, 223–227. e) Baek, J.; Rungtaweevoranit, B.; Pei, X.; Park, M.; Fakra, S. C.; Liu, Y.-S.; Matheu, R.; Alshmimri, S. A.; Alshehri, S.; Trickett, C. A.; Somorjai, G. A.; Yaghi, O. M. *J. Am. Chem. Soc.* **2018**, *140*, 18208–18216.

9. a) Godula, K.; Sames, D. *Science* **2006**, *312*, 67–72. b) Rech, J. C.; Yato, M.; Duckett, D.; Ember, B.; LoGrasso, P. V.; Bergman, R. G.; Ellman, J. A. *J. Am. Chem. Soc.* **2007**, *129*, 490–491. c) Davies, H. M. L.; Manning, J. R. *Nature* **2008**, *451*, 417–424. d) McMurray, L.; O'Hara, F.; Gaunt, M. J. *Chem. Soc. Rev.* **2011**, *40*, 1885–1898. e) Yamaguchi, J.; Yamaguchi, A. D.; Itami, K. *Angew. Chem. Int. Ed.* **2012**, *51*, 8960–9009. f) Wencel-Delord, J.; Glorius, F. *Nat. Chem.* **2013**, *5*, 369–375. g) He, J.; Hamann, L. G. H.; Davies, H. M. L.; Beckwith, R. E. J. *Nat. Commun.* **2015**, *6*, 5943.

10. a) Dimroth, O. *Ber. Dtsch. Chem. Ges.* **1898**, *31*, 2154–2156; b) Dimroth, O. *Ber. Dtsch. Chem. Ges.* **1902**, *35*, 2032–2045.

11. Chatt, J.; Watson, H. R. *J. Chem. Soc.* **1962**, 2545–2549.

12. a) Gol'dshleger, N.F.; Tyabin, M.B.; Shilov, A.E.; Shteinman, A. A. *Zh. Fiz. Khim.* **1969**, *43*, 2174–2175. b) Gol'dshleger, N. F.; Shteinman, A. A.; Shilov, A. E.; Eskova, V. V. *Zh. Fiz. Khim.* **1972**, *46*, 1353–1354.

13. a) Hartwig, J. F. *J. Am. Chem. Soc.* **2016**, *138*, 2–24. b) Altus, K.M.; Love, J.A.; *Commun. Chem*. **2021**, *4*, 173.

14. a) Roudesly, F.; Oble, J.; Poli, G. *J. Mol. Catal. A: Chem* **2017**, *426*, 275–296. b)Vastine, B. A.; Hall, M. B. *J. Am. Chem. Soc.* **2007**, *129*, 12068–12069.

15. Ess, D. H.; Bischof, S. M.; Oxgaard, J.; Periana, R. A.; Goddard, W. A. *Organometallics*, **2008**, *27*, 6440–6445.

16. Cheng, Y.-H.; Ho, Y.-S.; Yang, C.-J.; Chen, C.-Y.; Hsieh, C.-T.; Cheng, M.-J. *J. Phys. Chem. A* **2024**, *128*, 4638–4650.

17. a) Klei, S. R.; Tilley, T. D.; Bergman, R. G. *J. Am. Chem. Soc.* **2000**, *122*, 1816–1817. b) Balcells, D.; Clot, E.; Eisenstein, O.; *Chem. Rev.* **2010**, *110*, 749–823. c) Carlsen, R.; Wohlgemuth, N.; Carlson, L.; Ess, D. H. *J. Am. Chem. Soc.* **2018**, *140*, 11039–11045. d) Taw, F.L.; Mellows, H.; White, P. S.; Hollander, F. J.; Bergman, R. G.;Brookhart, M.; Heinekey, D. M. *J. Am. Chem. Soc.* **2002**, *124*, 5100–5108.

18. Shang, R.; Ilies, L.; Nakamura, E. *Chem. Rev.* **2017**, *117*, 9086–9139.

19. a) Moselage, M.; Li, J.; Ackermann, L. *ACS Catal.* **2016**, *6*, 498–525. b) Yoshino, T.; Matsunaga, S. *Adv. Organomet. Chem.* **2017**, *68*, 197–247.

20. a) Zhou, W.; Zheng, S.; Schultz, J. W.; Rath, N. P.; Mirica, L. M. *J. Am. Chem. Soc.* **2016**, *138,* 5777–5780. b) Chong, E.; Kampf, J. W.; Ariafard, A.; Canty, A. J.; Sanford, M. S. *J. Am. Chem. Soc.* **2017**, *139*, 6058–6061.

21. a) Gava, R.; Olmos, A.; Noverges, B.; Varea, T.; Álvarez, E.; Belderrain, T. R.; Caballero, A.; Asensio, G.; Pérez, P. J. *ACS Catal.* **2015**, *5,* 3726–3730. b) Guo, X.-X.; Gu, D.-W.; Wu, Z.; Zhang, W. *Chem. Rev.* **2015**, *115*, 1622–1651.

22. Crabtree, R. H., Mihelcic, J. M.; Quirk, J. M. *J. Am. Chem. Soc.* **1979**, *101*, 7738–7740.

23. Felkin, H.; Fillebeen-Khan, T.; Gault, Y.; Holmes-Smith, R.; Zakrzewski, J. *Tetrahedron Lett.* **1984**, *25*, 1279–1282.

24. Liu, F.; Pak, E. B.; Singh, B.; Jensen, C. M.; Goldman, A. S. *J. Am. Chem. Soc.* **1999**, *121*, 4086–4087.

25. Goldman, A. S.; Roy, A. H.; Huang, Z.; Ahuja, R.; Schinski, W.; Brookhart, M. *Science* **2006**, *312*, 257–261.

26. Conk, R. J.; Hanna, S.; Shi, J. X.; Yang, J.; Ciccia, N. R.; Qi, L.; Bloomer, B. J.; Heuvel, S.; Wills, T.; Su, J.; Bell, A. T.; Hartwig, J. F. *Science* **2022**, *377*, 1561–1566.

27. Green, M. L. H.; Knowles, P. J. *J. Chem. Soc. D* **1970**, 1677–1677.

28. Janowicz, A.H.; Bergman, R. G. *J. Am. Chem. Soc.* **1982**, *104*, 352–354.

29. Hoyano, J. K.; Graham, W.A.G. *J. Am. Chem. Soc.* **1982**, *104*, 3723–3725.

30. Arndtsen, B. A.; Bergman, R. G. *Science* **1995**, *270*, 1970–1973.

31. For a review on this topic see: Shilov, A. E.; Shul'pin, G. B. *Activation and Catalytic Reactions of Saturated Hydrocarbons in the Presence of Metal Complexes*, 2000, Kluwer Academic, Dordrecht.

32. Itoh, M.; Hirano, K.; Satoh, T.; Shibata, Y.; Tanaka, K.; Miura, M. *J. Org. Chem.* **2013**, *78,* 1365–1370.

33. a) Zhou, M.; Schley, N. D.; Crabtree, R. H. *J. Am. Chem. Soc.* **2010**, *132*, 12550–12551; b) Zhou, M.; Balcells, D.; Parent, A. R.; Crabtree, R. H.; Eisenstein, O. *ACS Catal.* **2012**, *2*, 208–218.

34. Weis, E.; Johansson, M.; Korsgren, P.; Martín-Matute, B.; Johansson, M. J. *JACS Au* **2022,** *2*, 906–916.

35. a) Kealy, T. J.; Pauson, P. L. *Nature* **1951**, *168*, 1039−1040. b) Miller, A.; Tebboth, J. A.; Tremaine, F. *J. Chem. Soc.* **1952**, 632−635.

36. Crabtree, R. H. *J. Organomet. Chem.* **2005**, *690*, 5451−5457.

37. a) Poli, R. *Chem. Rev*. **1991**, *91*, 509−551. b) Budzelaar, P. H. M.; Engelberts, J. J.; van Lenthe, J. H. *Organometallics* **2003**, *22*, 1562−1576. c) Evans, W. J. *Organometallics* **2016**, *35*, 3088−3100.

38. a) O'Connor, J. M.; Casey, C. P. *Chem. Rev.* **1987**, *87*, 307−318. b) Veiros, L. F. *Organometallics* **2000**, *19*, 3127−3136.

39. Deck, P. A. *Coord. Chem. Rev*. **2006**, *250*, 1032−1055.

40. a) Ruspic, C.; Moss, J. R.; Schürmann, M.; Harder, S. *Angew. Chem. Int. Ed*. **2008**, *47*, 2121−2126. b) Meyer, G. *Angew. Chem., Int. Ed.* **2008**, *47*, 4962−4964. c) Harder, S.; Naglav, D.; Schwerdtfeger, P.; Nowik, I.; Herber, R.H. *Inorg. Chem.* **2014**, *53*, 2188−2194. d) van Velzen, N. J. C.; Harder, S. *Organometallics* **2018**, *37*, 2263−2271. e) Giesbrecht, G. R.; Gordon, J. C.; Clark, D. L.; Scott, B. L. *Dalton Trans.* **2003**, *3*, 2658−2665. f) Orzechowski, L.; Piesik, D. F. J.; Ruspic, C.; Harder, S. *Dalton Trans.* **2008**, *35*, 4742−4746. g) Harder, S.; Ruspic, C. *J. Organomet. Chem.* **2009**, *694*, 1180−1184.

41. a) Blais, M. S.; Rausch, M. D. *J. Organomet. Chem.* **1995**, *502*, 1–8. b) Conway, B. G.; Rausch, M. D. *Organometallics* **1985**, *4*, 688–693.

42. a) Chen, E. Y.-X.; Kruper, W. J.; Roof, G.; Wilson, D. R. *J. Am. Chem. Soc.* **2001**, *123*, 745−746. b) Mitchell, J. P.; Hajela, S.; Brookhart, S. K.; Hardcastle, K. I.; Henling, L. M.; Bercaw, J. E. *J. Am. Chem. Soc.* **1996**, *118*, 1045−1053. c) Busico, V.; Cipullo, R. *J. Am. Chem. Soc.* **1994**, *116*, 9329−9330. d) Wang, B. *Coord. Chem. Rev*. **2006**, *250*, 242−258.

43. Mas-Roselló, J.; Herraiz, A. G.; Audic, B.; Laverny, A.; Cramer, N. *Angew. Chem., Int. Ed.* **2021**, *60*, 13198−13224.

44. a) Bernechea, M.; Berenguer, J. R.; Lalinde, E.; Torroba, J. *Organometallics* **2009**, *28*, 312−320. b) Fan, L.; Wei, C.; Aigbirhio, F. I.; Turner, M. L.; Gusev, O. V.; Morozova, L. N.; Knowles, D. R. T.; Maitlis, P. M. *Organometallics* **1996**, *15*, 98−104. c) Glueck, D. S.; Bergman, R. G. *Organometallics* **1990**, *9*, 2862−2863. d) Caldwell, H.; Pregosin, P. S. *Organometallics* **2008**, *27*, 1591−1595.

45. Moreno, J. J.; Espada, M. F.; Campos, J.; López-Serrano, J.; Macgregor, S. A.; Carmona, E. *J. Am. Chem. Soc.* **2019**, *141*, 2205−2210.

46. a) Takemoto, S.; Morita, H.; Karitani, K.; Fujiwara, H.;Matsuzaka, H. *J. Am. Chem. Soc.* **2009**, *131*, 18026−18027. b) Cloke, F. G. N.; Green, J. C.; Green, M. L. H.; Morley, C. P. *Chem. Commun*. **1985**, *14*, 945−946. c) Kupfer, V.; Thewalt, U.; Tišlerová, I.; Štěpnička, P.; Gyepes, R.; Kubiš ta, J.; Horáček, M.; Mach, K. *J. Organomet. Chem.* **2001**, *620*, 39−50. d) Sun, Y.; Spence, R. E. V. H.; Piers, W. E.; Parvez, M.; Yap, G. P.A. *J. Am. Chem. Soc.* **1997**, *119*, 5132−5143. e) Mori, Y.; Ando, T.; Matsumoto, T.; Yatabe, T.; Kikkawa, M.; Yoon, K.-S.; Ogo, S. *Angew. Chem., Int. Ed.* **2018**, *57*, 15792−15796. f) Rodríguez-Bárzano, A.; Blacker, A. J.; McGowan, P. C. *Dalton Trans*. **2013**, *42*, 16669−16671. g) Holland, P. L.; Andersen, R. A.; Bergman, R. G.; Huang, J.; Nolan, S. P. *J. Am. Chem. Soc.* **1997**, *119*, 12800−12814. h) Rüba, E.; Mereiter, K.; Schmid, R.; Kirchner, K.; Bustelo, E.; Puerta, M. C.; Valerga, P. *Organometallics* **2002**, *21*, 2912−2920.

47. a) Klet, R. C.; Kaphan, D. M.; Liu, C.; Yang, C.; Kropf, A. J.; Perras, F. A.; Pruski, M.; Hock, A. S.; Delferro, M. *J. Am. Chem. Soc*. **2018**, *140*, 6308−6316. b) Li, S.; Wang, X.; Zhang, Z.; Zhao, Y.; Wang, X. *Dalton Trans*. **2015**, *44*, 19754−19757. c) Meredith, J. M.; Goldberg, K. I.; Kaminsky, W.; Heinekey, D.M. *Organometallics* **2012**, *31*, 8459−8462.

48. a) Einstein, F. W. B.; Jones, R. H.; Zhang, X.; Yan, X.; Nagelkerke, R.; Sutton, D. *Chem. Commun.* **1989**, *19*, 1424−1426. b) Wang, W.; Davis, H. B.; Einstein, F. W. B.; Pomeroy, R. K. *Organometallics* **1994**, *13*, 5113−5121. c) Evans, W. J.; Perotti, J. M.; Ziller, J. W. *Inorg. Chem.* **2005**, *44*, 5820−5825. d) Takahashi, Y.; Fujita, K.; Yamaguchi, R. *Eur. J. Inorg. Chem.* **2008**, *28*, 4360−4368. e) Carbó, J. J.; García-López, D.; Gómez-Pantoja, M.; González-Pérez, J. I.; Martín, A.; Mena, M.; Santamaría, C. *Organometallics* **2017**, *36*, 3076−3083. f) Dyllick-Brenzinger, R.; Olsen, H. *J. Am. Chem. Soc.* **1981**, *103*, 704−706. g) Chung, C.; Tseng, W.-C.; Chi, Y.; Peng, S.-M.; Lee, G.-H. *Organometallics* **1998**, *17*, 2207−2214. h) Shima, T.; Hou, Z. *Organometallics* **2009**, *28*, 2244−2252.

49. a) McDade, C.; Green, J. C.; Bercaw, J. E. A. *Organometallics* **1982**, *1*, 1629−1634. b) Bulls, A. R.; Schaefer, W. P.; Serfas, M.; Bercaw, J. E. *Organometallics* **1987**, *6*, 1219−1226. c) Bercaw, J. E. *J. Am. Chem. Soc.* **1974**, *96*, 5087−5095. d) Cloke, F. G. N.; Day, J. P.; Green, J. C.; Morley, C. P.; Swain, A. C. *Dalton Trans*. **1991**, 789−796.

50. Alférez, M. G.; Moreno, J. J.; Hidalgo, N.; Campos, J. *Angew. Chem., Int. Ed.* **2020**, *59*, 20863−20867.

51. a) Chalkley, M. J.; del Castillo, T. J.; Matson, B. D.; Roddy, J. P.; Peters, J. C. *ACS Cent. Sci.* **2017**, *3*, 217−223. b) Chalkley, M. J.; del Castillo, T. J.; Matson, B. D.; Peters, J. C. *J. Am. Chem. Soc*. **2018**, *140*, 6122−6129. c) Chalkley, M. J.; Oyala, P. H.; Peters, J. C. *J. Am. Chem. Soc*. **2019**, *141*, 4721−4729. d) Quintana, L. M. A.; Johnson, S. I.; Corona, S. L.; Villatoro, W.; Goddard, W. A.; Takase, M. K.; VanderVelde, D. G.; Winkler, J. R.; Gray, H. B.; Blakemore, J. D. *Proc. Natl. Acad. Sci. U. S. A*. **2016**, *113*, 6409−6414. e) Pitman, C. L.; Finster, O. N. L.; Miller, A. J. M. *Chem. Commun.* **2016**, *52*, 9105−9108. f) Pal, S.; Kusumoto, S.; Nozaki, K. *Organometallics* **2018**, *37*, 906−914. g) Kefalidis, C. E.; Perrin, L.; Burns, C. J.; Berg, D. J.; Maron, L.; Andersen, R. A. *Dalton Trans.* **2015**, *44*, 2575−2587.

52. a) Gusev, O.; Denisovich, L. I.; Peterleitner, M. G.; Rubezhov, A. Z.; Ustynyuk, N. A.; Maitlis, P. M. *J. Organomet. Chem.* **1993**, *452*, 219−222. b) Gusev, O. V.; Peterleitner, M. G.; Ievlev, M. A.; Kal'sin, A. M.; Petrovskii, P. V.; Denisovich, L. I.; Ustynyuk, N. A. *J. Organomet. Chem.* **1997**, *531*, 95−100. c) Blaha, J. P.; Wrighton, M. S. *J. Am. Chem. Soc.* **1985**, *107*, 2694−2702.

53. Tellers, D. M.; Yung, C. M.; Arndtsen, B.; Adamson, D. R.; Bergman, R. G. *J. Am. Chem. Soc.* **2002**, *124*, 1400–1410.

54. Moreno, J. J.; Espada, M. F.; Maya, C.; Campos, J.; López-Serrano, J.; Macgregor, S. A.; Carmona, E. *Polyhedron* **2021**, *207*, 115363.

55. a) Campos, J.; López-Serrano, J.; Álvarez, E.; Carmona, E. *J. Am. Chem. Soc.* **2012**, *134*, 7165–7175. b) Campos, J.; Esqueda, A. C.; Carmona, E. *Chem. Eur. J.* **2010**, *16*, 419–422.

56. a) Yao, Z.-J.; Lin, Y.-J.; Xu, B.; Jin, G.-X. *Dalton Trans*. **2014**, *43*, 4938−4940. b) Moseley, K.; Kang, J. W.; Maitlis, P.M. *J. Chem. Soc. A: Inorg. Phys. Theor.* **1970**, 2875−2883. c) Razuvaev, G. A.; Maryin, V. P.; Vyshinskaya, L. I.; Ya, G.; Mal'kova, Y.; Andrianov, A.; Druzhkov, O.N. *Dokl. Akad. Nauk SSSR* **1987**, *294*, 614–617. d) Kochi, T.; Nomura, Y.; Tang, Z.; Ishii, Y.; Mizobe, Y.; Hidai, M. *Dalton Trans.* **1999**, *15*, 2575−2582.

57. a) de Azevedo, C. G.; Calhorda, M. J.; de Carrondo, M. A. A. F.; Dias, A. R.; Duarte, M. T.; Galvão, A. M.; Gamelas, C. A.; Gonçalves, I. S.; da Piedade, F. M.; Romão, C. C. *J. Organomet. Chem.* **1997**, *544*, 257−276. b) Comte, V.; Blacque, O.; Kubicki, M. M.; Moïse, C. *Organometallics* **1997**, *16*, 5763−5769. c) Hughes, R. P.; Maddock, S. M.; Guzei, I. A.; Liable-Sands, L.M.; Rheingold, A. L. *J. Am. Chem. Soc.* **2001**, *123*, 3279−3288. d) Hughes, R. P.; Maddock, S. M.; Rheingold, A. L.; Liable-Sands, L. M. *J. Am. Chem. Soc.* **1997**, *119*, 5988−5989. e) Liu, R.; Zhou, X. *Chem. Commun*. **2013**, *49*, 3171−3187. f) Comte, V.; Blacque, O.; Kubicki, M. M.; Moïse, C. *Organometallics* **2001**, *20*, 5432−5439. g) Forschner, T. C.; Cooper, N. J. *J. Am. Chem. Soc*. **1989**, *111*, 7420−7424. h) Basato, M.; Biffis, A.; Buscemi, G.; Callegaro, E.; Polo, M.; Tubaro, C.; Venzo, A.; Vianini, C.; Graiff, C.; Tiripicchio, A.; Benetollo, F. *Organometallics* **2007**, *26*, 4265−4270. i) Basato, M.; Biffis, A.; Tubaro, C.; Graiff, C.; Tiripicchio. *Dalton Trans.* **2004**, *24*, 4092−409. j) Fischer, E. O.; Herberich, G. E. *Chem. Ber*. **1961**, *94*, 1517−1523. k) Fischer, E. O.; Angelici, R. J. *J. Am. Chem. Soc.* **1963**, *85*, 3733−3735.

58. a) Millward, D. B.; Waymouth, R. M. *Organometallics* **1997**, *16*, 1153−1158. b) Suzuki, N.; Kondakov, D. Y.; Takahashi, T. *J. Am. Chem. Soc.* **1993**, *115*, 8485−8486. c) Dzhemilev, U. M.; D'yakonov, V. A.; Khafizova, L. O.; Ibragimov, A. G. *Tetrahedron* **2004**, *60*, 1287−1291. c) Morken, J. P.; Didiuk, M. T.; Hoveyda, A. H. *J. Am. Chem. Soc.* **1993**, *115*, 6997−6998. d) Negishi, E.-I.; Takahashi, T. *Acc. Chem. Res.* **1994**,

27, 124−130. e) Takahashi, T.; Seki, T.; Nitto, Y.; Saburi, M.; Rousset, C. J.; Negishi, E. *J. Am. Chem. Soc.* **1991**, *113*, 6266−6268. f) Farády, L.; Bencze, L.; Markó, L. *J. Organomet. Chem.* **1967**, *10*, 505−510. g) Farády, L.; Markó, L. *J. Organomet. Chem.* **1971**, *28*, 159−165. h) Negishi, E.; Rousset, C. J.; Choueiry, D.; Maye, J. P.; Suzuki, N.; Takahashi, T. *Inorg. Chim. Acta* **1998**, *280*, 8−20.

59. a) Uemura, M.; Yorimitsu, H.; Oshima, K. *Chem. Commun*. **2006**, *45*, 4726−4728. b) Fürstner, A.; Martin, R.; Krause, H.; Seidel, G.; Goddard, R.; Lehmann, C. W. *J. Am. Chem. Soc.* **2008**, *130*, 8773−8787. c) Monnereau, L.; Sémeril, D.; Matt, D.; Toupet, L.; Mota, A. J. *Adv. Synth. Catal.* **2009**, *351*, 1383−1389. d) Goetz, A. E.; Garg, N. K. *Nat. Chem.* **2013**, *5*, 54−60. e) Macklin, T. K.; Snieckus, V. *Org. Lett*. **2005**, *7*, 2519−2522. f) Teo, W. J.; Wang, Z.; Xue, F.; Andy Hor, T. S.; Zhao, J. *Dalton Trans.* **2016**, *45*, 7312−7319.

60. Tamba, S.; Fuji, K.; Meguro, H.; Okamoto, S.; Tendo, T.; Komobuchi, R.; Sugie, A.; Nishino, T.; Mori, A. *Chem. Lett.* **2013**, *42*, 281−283.

61. a) Yanlong, Q.; Lu; Jiaqui; Weihua, X. *J. Mol. Catal.* **1986**, *34*, 31−38. b) Tao, X.; Qian, F.; Yong, L.; Qian, Y. *J. Mol. Catal. A: Chem*. **2000**, *156*, 121−126.

62. a) Dysard, J. M.; Tilley, T. D. *J. Am. Chem. Soc.* **2000**, *122*, 3097−3105. b) Mohapatra, S. K.; Büschel, S.; Daniliuc, C.; Jones, P. G.; Tamm, M. *J. Am. Chem. Soc*. **2009**, *131*, 17014−17023. c) Chiu, M.; Hoyt, H. M.; Michael, F. E.; Bergman, R. G.; vanHalbeek, H. *Angew. Chem. Int. Ed.* **2008**, *47*, 6073−6076. d) Martín, A.; Mena, M.; Morales-Varela, M. D. C.; Santamaría, C. *Eur. J. Inorg. Chem.* **2004**, *9*, 1914−1921. e) Hernán-Gómez, A.; Martín, A.; Mena, M.; Santamaría, C. *Dalton Trans.* **2013**, *42*, 5076−5084. f) Visser, C.; Meetsma, A.; Hessen, B. *Organometallics* **2002**, *21*, 1912−1918. g) Kirchbauer, F. G.; Pellny, P.-M.; Sun, H.; Burlakov, V. V.; Arndt, P.; Baumann, W.; Spannenberg, A.; Rosenthal, U. *Organometallics* **2001**, *20*, 5289−5296. h) García-Castro, M.; Martín, A.; Mena, M.; Yélamos, C. *Organometallics* **2004**, *23*, 1496−1500. i) Schock, L. E.; Marks, T. J. *J. Am. Chem. Soc.* **1988**, *110*, 7701−7715.

63. a) Golden, J. T.; Peterson, T. H.; Holland, P. L.; Bergman, R. G.; Andersen, R. A. *J. Am. Chem. Soc.* **1998**, *120*, 223−224. b) Bretschneider-Hurley, A.; Winter, C. H. *J. Am. Chem. Soc*. **1994**, *116*, 6468−6469. c) Ohashi, M.; Matsubara, K.; Iizuka, T.; Suzuki, H. *Angew. Chem., Int. Ed.* **2003**, *42*, 937−940. d) Seneviratne, K. N.; Bretschneider-Hurley, A.;

Winter, C. H. *J. Am. Chem. Soc.* **1996**, *118*, 5506−5507. e) Chao, S.; Robbins, J. L.; Wrighton, M. S. *J. Am. Chem. Soc.* **1983**, *105*, 181−188. f) Sun, X.; Singh, A. K.; Yadav, R.; Jin, D.; Haimerl, M.; Scheer, M.; Roesky, P. W. *Chem. Commun.* **2022**, *58*, 673−676. g) Weng, W.; Bartik, T.; Brady, M.; Bartik, B.; Ramsden, J. A.; Arif, A. M.; Gladysz, J. A. *J. Am. Chem. Soc*. **1995**, *117*, 11922−11931. h) Herring, F. G.; Legzdins, P.; Richter-Addo, G. B. *Organometallics* **1989**, *8*, 1485−1493. i) Glassman, T. E.; Liu, A. H.; Schrock, R. R. *Inorg. Chem.* **1991**, *30*, 4723−4732.

64. Crabtree, R. H. *Chem. Rev.* **2015**, *115*, 127−150.

65. a) Maimone, T. J.; Milner, P. J.; Kinzel, T.; Zhang, Y.; Takase, M.K.; Buchwald, S. L. *J. Am. Chem. Soc.* **2011**, *133*, 18106−18109. b) Milner, P. J.; Maimone, T. J.; Su, M.; Chen, J.; Müller, P.; Buchwald, S. L. *J. Am. Chem. Soc.* **2012**, *134*, 19922−19934. c) Sather, A. C.; Lee, H. G.; de La Rosa, V. Y.; Yang, Y.; Müller, P.; Buchwald, S. L. *J. Am. Chem. Soc.* **2015**, *137*, 13433−13438.

66. a) Janowicz, A. H.; Bergman, R. G. C-H. *J. Am. Chem. Soc.* **1982**, *104*, 352−354. b) Marinelli, G.; Rachidi, I. E. I.; Streib, W. E.; Eisenstein, O.; Caulton, K. G. *J. Am. Chem. Soc*. **1989**, *111*, 2346−2347.

67. te Velde, G.; Bickelhaupt, F. M.; Baerends, E. J.; Fonseca Guerra, C.; van Gisbergen, S. J. A.; Snijders, J. G.; Ziegler, T. *J. Comput. Chem*. **2001**, *22*, 931−967.

68. Moreno, J. J.; Espada, M. F.; Krüger, E.; López-Serrano, J.; Campos, J.; Carmona, E. *Eur. J. Inorg. Chem.* **2018**, 2309−2321.

69. a) Yanlong, Q.; Lu; Jiaqui; Weihua, X. *J. Mol. Catal.* **1986**, *34*, 31−38. b) Tao, X.; Qian, F.; Yong, L.; Qian, Y. *J. Mol. Catal. A: Chem.* **2000**, *156*, 121−126.

70. Craig, N. C.; Groner, P.; McKean, D. C. *J. Phys. Chem. A* **2006**, *110*, 7461−7469.

71. Brookhart, M.; Green, M. L. H.; Parkin, G. *Proc. Natl. Acad. Sci. U. S. A*. **2007**, *104*, 6908–6914.

72. Popelier, P. L. A. The QTAIM Perspective of Chemical Bonding. In *The Chemical Bond*; Frenking, G.; Shaik, S., Eds.; Wiley, 2014. pp. 271–308.

73. a) Varadwaj, P. R.; Cukrowski, I.; Marques, H. M. *J. Phys. Chem. A* **2008**, *112*, 10657–10666. b) Varadwaj, P. R.; Varadwaj, A.; Marques, H. M. *J. Phys. Chem*. *A* **2011**, *115*, 5592–5601. c) Espinosa, E.; Alkorta, I.; Elguero, J.; Molins, E. *J. Chem. Phys*. **2002**, *117*, 5529–5542.

74. Marín, M.; Moreno, J. J.; Navarro-Gilabert, C.; Álvarez, E.; Maya, C; Peloso, R.; Nicasio, M. C.; Carmona, E. *Chem. Eur. J.* **2019**, *25*, 260–272.

75. Marín, M.; Moreno, J. J.; Alcaide, M. M.; Álvarez, E.; López-Serrano, J.; Campos, J.; Nicasio, M. C.; Carmona, E. *J. Organomet. Chem.* **2019**, *896*, 120–128.

76. For reviews on this topic see: a) Bickelhaupt, F. M.; Houk, K. N. *Angew. Chem., Int. Ed.* **2017**, *56*, 10070–10086. b) Wolters, L. P.; Bickelhaupt, F. M. *WIREs Comput. Mol. Sci.* **2015**, *5*, 324–343.

77. Fernández, I.; Bickelhaupt, F. M. *Chem. Soc. Rev.* **2014**, *43*, 4953–4967.

78. White, C.; Yates, A.; Maitlis, P. M.; Heinekey, D. M. *Inorg. Synth.* **1992**, *29*, 228–234.

79. Yakelis, N. A.; Bergman, R. G. *Organometallics* **2005**, *24*, 3579–3581.

80. a) Campos, J.; Ortega-Moreno, L.; Conejero, S.; Peloso, R.; López-Serrano, J.; Maya, C.; Carmona, E. *Chem. Eur. J.* **2015**, *21*, 8883–8896. b) Ortega-Moreno, L.; Peloso, R.; Maya, C.; Suárez, A.; Carmona, E. *Chem. Commun.* **2015**, *51*, 17008–17011.

81. Frisch, M. J.; Trucks, G. W.; Schlegel, H. B.; Scuseria, G. E.; Robb, M. A.; Cheeseman, J. R.; Scalmani, G.; Barone, V.; Mennucci, B; Petersson, G. A.; Nakatsuji, H.; Caricato, M.; Li, X.; Hratchian, H. P.; Izmaylov, A. F.; Bloino, J.; Zheng, G.; Sonnenberg, J. L.; Hada, M.; Ehara, M.; Toyota, K.; Fukuda, R.; Hasegawa, J.; Ishida, M.; Nakajima, T.; Honda, Y.; Kitao, O.; Nakai, H.; Vreven, T.; Montgomery, J. A. J.; Peralta, J. E.; Ogliaro, F.; Bearpark, M.; Heyd, J. J.; Brothers, E.; Kudin, K. N.; Staroverov, V. N.; Kobayashi, R.; Normand, J.; Raghavachari, K.; Rendell, A.; Burant, J. C.; Iyengar, S. S.; Tomasi, J.; Cossi, M.; Rega, N.; Millam, J. M.; Klene, M.; Knox, J. E.; Cross, J. B.; Bakken, V.; Adamo, C.; Jaramillo, J.; Gomperts, R.; Stratmann, R. E.; Yazyev, O.; Austin, A. J.; Cammi, R.; Pomelli, C.; Ochterski, J. W.; Martin, R. L.; Morokuma, K.; Zakrzewski, V. G.; Voth, G. A.; Salvador, P.; Dannenberg, J. J.; Dapprich, S.; Daniels, A. D.;

Farkas, O.; Foresman, J. B.; Ortiz, J. V.; Cioslowski, J.; Fox, D. J.; Gaussian 09, Revision D.01, Gaussian, Inc.: Wallingford CT, 2013.

82. Perdew, J. P.; Burke, K.; Ernzerhof, M. *Phys. Rev. Lett.* **1996**, *77*, 3865–3868.

83. Grimme, S.; Antony, J.; Ehrlich, S.; Krieg, H. *J. Chem. Phys*. **2010**, *132*, 154104.

84. a) Hehre, W. J.; Ditchfield, R.; Pople, J. A. *J. Phys. Chem.* **1972**, *56*, 2257–2261. b) Hariharan, P. C.; Pople, J. A. *Theor. Chim. Acta.* **1973**, *28*, 213–222. c) Francl, M. M.; Pietro, W. J.; Hehre, W. J.; Binkley, J. S.; Gordon, M. S.; Defrees, D. J.; Pople, J. A. *J. Chem. Phys.* **1982**, *77*, 3654–3665.

85. Andrae, D.; Haeussermann, U.; Dolg, M.; Stoll, H.; Preuss, H. *Theor. Chim. Acta* **1990**, *77*, 123–141.

86. Marenich, A. V.; Cramer, C. J.; Truhlar, D. G. *J. Phys. Chem. B* **2009**, *113*, 6378–6396.

87. Lu, T.; Chen, F. *J. Comput. Chem.* **2012**, *33*, 580–592.

88. Peltzer, R. M.; Gauss, J.; Eisenstein, O.; Cascella, M. *J. Am. Chem. Soc*. **2020**, *142*, 2984–2994.

89. Kwon, O.; Sevin, F.; McKee, M. L. *J. Phys. Chem. A* 2001**,** *105,* 913–922.

90. a) Sharma, A. K.; Sameera, W. M. C.; Jin, M.; Adak, L.; Okuzono, C.; Iwamoto, T.; Kato, M.; Nakamura, M.; Morokuma, K. *J. Am. Chem. Soc.* **2017,** *139*, 16117–16125. b) Gutsev, L. G.; Gutsev, G. L.; Tibbetts, K. M.; Jena, P. *J. Phys. Chem. A* **2019**, *123*, 9693–9700. c) Ikuma, N.; Nakagawa, K.; Kokubo, K.; Oshima, T. *Org. Biomol. Chem.* **2016,** *14,* 7103–7108.

91. Tammiku-Taul, J.; Burk, P.; Tuulmets, A. *J. Phys. Chem. A* **2004,** *108*, 133–139

92. a) Lebon, J.; Mortis, A.; Maichle-Mössmer, C.; Manßen, M.; Sirsch, P.; Anwander, R. *Angew. Chem. Int. Ed.* **2023,** *62,* e202214599. b) Davison, N.; Falbo, E.; Waddell, P. G.; Penfold, T. J.; Lu, E. *Chem. Commun.* **2021,** *57,* 6205–6208.

93. ADF 2021.104, SCM, Theoretical Chemistry, Vrije Universiteit, Amsterdam, The Netherlands, http://www.scm.com.

94. Snijders, J. G.; Baerends, E. J.; Vernooij, P. *At. Data. Nucl. Data Tables* **1981**, *26*, 483–509.

95. Krijn, A.; Baerends, E. J. *Fit Functions in the HFS-Method, Internal Report (in Dutch),* Vrije Universiteit Amsterdam, The Netherlands, 1984.

96. a) van Lenthe, E.; Baerends, E. J.; Snijders, J. G. *J. Chem. Phys.* **1993**, *99*, 4597–4610. b) van Lenthe, E.; Baerends, E. J.; Snijders, J. G. *J. Chem. Phys.* **1994**, *101*, 9783–9792. c) van Lenthe, E.; Ehlers, A.; Baerends, E. J. *J. Chem. Phys.* **1999**, *110*, 8943–8953.